NOAA Technical Memorandum ERL NSSL-98

# WIND PROFILING OF STORMY AND QUIESCENT ATMOSPHERES WITH MICROWAVE RADARS

Dusan S. Zrnic'
Steven D. Smith
Arthur Witt
Robert M. Rabin
Mangalore Sachidananda



National Severe Storms Laboratory
Norman, Oklahoma
February 1986


**UNITED STATES DEPARTMENT OF COMMERCE**

**Malcolm Baldrige, Secretary**

NATIONAL OCEANIC AND ATMOSPHERIC ADMINISTRATION

Anthony J. Calio, Administrator

Environmental Research Laboratories

Vernon E. Derr, Director

Table of Contents

ABSTRACT

We examine the feasibility of wind measurement in the lower atmosphere with centimeter wavelength (microwave) Doppler radars. Because it is assumed that only natural scatterers contribute echoes, their frequency and distribution over continental United States is presented. A method to retrieve environmental winds from radial velocity fields measured in isolated cells is developed and demonstrated through comparisons with winds synthesized from two radars and with rawinsonde observations. It is shown that 10 cm wavelength radars should be consistently capable of profiling winds in the planetary boundary layer. In the winter during stable atmospheric conditions, the echoes are primarily due to turbulent mixing of refractivity gradients whereas in warmer months convective mixing and insects are the main contributors.

# WIND PROFILING OF STORMY AND QUIESCENT ATMOSPHERES WITH MICROWAVE RADARS

Dusan S. Zrnic', Steven D. Smith, Arthur Witt,
Robert M. Rabin, and Mangalore Sachidananda*

## 1. INTRODUCTION

This report investigates the feasibility of measuring winds in the lower atmosphere with microwave Doppler radars. It is assumed that natural scatterers such as hydrometeors and/or refractive index irregularities are the only ones present. Thus, techniques based on tracking balloons or on obtaining echo from chaff are not considered. Echo strengths from refractive index irregularities at microwave wavelengths are very weak or nonexistent above the planetary boundary layer (Doviak and Zrnic', 1984). Therefore, for measurements of winds outside the lowest 1 to 2 km of the atmosphere, radars may have to rely on the presence of clouds bearing hydrometeors. For that reason we examine the distribution of radar echoes in the continental U.S.A. and give typical reflectivity values for some cloud types.

A technique to obtain environmental winds from measurements in isolated storms observed with a single radar is examined. Results are compared with those from two radars and from nearby rawinsondes.

Echoes in clear air are examined and several case studies are discussed. Some of the measurements were made specifically for this task in the winter of 1985 when echoes were very weak. Other measurements were obtained in earlier experiments in the spring of 1983. Reflectivities are compared with theoretical values based on turbulent mixing of refractivity gradients and convective mixing driven by solar radiation. The Appendices discuss the theories and provide other calculation details.

## 2. THE FREQUENCY AND DISTRIBUTION OF RADAR ECHOES OVER THE UNITED STATES

The frequency and the distribution of radar echoes over the U.S. are highly variable. In order to investigate the seasonal and geographic variations, data from 31 WSR-57 radar stations for 1962 to 1964 were examined. Grantham and Kantor (1967) determined mean monthly frequencies and probabilities of radar echoes within 100 miles of the radar site in 3-hour time intervals for each of the 31 radar stations. In addition, the echo coverage

*Dr. Sachidananda is a Postdoctoral Research Associate of the National Research Council and guest investigator at the National Severe Storms Laboratory.

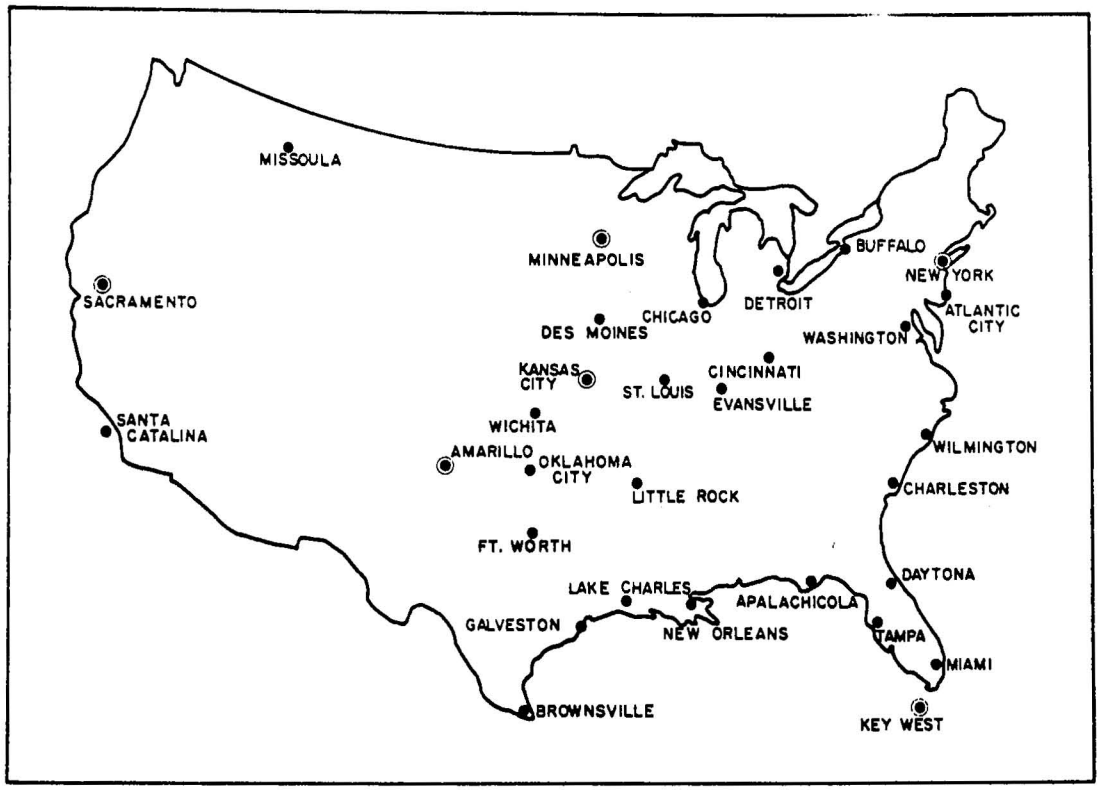


*Figure 2.1.--WSR-57 network.*

probabilities were estimated from low-level pulse position indicator (PPI) for a six-station sample: Sacramento, Amarillo, Minneapolis, Kansas City, New York, and Key West. The lowest echo power that was used in obtaining these statistics corresponds to 7 dBZ. Climates at the six stations are given in Appendix A.

## 2.1 Frequency of Radar Echoes Across the U.S.

The locations of the 31 radar stations are shown in Fig. 2.1. For each station the probabilities that radar echoes existed between given height intervals were calculated. The data for four seasonal months - January, April, July, and October - are shown in Fig. 2.2. In January (winter), we see fairly low probabilities (10-25%) in California, the Southern Plains states, and the western portion of the Midwest. Somewhat higher probabilities (26-45%) are found east of the Mississippi River, in western Montana, and along the Gulf Coast of Louisiana and eastern Texas. The highest probabilities (> 50%) occur in southern Florida and at Buffalo (this being caused by lake-effect snows). Unfortunately, large data void regions exist in the Pacific


*Figure 2.2a.--Frequency of radar echoes (percent of time) within a 100 mile radius of the radar, for January.*

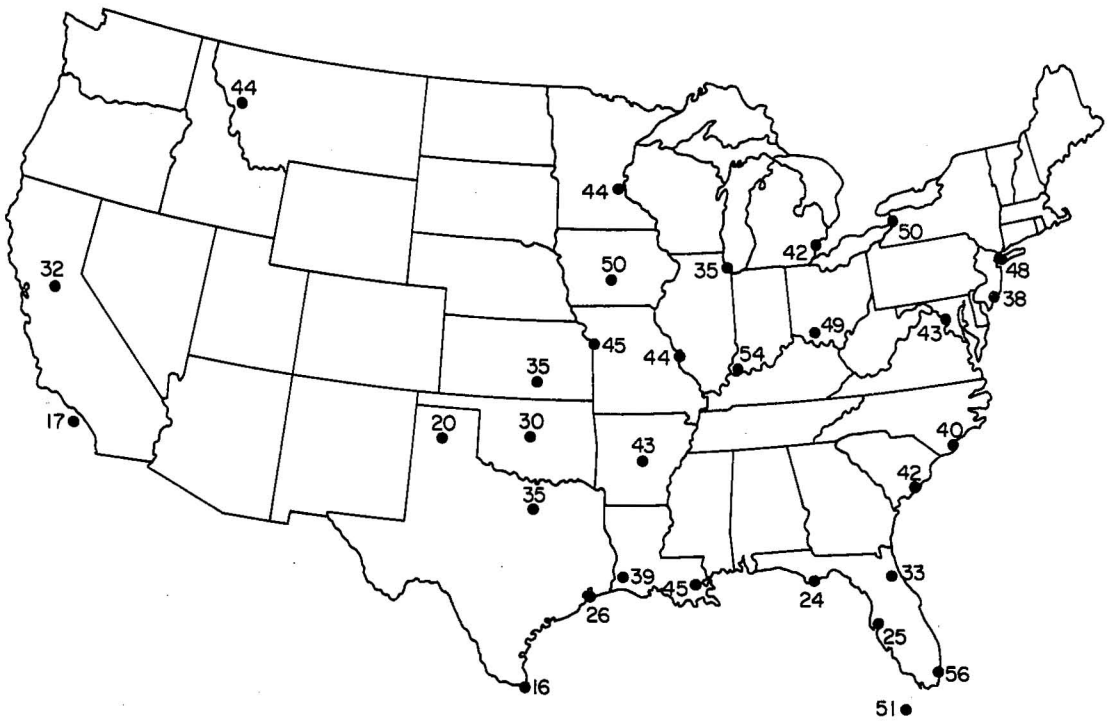


*Figure 2.2b.--Frequency of radar echoes (percent of time) within a 100-mi. radius of the radar, for April.*

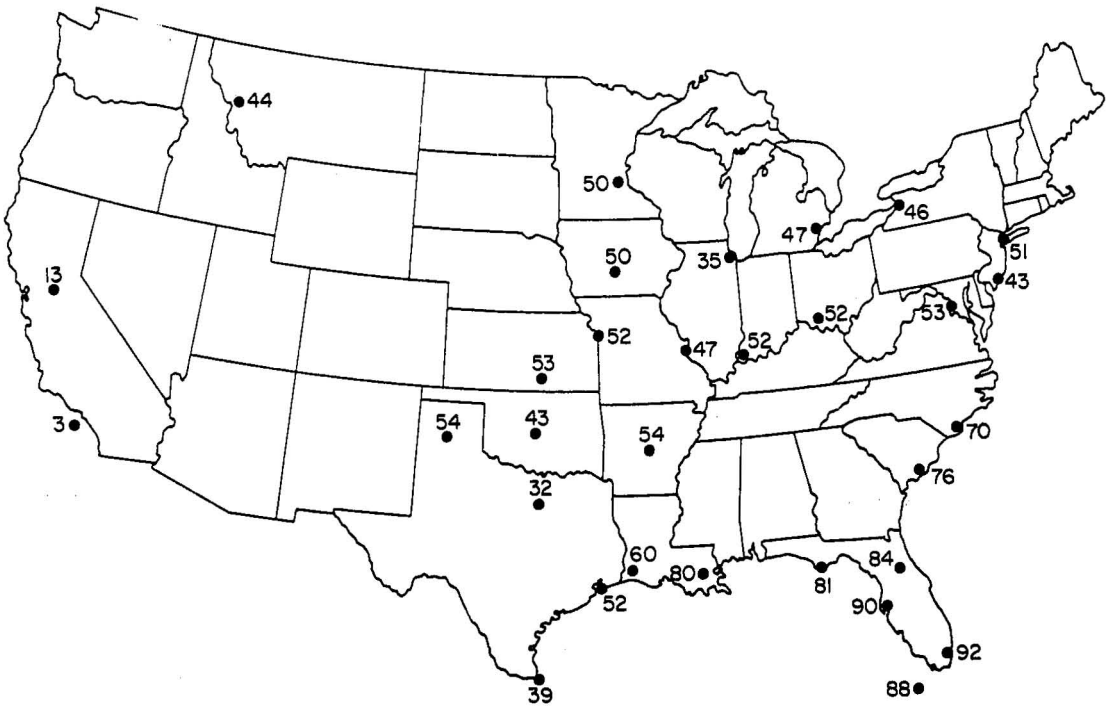


*Figure 2.2c.--Frequency of radar echoes (percent of time) within a 100-mi. radius of the radar, for July.*

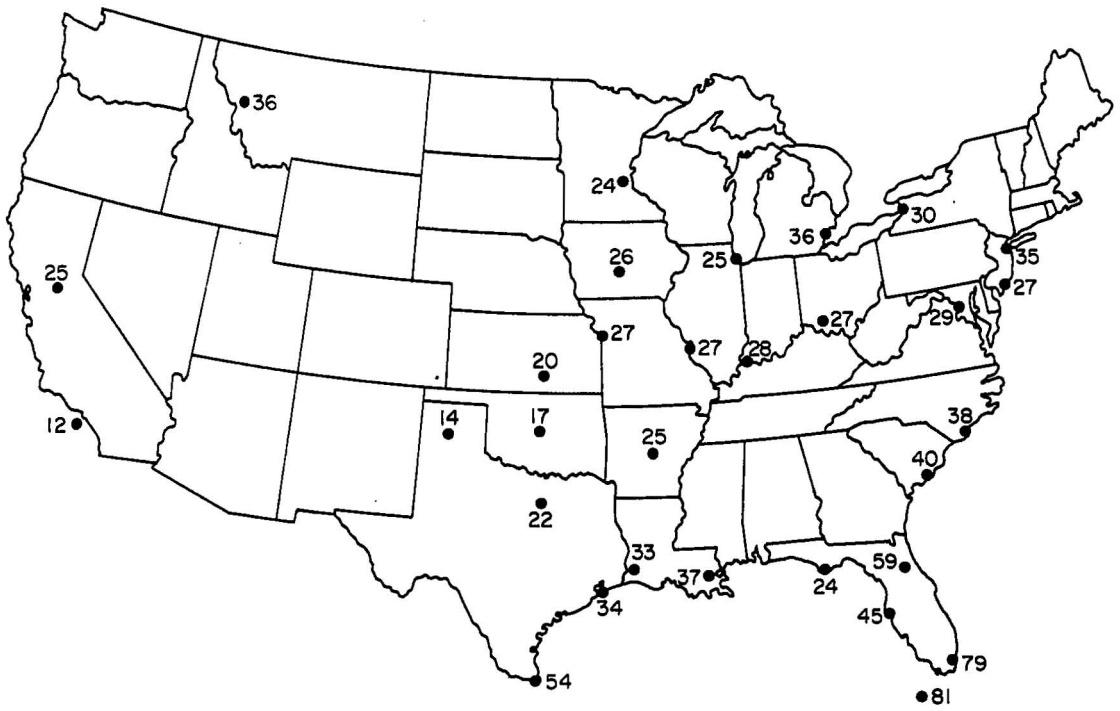


*Figure 2.2d.--Frequency of radar echoes (percent of time) within a 100-mi. radius of the radar, for October.*

Northwest, the Rocky Mountain states, the Northern Plains, New England, and the interior Southeast.

For April (spring) the probabilities have risen slightly (<10%) in California and western Montana and also along the East Coast. Probabilities have risen considerably (>10%) in the Southern Plains and western Midwest states but are lower in Florida.

In July (summer) most sites reach their maximum probabilities, with the exception of California, which is at a minimum. Almost three-fourths of the radar stations east of the Rockies have probabilities > 50%, with high probabilities (> 75%) occurring along the southeastern coast.

In October (autumn) most probabilities drop off significantly from their summer maximums, except in southern Florida where probabilities still remain high (~80%), and in California where they rise slightly from their summer minimums. A more detailed listing of radar echo probabilities for different heights above mean sea level is given in Appendix A.

## 2.2 Diurnal Variations

For six radar stations - Sacramento, Amarillo, Minneapolis, Kansas City, New York, and Key West - histograms were constructed to depict the diurnal variations of echo probability by 3-hour periods for each season (Fig. 2.3).

Variations in echo probabilities (Fig. 2.3) tend to be less in autumn and winter; greater in spring and summer. The smallest diurnal variation occurs at Amarillo and Kansas City in January; the largest occurs at Amarillo in July. The peak probabilities occurring during the afternoon and early evening hours are associated with the time of maximum convective activity. We note that generally low probability levels (≤ 30%) occur for Sacramento (except between 1300 and 2100 local standard time (LST) in April), for Amarillo (except in July), and for Minneapolis and Kansas City during January and October. Moderate values (~ 30 - 70%) occur for Sacramento in April between 1300 and 2100 LST, for Amarillo in July, for Minneapolis and Kansas City in April and July, for Key West in January and April, and for New York year-round. High values (>70%) occur only at Key West during July and October.

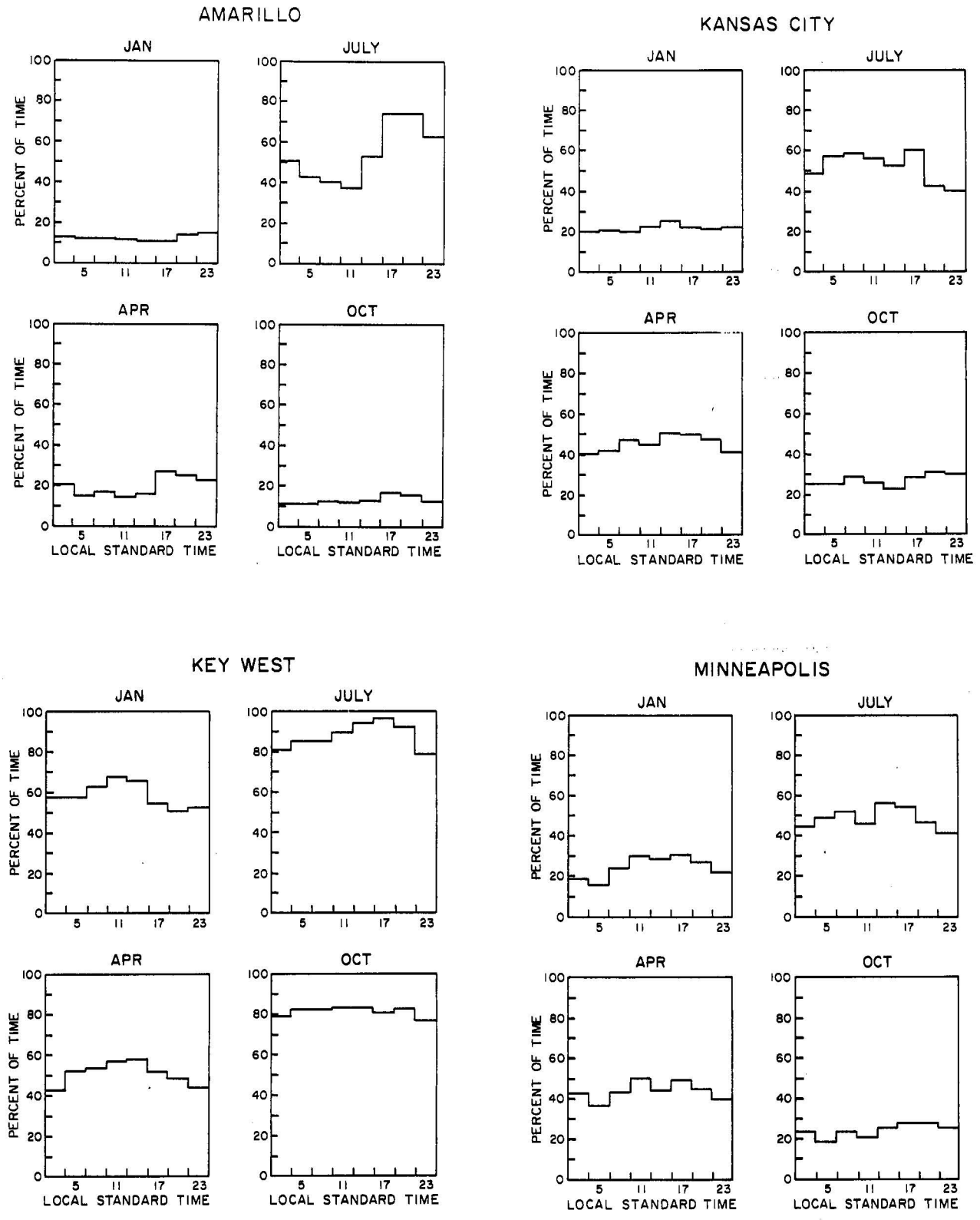


*Figure 2.3.--Diurnal variations in radar echo frequency, for six locations and four seasonal months.*

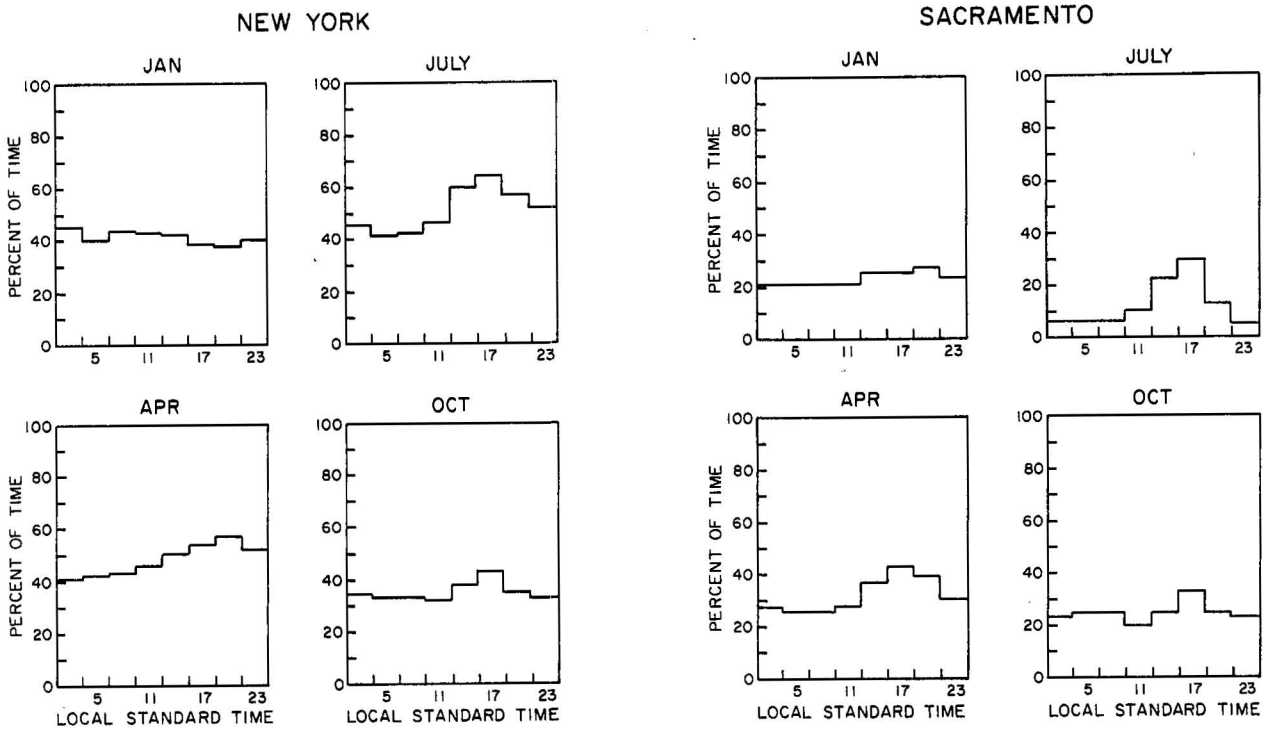


*Figure 2.3. (Continued)*

## 2.3 Echo Coverage Probabilities

For the same six stations, probabilities of echo coverage of a radar PPI scope out to a 100-mile range are presented for four seasonal months along with the diurnal variations (Fig. 2.4). The amount of echo coverage is divided into four groups: no echoes, 0%; low coverage, 1-30%; moderate coverage, 31-70%; and high coverage, 71-100%. Note that the probabilities of no echoes in Fig. 2.4 equal 100% minus the probabilities in Fig. 2.3. From Fig. 2.4 we see that, although the probabilities of at least low coverage reach a maximum in summer (except at Sacramento), the probabilities for high coverage remain roughly equal year-round, except in Key West where they are much higher in summer and autumn, and in Sacramento where they are near zero in summer.

## 2.4 Average Number of Clear, Cloudy, and Precipitation Days in the U.S.A.

NOAA data on cloudiness and precipitation for 39 U.S.A. cities are listed in Appendix A (Table A.7) and are summarized in Table 2.1. We conclude from these data that on a national average, 110 days per year (or 30% of the time) are clear with no radar echoes. From Table 2.2 we see that 38% of the time echo tops exceed 10,000 ft. Of these 38%, about 12% of the time, there is

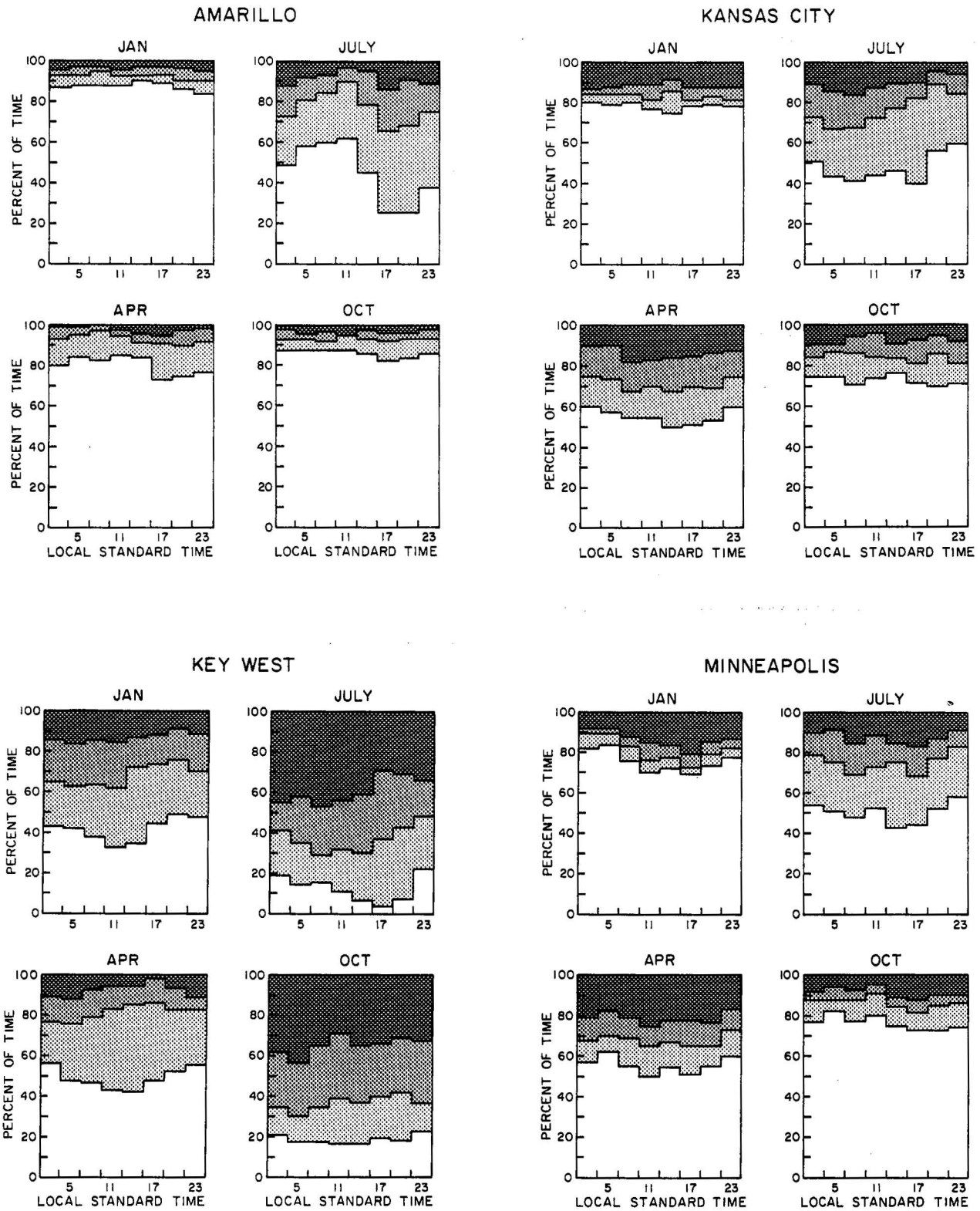


*Figure 2.4.--Echo coverage probabilities during four seasonal months, for the six locations represented in Fig. 2.3.*

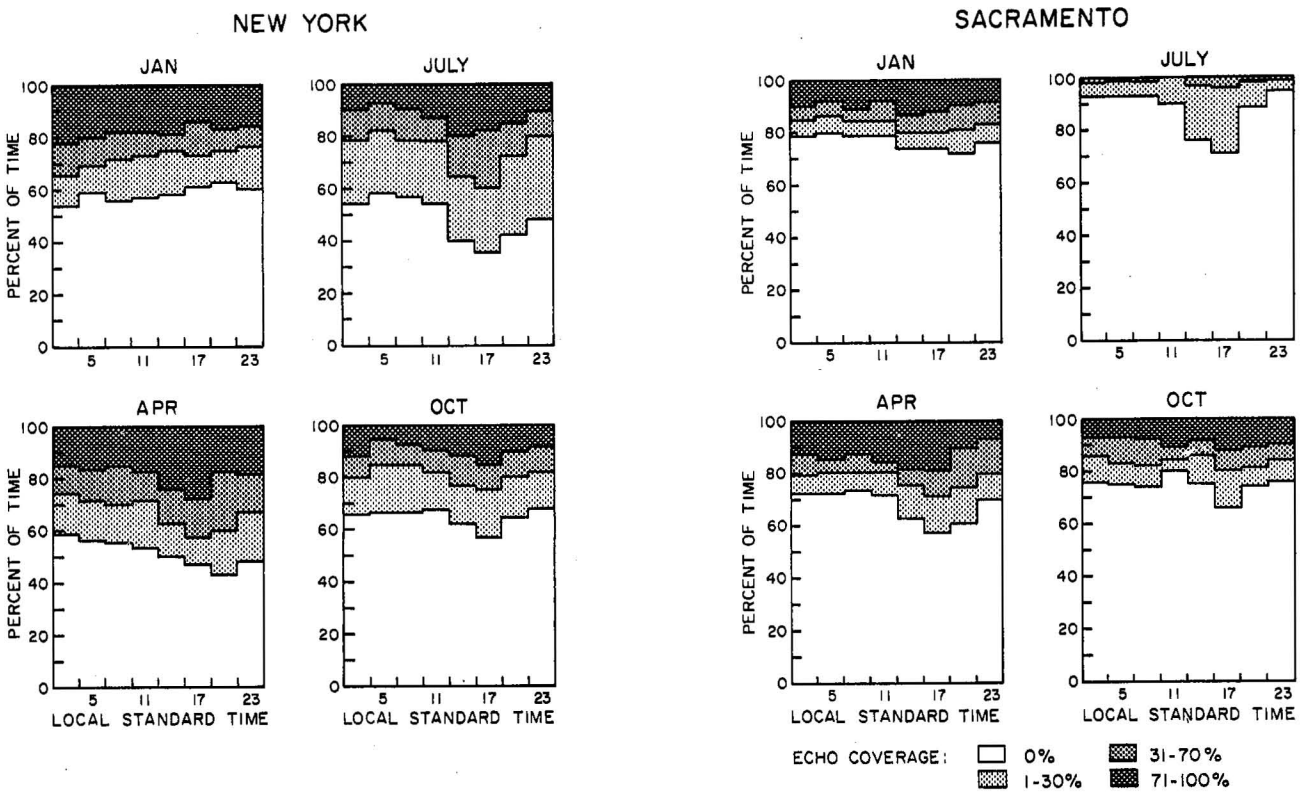


*Figure 2.4. (Continued)*

sufficient cloudiness and scattered light precipitation to allow velocity azimuth display (VAD) analysis. The remaining 26% of the time rain is sufficiently widespread to expect rain at the radar site (or any other point). Thus we expect to be able to make wind measurements to at least 3 km (10,000 ft) above ground level (AGL) more than 38% of the time.

Our summary of radar echo frequency data (Table 2.2) shows monthly variability of about 20-30%. The values in this table are averages of data from the 31 stations listed in Appendix A. We see that in late spring and summer more than 50% of the time, radars will be able to make measurements to over 3 km. This drops to about 30% in winter. Overall we expect to make measurements to at least 3 km 38% of the time.

With sensitive Doppler radars we expect to be able to make some measurements even in nonprecipitating clouds (see Appendix B). The cross section per unit volume for weakly reflecting clouds is given in Table 2.3 together with the effective reflectivity factor $Z_e$ (see Doviak and Zrnic', 1984).

Table 2.1.--Summary of Data on Clouds and Precipitation in the U.S.A.

| Average number of days | Mean % | Standard deviation % |
|---|---|---|
| 110 clear days | 30% | ±11% |
| 149 cloudy days | 41% | ±10% |
| 106 precipitation days | 29% | ±9% |

Table 2.2.--Summary of Radar Echo Frequency Data

| | Height (kft above sea level) | | | | | | |
|---|---|---|---|---|---|---|---|
| Month | 0-4.9 | 5-9.9 | 10-14.9 | 15-19.9 | 20-24.9 | 25-29.9 | 30+ |
| Jan | 33.47 | 32.63 | 28.23 | 19.68 | 10.27 | 3.90 | 1.50 |
| Feb | 34.00 | 33.32 | 28.15 | 20.51 | 11.97 | 5.39 | 2.90 |
| Mar | 34.27 | 35.50 | 33.36 | 26.03 | 17.86 | 7.76 | 4.71 |
| Apr | 38.57 | 38.52 | 36.55 | 30.36 | 20.88 | 12.77 | 8.17 |
| May | 50.20 | 41.28 | 39.34 | 35.58 | 30.61 | 21.53 | 15.59 |
| Jun | 51.80 | 51.87 | 51.53 | 49.18 | 43.35 | 35.17 | 26.01 |
| Jul | 54.33 | 54.32 | 57.07 | 52.58 | 48.01 | 39.30 | 30.12 |
| Aug | 52.83 | 52.82 | 52.49 | 43.80 | 37.64 | 35.72 | 28.31 |
| Sep | 49.35 | 49.34 | 48.70 | 47.25 | 39.47 | 29.20 | 21.50 |
| Oct | 33.39 | 33.36 | 32.34 | 28.57 | 21.15 | 13.58 | 8.18 |
| Nov | 34.68 | 34.62 | 29.92 | 21.97 | 14.15 | 6.76 | 3.70 |
| Dec | 32.72 | 32.05 | 27.20 | 17.58 | 9.53 | 3.92 | 1.93 |
| Yearly Av. | 41.64 | 40.14 | 38.49 | 32.76 | 25.41 | 17.92 | 12.72 |

Table 2.3.--Cross Sections for Various Cloud Types

| Cloud type | Cross section ($m^{-1}$) | Effective reflectivity factor (dBZ) |
|---|---|---|
| Fair weather cumulus | $1.8 \times 10^{-15}$ | -32 |
| Cumulus congestus | $2.6 \times 10^{-12}$ to $4.3 \times 10^{-14}$ | -1 to -19 |
| Stratocumulus | $9 \times 10^{-14}$ | -16 |
| Altocumulus | $9 \times 10^{-12}$ | 4 |
| Altostratus | $4 \times 10^{-13}$ | -11 |
| Cirrus | $9 \times 10^{-13}$ | 2 |

# 3. USE OF STORMS FOR ENVIRONMENTAL WIND PROFILING

## 3.1 Methodology

We estimate Cartesian wind components by analyzing single Doppler radar data. A Doppler radar samples only the radial component and therefore provides an incomplete description of the vector wind. If one can describe the

vector wind by some assumed model, it may be possible to deduce the parameters of such a model. For simplicity we describe the wind as being horizontal, invariant over the data acquisition time, and spatially uniform within some analysis domain. For a radar scanning a uniform horizontal wind, the radial component $v_r$ is related to the radar beam azimuth $\phi$ and elevation angle $\theta_e$ through the following relationship (in matrix notation):

$$v_r = \mathbf{P}\,\mathbf{K}_2$$

where

$$\mathbf{P} = [\cos\theta_e' \sin\phi,\ \cos\theta_e' \cos\phi], \tag{3.1}$$

$$\mathbf{K}_2 = \begin{bmatrix} u_o \\ v_o \end{bmatrix},$$

$u_o$ and $v_o$ are constants denoting the east-west and north-south uniform wind components which must be estimated, and $\theta_e' = \theta_e + \theta_c$ is elevation angle corrected for the earth's curvature (see Koscielny et al., 1982). The angle $\theta_c$ is given by

$$\theta_c = \tan^{-1}\left[\frac{r\cos\theta_e}{a_e + r\sin\theta_e}\right] \tag{3.2}$$

where r is slant range and $a_e$ is the earth's radius adjusted for beam bending due to vertical gradients of refractive index (Doviak and Zrnic', 1984).

It will be shown that estimates of $\mathbf{K}_2$ are the solutions to a multivariate regression problem. Consider an analysis domain within which there are n radial velocity estimates. (This analysis domain is chosen to be either a circular arc of azimuthal width $\Delta\phi$ or a sector of azimuthal width $\Delta\phi$ and small range width $\Delta r$ to keep contamination by vertical wind shear small). The i-th estimate can be expressed as the sum of two terms:

$$\hat{v}_i = \mathbf{P}_i\,\mathbf{K}_2 + \varepsilon_i \tag{3.3}$$

of which the additional term $\varepsilon_i$ expresses that part of radial velocity $\hat{v}_i$ not explained by the uniform wind model. Factors that contribute to $\varepsilon_i$ are errors due to velocity measurement, nonuniformities of the wind, and (if the measurements are taken in precipitation) raindrop terminal fallspeeds. Collecting

the n velocities into a column vector $\hat{\mathbf{V}}_n$, least-squares estimates $\hat{\mathbf{K}}_2$ are given by

$$\hat{\mathbf{K}}_2 = (\mathbf{P}_{n2}^T \mathbf{P}_{n2})^{-1} \mathbf{P}_{n2}^T \hat{\mathbf{V}}_n. \tag{3.4}$$

The superscripts -1 and T indicate the matrix inverse and transpose respectively (Draper and Smith, 1981), and $\mathbf{P}_{n2}^T = (\mathbf{P}_1^T, \mathbf{P}_2^T, \ldots, \mathbf{P}_n^T)$.

In general, $\hat{\mathbf{K}}_2$ and the true $\mathbf{K}_2$ differ and these differences can be decomposed into bias and variance errors. The estimates $\hat{\mathbf{K}}_2$ are biased if $E[\hat{\mathbf{K}}_2] \neq \mathbf{K}_2$, which occurs when the uniform wind model (3.1) is inadequate. Raindrop terminal fallspeeds and nonuniformities of the wind are the major contributors to biases of $\hat{\mathbf{K}}_2$. The degree to which wind estimates are biased depends on the geometry of the analysis domain and the magnitudes of the nonuniformities of the wind.

Variance errors depend on both the geometry of the analysis domain and velocity measurement uncertainty. The variances of the uniform wind estimates (i.e., $\hat{u}_o$, $\hat{v}_o$) are given by the diagonal elements of the variance-covariance matrix

$$\mathbf{C}_{22} \equiv \mathrm{VAR}(\hat{\mathbf{K}}_2) = (\mathbf{P}_{n2}^T \mathbf{P}_{n2})^{-1} \sigma_\varepsilon^2 \tag{3.5}$$

where $\sigma_\varepsilon^2$ is velocity estimate variance due to measurement error. If $\sigma_\varepsilon^2$ is unknown, an estimate is given by the residual variance $s^2 = \hat{\mathbf{E}}_n^T \hat{\mathbf{E}}_n/(n-2)$ where $\hat{\mathbf{E}}_n = (\hat{\mathbf{V}}_n - \mathbf{P}_{n2} \hat{\mathbf{K}}_2)$.

Expression (3.5) is useful in determining the appropriate geometry of the analysis domain so as to keep $\mathrm{VAR}(\hat{\mathbf{K}}_2)$ tolerable. It can be shown that the trace of $\mathbf{C}_{22}$ (equal to the sum $\mathrm{VAR}(\hat{u}_o) + \mathrm{VAR}(\hat{v}_o)$) for a circular arc of data is given (approximately) by

$$T_r(\mathbf{C}_{22}) \approx \frac{12 \sec^2 \theta_e'}{n \Delta\phi^2} \sigma_\varepsilon^2 \tag{3.6}$$

(Doviak and Zrnic', 1984). Equation (3.6) expresses the need for a large azimuthal width of data when single Doppler velocities are processed to obtain the uniform wind. Evaluation of (3.6) shows that accurate wind estimates are made when $\Delta\phi \geq \pi/6$ radians (i.e., $\geq 30°$) and $\sigma_\varepsilon \lesssim 1\mathrm{m\ s}^{-1}$.

Data acquisition schemes limit n for a given $\Delta\phi$ and therefore the minimum variance. To take further advantage of the $n^{-1}$ dependence on estimate variance, velocity data can be processed within a sector of range width $\Delta r$. Two related methods can be used to retrieve $\hat{u}_o$ and $\hat{v}_o$ from such a sector. In one, the fit is done for each data point as just outlined. Alternately we can average velocities over the range interval $\Delta r$ and fit the resulting data on an arc (see Appendix C). Although fewer data are used in this type of analysis, there is an $n_r^{-1}$ decrease in $\sigma_\varepsilon^2$ ($n_r$ is the number of data averaged in range). Two advantages of range averaging are that both computer memory requirements and the number of computations necessary to evaluate $\hat{K}_2$ are reduced. In order to constrain biases at higher elevations due to vertical wind shear, the range averaging interval must be kept less than 10 km; this also helps reduce the effects of differences of the angles between the beam and the local horizon.

Above the planetary boundary layer (1.5 - 2.0 km AGL), backscatter at microwave frequencies from refractive index fluctuations is generally too weak for accurate velocity estimation. To obtain velocities at these higher levels, we must rely on radar targets of opportunity such as storms and convective cells with sufficiently large backscatter. If these are unavailable, artificial targets such as chaff or balloons must be introduced to the atmosphere. We do not consider these latter alternatives but rather attempt to profile the winds using storm data.

Doppler data collected within storms on two days (June 19, 1980, and May 17, 1981) were processed to produce wind profiles using the uniform wind algorithm. On both days, volume scans allowed sampling of the in-storm winds up to heights of nearly 15 km with good spatial resolution (data spaced 1° in azimuth and 150 m in range). Prior to data analysis, radial velocities were edited to remove anomalous data resulting from weak signal (SNR < 5 dB) and overlaid echoes. Also to reduce as much as possible contamination of velocities by raindrop terminal fallspeeds, data within 40 dBZ contours were not used. When necessary, velocities were dealiased.

The sectors over which the uniform wind components were estimated subtended 30° in azimuth (primarily because of limitations on the availability of data) and approximately 10 km in range. For sectors this size, the maximum number of processed data, n, was ~ 2000. Because some data are missing after editing, a minimum threshold on n was set at one-half this value. In general,

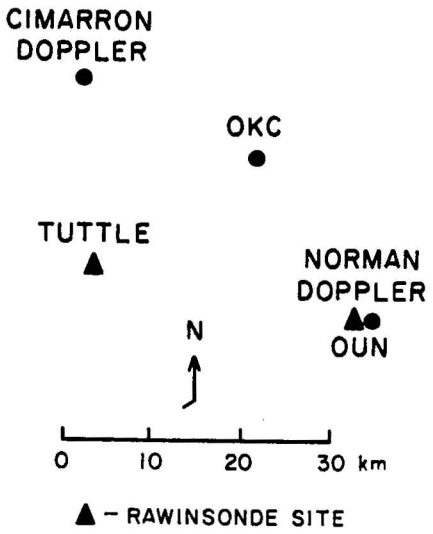


*Figure 3.1.--Relative positions of NSSL's radars and the rawinsonde sites.*

uniform wind estimates have unacceptably large variance when n decreases below this threshold (when processing velocity data in real-time, a minimum threshold on the azimuthal extent of the data should also be imposed).

The results of the uniform wind analysis for the two days are shown in sections 3.2.1 and 3.2.2. Also shown are profiles derived from dual Doppler reconstructed wind fields at various levels through the storms and storm proximity soundings. Comparisons between single and dual Doppler derived profiles are made to determine how well uniform winds represent the average flow within storms. A second comparison between rawinsonde and Doppler derived profiles helps determine whether in-storm winds represent the environmental flow. Figure 3.1 shows the relative positions of NSSL's Doppler radars and rawinsonde sites used for these comparisons.

## 3.2 Results of the Uniform Wind Analysis

### 3.2.1 June 19, 1980

On this day, a storm first formed in west-central Oklahoma and was tracked on radar from 1942 to 2215 CST as it moved to the southeast (Vasiloff and Brandes, 1984). Early in the storm's lifetime (2016 CST) echo intensities were less than 50 dBZ and in-storm winds were relatively unperturbed. By 2215 CST, maximum reflectivities exceeded 60 dBZ, peak updraft speeds were in excess of 60 $ms^{-1}$, and a mesocyclone had formed on the southwest flank of the storm both at middle and low levels. Maximum echo tops at this time were near

16 km AGL. Figures 3.2 and 3.3 show dual Doppler reconstructed winds within the storm and the reflectivity factor contours at 4 km AGL for 2016 and 2215.

Profiles derived from uniform wind estimates at 2016 CST for sectors 30° x 2.5 km are shown in Figs. 3.4a and 3.4b. These figures illustrate how uniform wind estimates can differ considerably even though they were derived from data separated by short range intervals. Although some of the variation between profiles can be explained by wind estimation errors, the larger differences are the result of nonuniformities of the wind, which bias the uniform wind estimates to different degrees. As stated previously, bias errors can be reduced by selecting appropriate analysis volume geometry. However, the choice of analysis volume geometry must depend on the type and magnitude of the nonuniformities that cause these biases. Also, in many cases, variance errors are compromised when bias errors are reduced. Since the exact model of the wind field is unknown, we cannot reduce bias errors but must be aware of their presence. We can, however, reduce variance errors by processing data over larger sectors (e.g., 30° x 10 km).

Figures 3.5a and 3.5b compare profiles from dual Doppler reconstructed winds, a uniform wind analysis (single radar) over the (30° x 10 km) sector shown in Fig. 3.2 and the 2015 CST OUN rawinsonde (OUN is collocated at the Norman Doppler radar site). Figures 3.6a and 3.6b quantify discrepancies between the three profiles in terms of wind speed and direction differences.

A second uniform wind analysis was performed at 2215 CST. At this time there was nearly 40 km of useable data at each elevation, so for 30° x 10 km sectors there were four estimates of $u_0$ and $v_0$ in range. (The data used in this analysis are outside the boundary of Fig. 3.3). These estimates are shown in Figs. 3.7a and 3.7b.

Comparisons similar to those in Figs. 3.5 and 3.6 are shown in Figs. 3.8 and 3.9. A mean profile from the uniform wind estimates was obtained by averaging $\hat{u}_0$ and $\hat{v}_0$ over 1 km height intervals. The rawinsonde data are from OUN at 2215 CST.

### 3.2.2 May 17, 1981

On this day, two storms had developed in west-central Oklahoma in advance of a dryline. The northern cell was almost directly west and the southern cell southwest of the Norman Doppler. Dual Doppler coverage of both storms

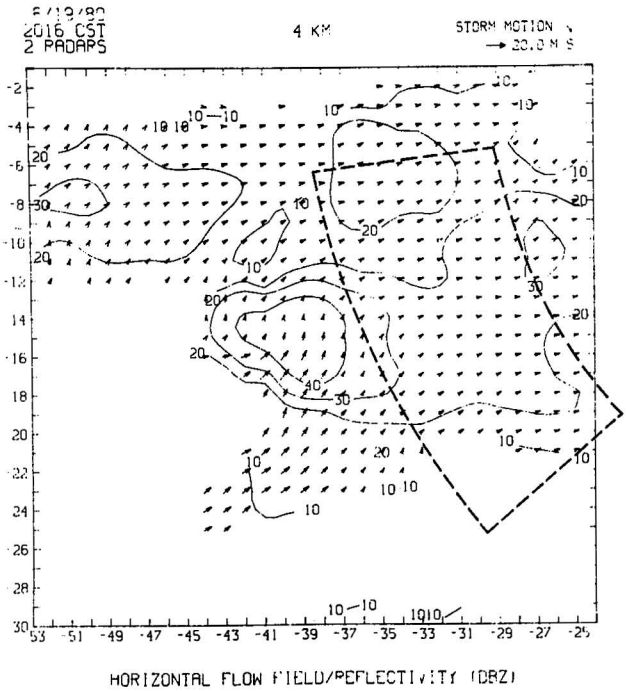


*Figure 3.2.--Horizontal flow field and reflectivity factor in dBZ at 2016 CST on June 19, 1980. The height is 4 km AGL. The grid border numbers represent distance from the Norman radar. The wind vectors have had the storm motion vector (shown in the upper right-hand corner) subtracted out. The dashed annulus sector is the region where winds were estimated from single Doppler analysis.*

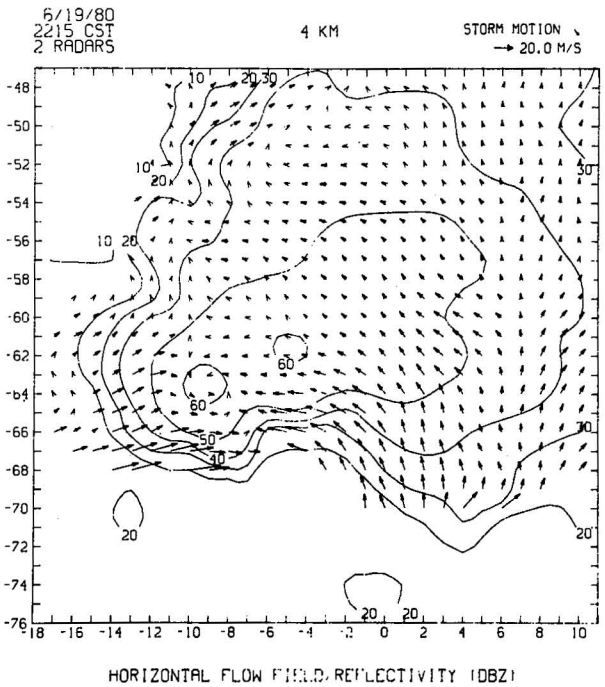


*Figure 3.3.--Horizontal flow field and reflectivity factor on 19 June 1980, except at 2215 CST (see Fig. 3.2).*

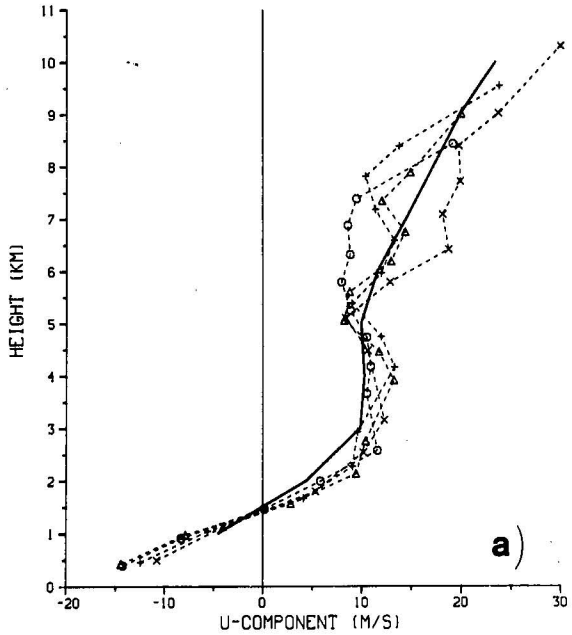


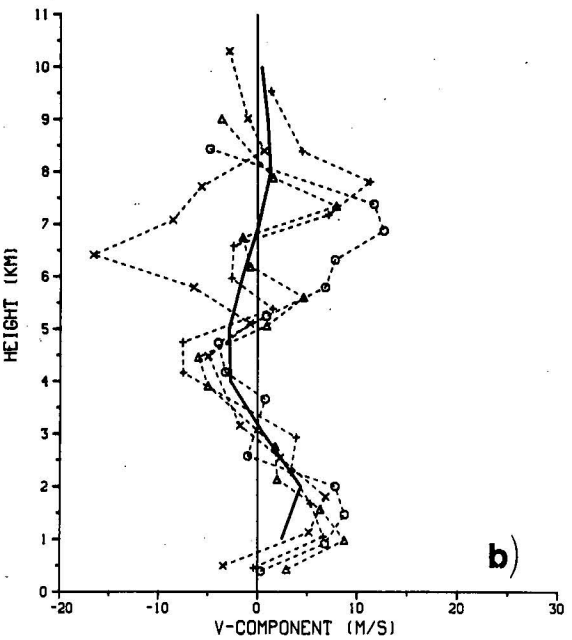


*Figure 3.4.--Profiles of (a) the u-component and (b) the v-component at 2016 CST on June 19, 1980. The short dashed lines are from single Doppler analysis over 30° x 2.5 km sectors. The solid line is the profile derived from dual Doppler analysis. The dual Doppler wind at each level represents an average of all horizontal wind vectors within 10 dBZ contours.*

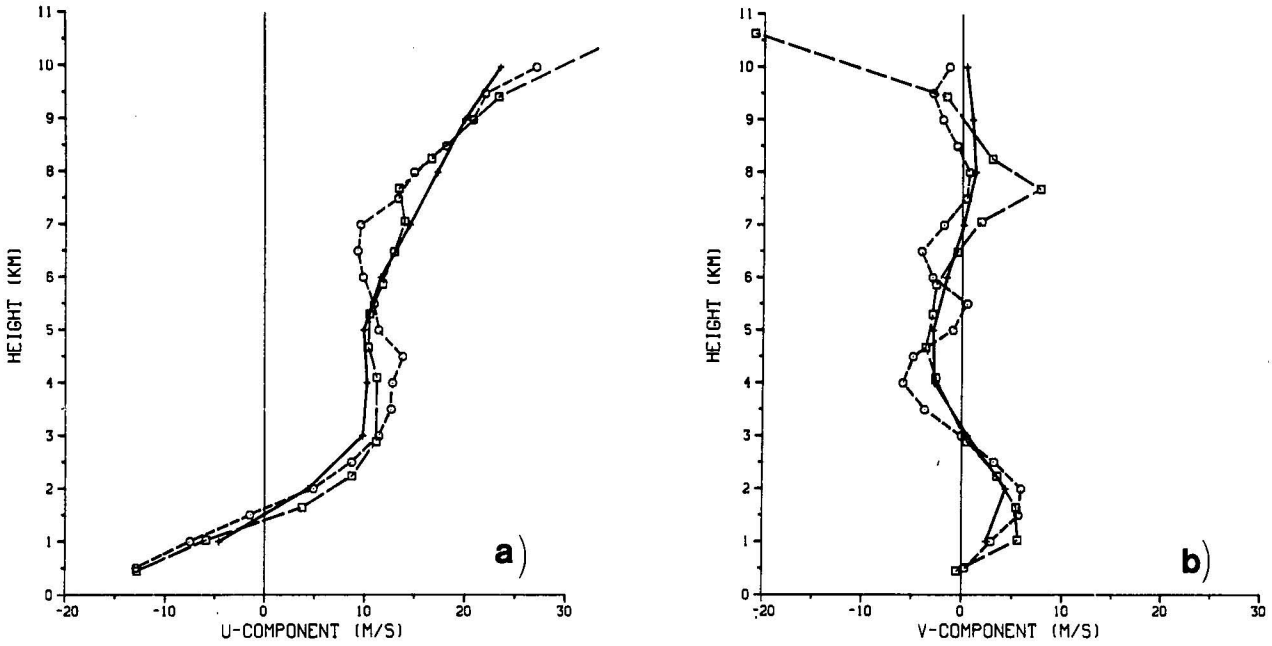


*Figure 3.5.--Comparison of (a) u-component and (b) v-component profiles at 2016 CST. The solid line is from dual Doppler analysis, the long dashed line is from single Doppler analysis, and the short dashed line is from the 2016 CST OUN rawinsonde.*

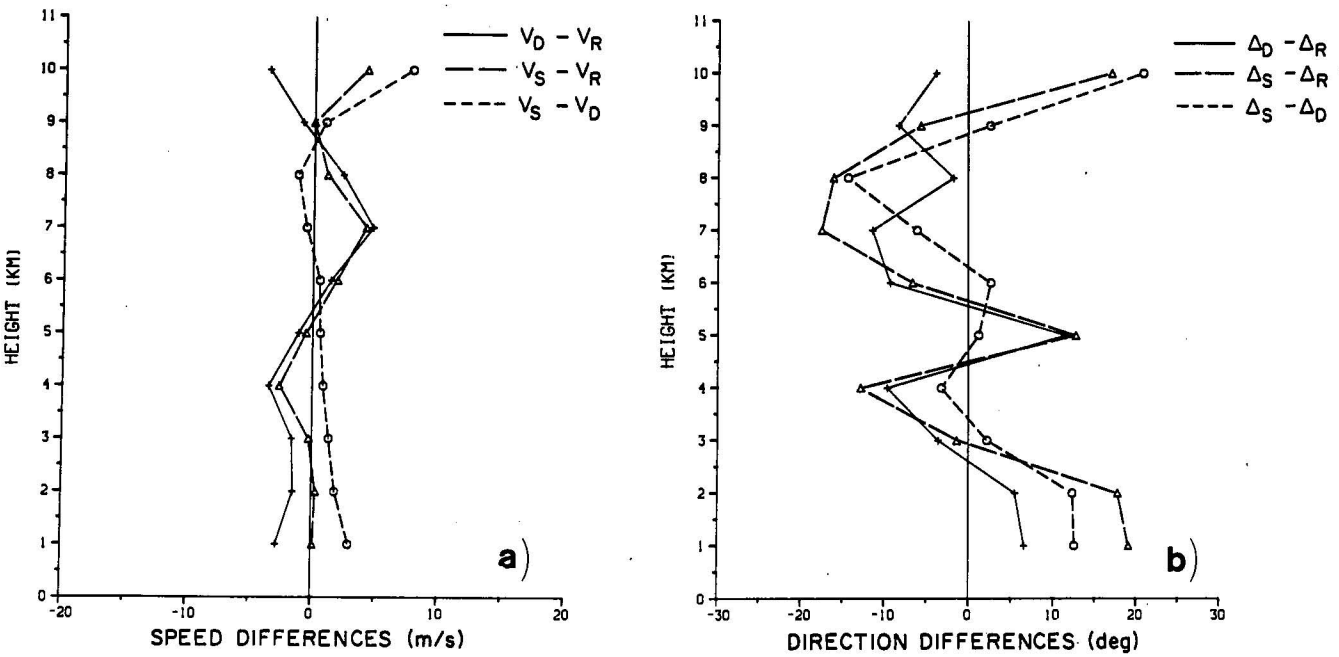


*Figure 3.6.--Differences between (a) wind magnitudes V and (b) wind directions Δ obtained from dual Doppler derived winds (D), single Doppler derived winds (S), and rawinsonde (R).*

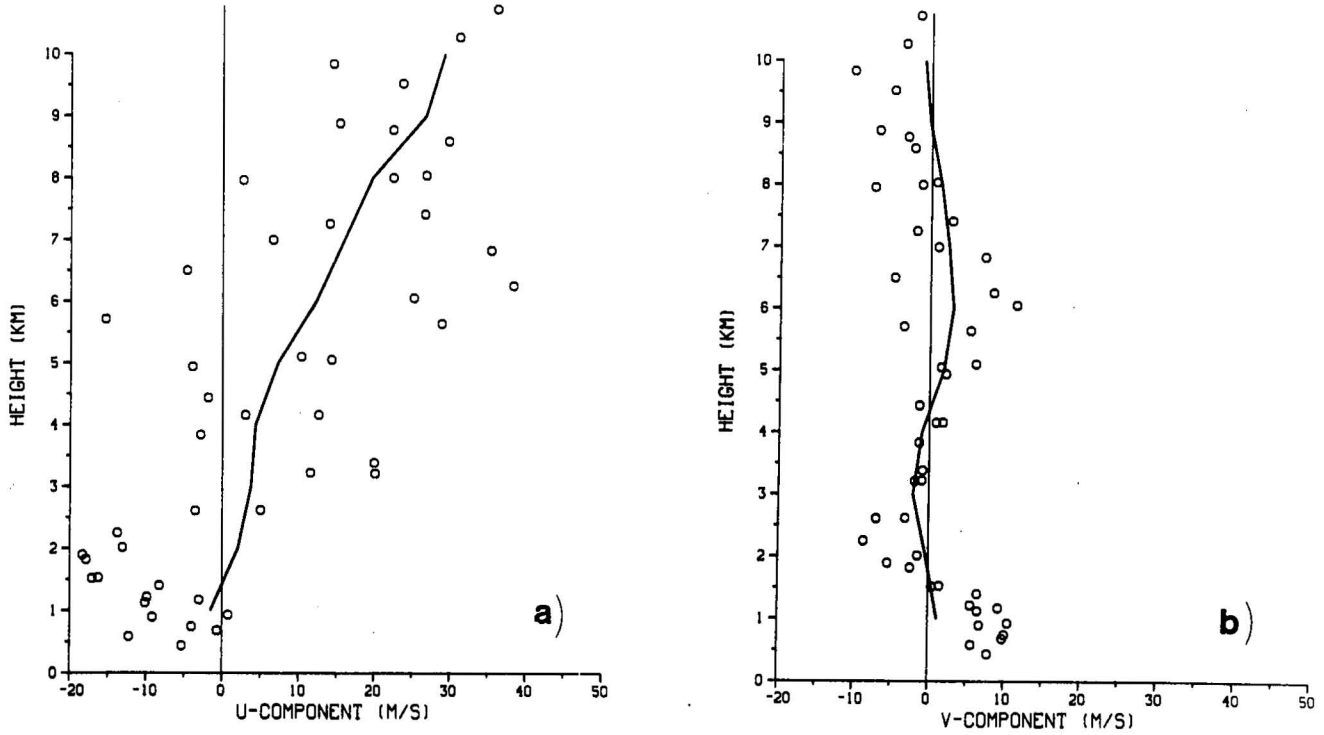


*Figure 3.7.--Estimates of (a) u-component and (b) v-component from single Doppler analysis (circles) at 2215 CST on June 19, 1980. The solid line represents the profile from dual Doppler analysis at the same time.*

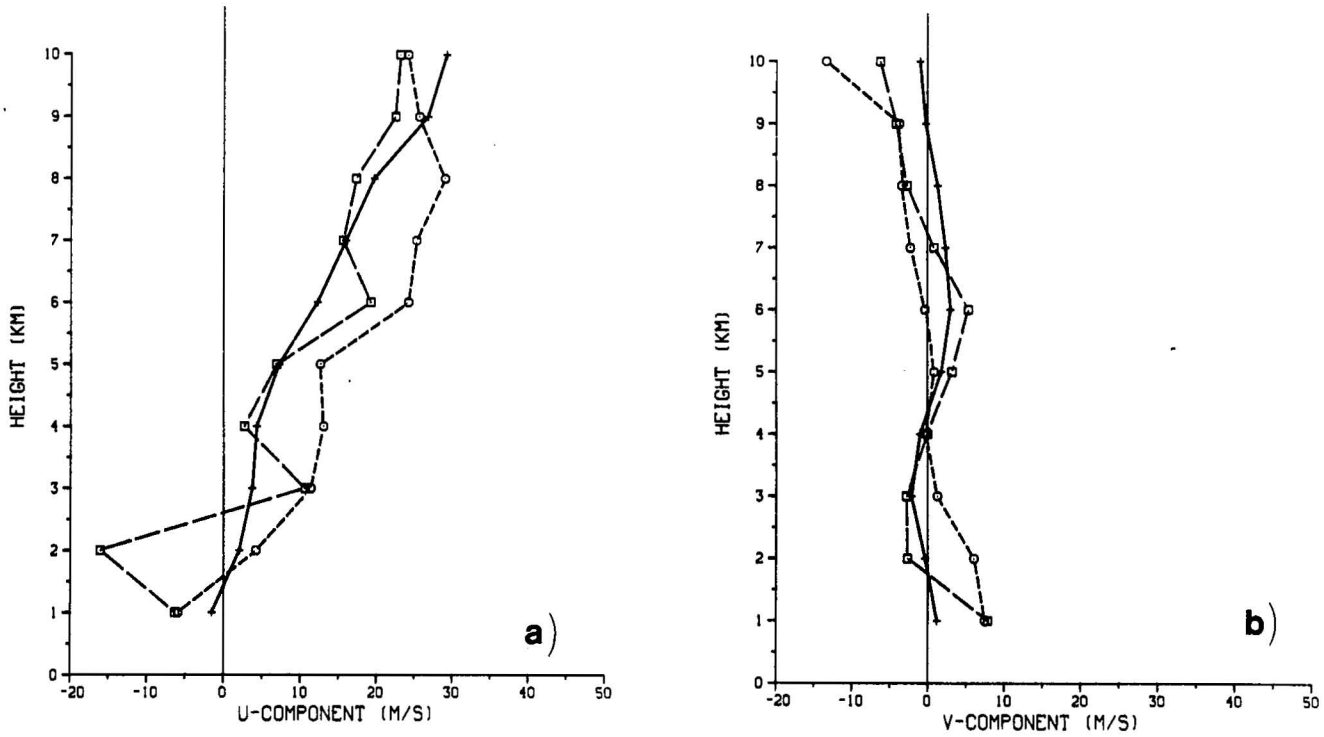


*Figure 3.8.--Profiles of (a) u-component and (b) v-component at 2215 CST. The solid line is from dual Doppler analysis, the long dashed line is from single Doppler analysis, and the short dashed line is from the 2215 CST rawinsonde.*

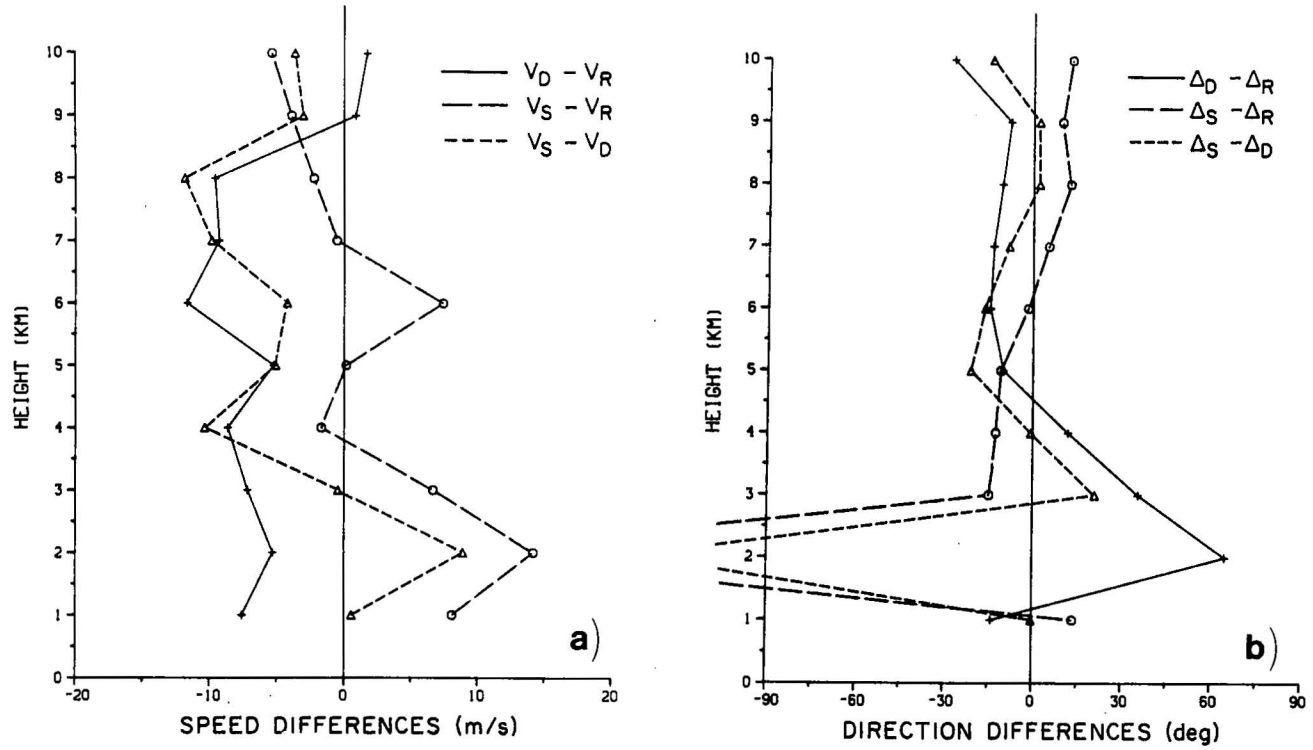


*Figure 3.9.--Differences between (a) wind magnitudes V and (b) wind directions Δ obtained from dual Doppler derived winds (D), single Doppler derived winds (S), and rawinsonde (R) at 2215 CST.*

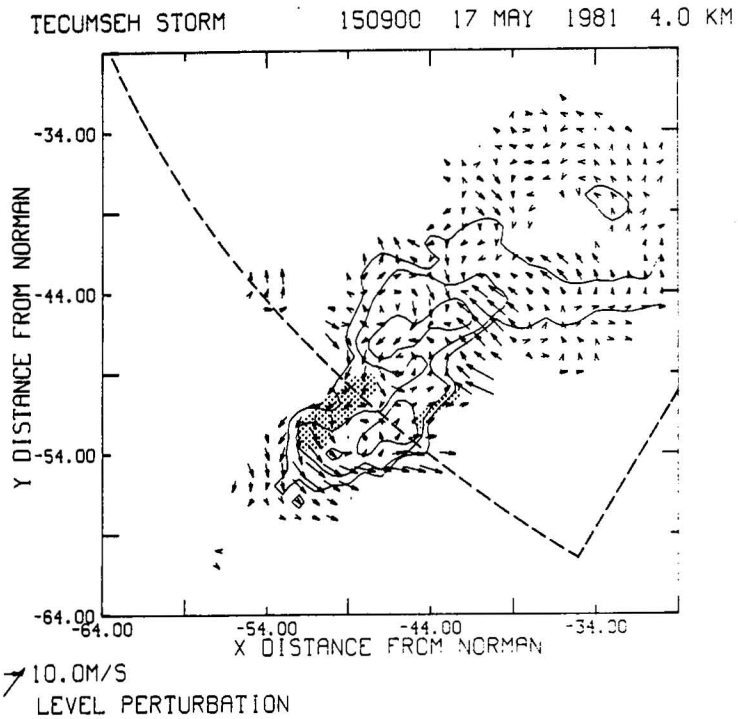


*Figure 3.10.--Horizontal flow field and reflectivity factor in dBZ at 1509 CST on May 17, 1981. The height is 4.0 km AGL. The mean wind vector (shown in the lower left-hand corner) has been subtracted from the flow field. The beginning reflectivity contour is 20 dBZ with increments of 10 dBZ.*

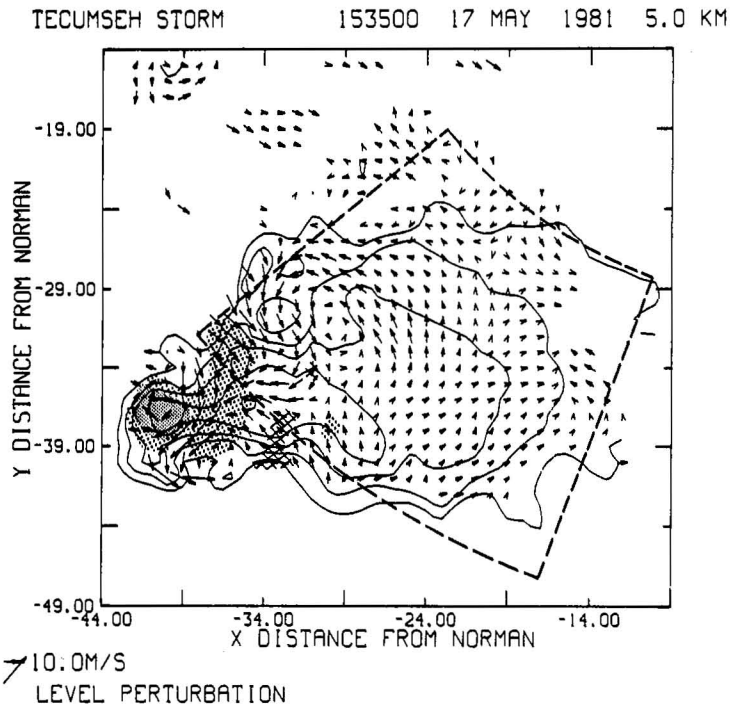


*Figure 3.11.--Horizontal flow field and reflectivity factor at 1535 CST and 5.0 km AGL (see Fig. 3.10).*

began at 1445 CST and continued until 1525 when dual mapping continued only for the southern storm.

During the first half-hour of radar coverage, the cells appeared narrow (each cell subtended no more than 15° in azimuth) and they were relatively weak. Maximum reflectivities at this time were still under 50 dBZ and updraft speeds approached 20 $ms^{-1}$ (Brewster, 1985). By 1535 CST, the southern cell (referred to as the Tecumseh storm) had grown in areal coverage; maximum reflectivities were near 60 dBZ and updraft speeds were measured in excess of 20 $ms^{-1}$. Figures 3.10 and 3.11 are examples of the in-storm winds and reflectivity factor at middle levels of the Tecumseh storm for 1509 and 1535 CST.

For the first analysis time (1503 CST), the individual storm cells were too narrow in azimuthal extent for an adequate uniform wind analysis on each cell. Because the storms were in close proximity, we decided to use Doppler data from both storms to estimate the winds. The sector sizes chosen to encompass both storms were then quite large (70° x 10 km); however, the data voids between storms were near 40°. In this particular case the two cells

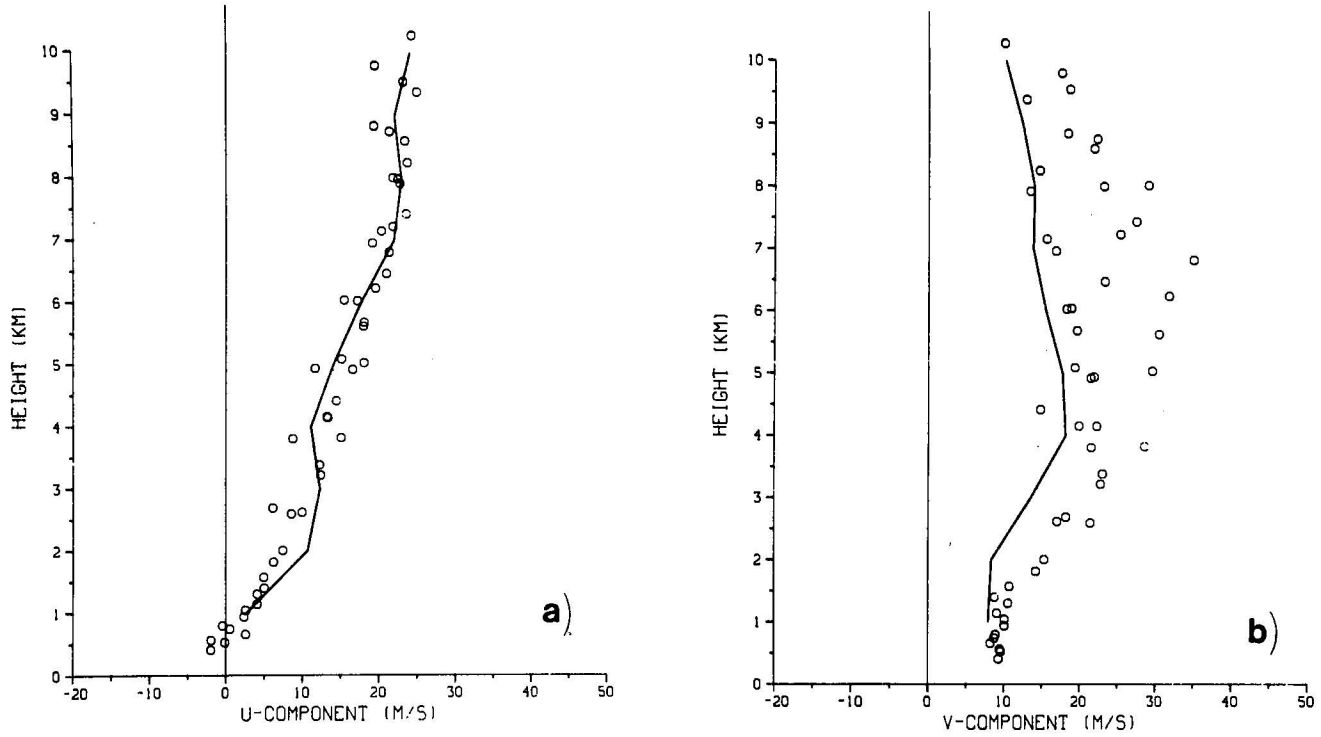


*Figure 3.12.--Estimates of (a) u-component and (b) v-component from single Doppler analysis (circles) at 1503 CST on May 17, 1981. The solid line is a profile from dual Doppler analysis at 1535 CST.*

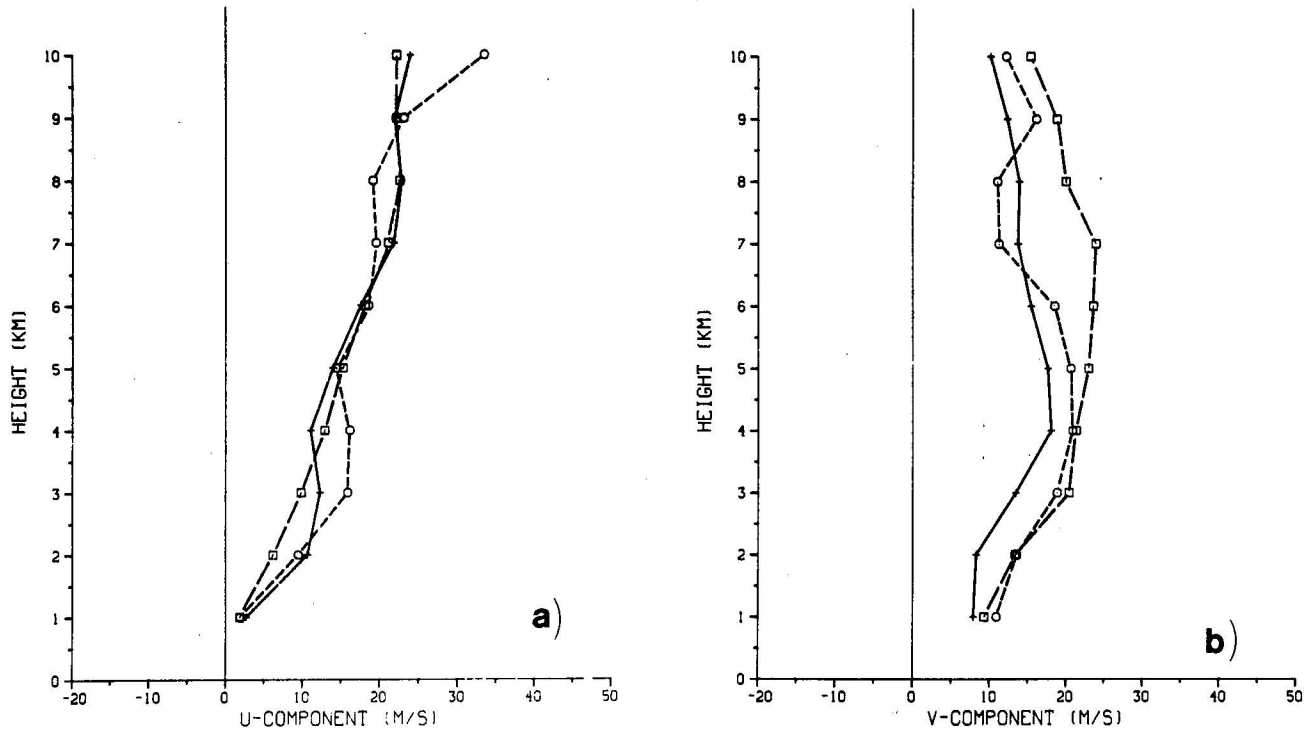


*Figure 3.13.--Profiles of (a) u-component and (b) v-component at 1503 CST. The solid line is from dual Doppler analysis at 1535 CST. The long dashed line is from single Doppler analysis and the short dashed line is from the 1516 CST rawinsonde.*

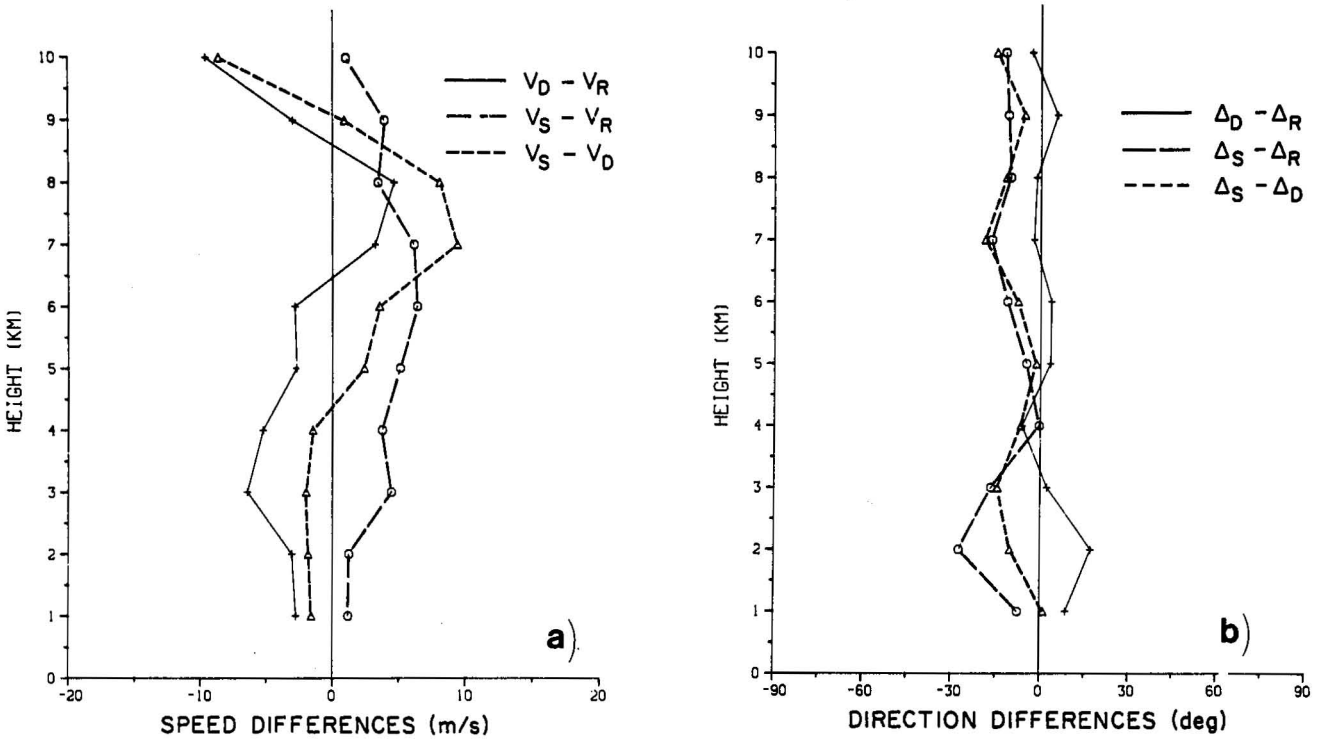


*Figure 3.14.--Differences between (a) wind magnitudes V and (b) wind directions Δ obtained from dual Doppler analysis (D), rawinsonde (R), and single Doppler analysis (S) at 1503 CST.*

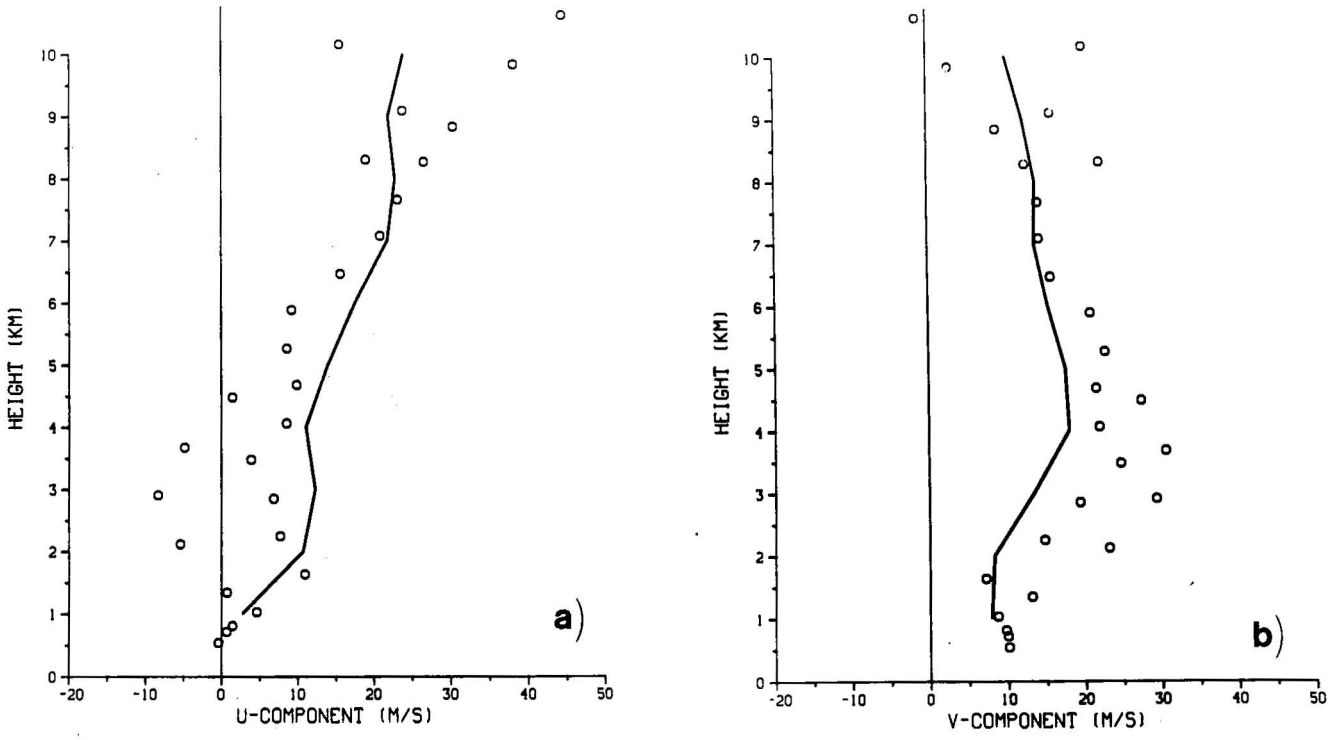


*Figure 3.15.--Estimates of (a) u-component and (b) v-component from single Doppler analysis (circles) at 1535 CST on May 17, 1981. The solid line is from dual Doppler analysis at the same time.*

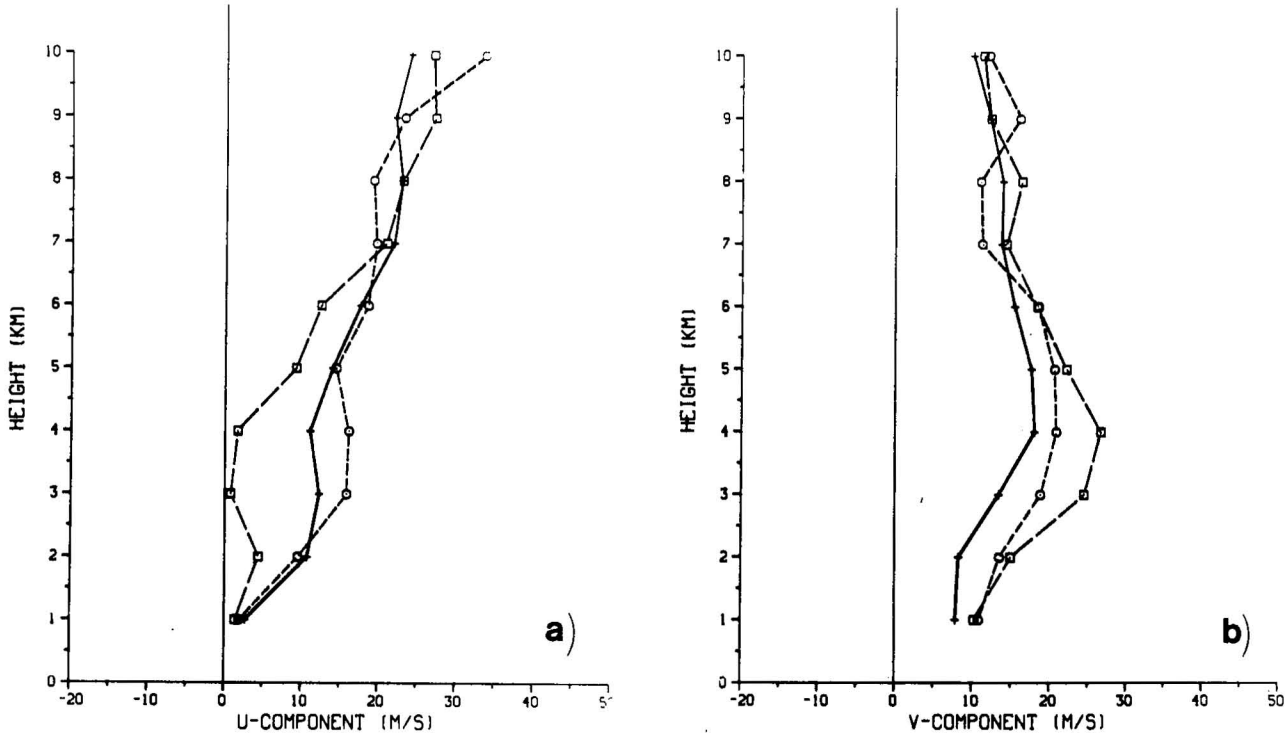


*Figure 3.16.--Profiles of (a) u-component and (b) v-component at 1535 CST. The solid line is from dual Doppler analysis, the long dashed line is from single Doppler analysis, and the short dashed line is from the 1516 CST TTS rawinsonde.*

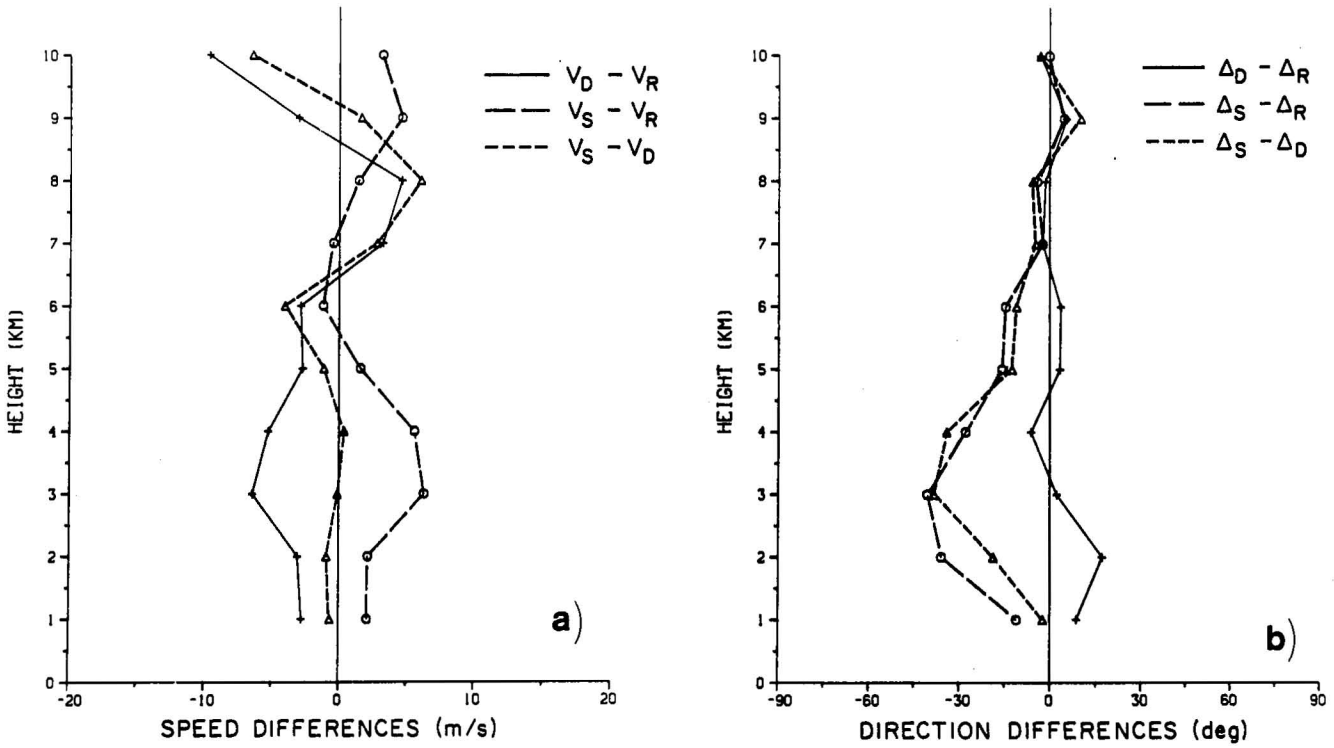


*Figure 3.17.--Differences between (a) wind magnitudes V and (b) wind directions Δ obtained from dual Doppler derived winds (D), single Doppler derived winds (S), and the 1516 CST TTS rawinsonde.*

were at approximately the same range from the Norman Doppler so that the data had been incorporated into the uniform wind algorithm without any modifications. This technique can also be applied when storms are at different ranges but then data from different elevations may have to be combined to assure that they are from approximately the same height. The results of this single Doppler analysis along with dual Doppler analysis and rawinsonde are shown in Figs. 3.12 through 3.14. The dual Doppler wind profiles are from 1535 CST and the rawinsonde data come from TTS at 1516 CST (TTS is Tuttle, Oklahoma, located approximately 30 km west of Norman).

By the second analysis time (1535 CST), the Tecumseh storm was large enough in azimuthal extent for a uniform wind analysis. These results are given in Figs. 3.15 through 3.17. The dual Doppler wind profiles and the rawinsonde data are the same as before since they were the only ones available.

## 3.3 Conclusions

We have shown that it is possible to profile the winds up to 10 km AGL with a single Doppler radar using storms as targets. To assess the accuracy of the uniform wind algorithm in profiling the winds, comparisons between profiles derived from single and dual Doppler analysis and rawinsonde were made. From these, questions concerning the representativeness of single Doppler winds to in-storm winds and in-storm winds to the environmental flow can be addressed.

As a general observation, profiles from all three techniques show a certain degree of similarity. Closer examination reveals differences in wind speed and direction between profiles generally less than 10 $ms^{-1}$ and 30° respectively. Such discrepancies are to be expected when one considers the inherent errors in each technique. For example, dual Doppler reconstructed winds suffer from the vertical smoothing that occurs when data are interpolated to constant height surfaces. Rawinsonde winds contain uncertainties resulting from elevation tracking errors. The expected wind vector errors in rawinsonde wind measurements are discussed by Ference (1951). More recent work by Hoehne (1980) found 3.1 $ms^{-1}$ to be the standard deviation of the difference between winds measured by tracking with independent systems two sondes suspended from the same balloons. Bias and variance errors for single Doppler wind estimates have already been discussed.

In deriving the wind profiles, not all the data were common to both single and dual Doppler analyses. For a good dual Doppler analysis, the two beams should intersect at angles between 60° and 120°. In our single Doppler analyses, we have not included data with reflectivities above 40 dBZ, in order to avoid contamination by hydrometeor fallspeeds and the perturbations expected near the storm core. Only when the in-storm winds are relatively unperturbed, as would occur in weak cells, we expect single Doppler estimates to agree with dual Doppler estimates.

Finally, important philosophical questions must be addressed: What is it that the measurements represent, and what is it that we would like them to represent? The second question is easily answered -- we know that practically every meteorologist has interest in the wind at various altitudes. A radar that can measure in clear air over large range intervals would then be the choice instrument. In environments perturbed by storms, we believe that either technique (radar versus rawinsonde) would be equivalent. As a matter of fact, the radar might have an advantage over a rawinsonde because it can obtain several profiles (in various directions and ranges where cells are located), each of which would be an average representation of winds in a given region. The rawinsonde winds are representative of conditions along the balloon path which may be considerably perturbed in the presence of cells.

# 4. ECHOES FROM CLEAR AIR

## 4.1 Reflectivity of the Planetary Boundary Layer (PBL)

Experience with 10 cm wavelength radars has shown that the mixed layer provides enough reflectivity that, even with modest performance, these radars can map velocities in the PBL. The exact nature of tracers is not always known but generally these are refractive index fluctuations, insects, and debris (airborne particulates). Our observations in Oklahoma during spring, summer, and autumn suggest that the boundary layer during daytime provides ample reflectivity to make meaningful measurements, often to more than 100 km in range. Sometimes the echoes extend to greater heights, and limited observations during storm days suggest that good measurements are possible in the evenings as well. These findings are summarized in Section 4.4. We briefly

examine the echoes in winter associated with arctic air masses since then the atmosphere is most stable and there are no flying insects. Under these conditions we expect the weakest echoes and thus the most demanding performance of the radar. We have made measurements on several days and discuss three of these.

There is no single theory to explain reflectivity at a 10 cm wavelength that we observe in the PBL. Rather, depending on the situation, it is possible to use appropriate models and obtain order-of-magnitude effects. When scattering is from layers, the theory in Appendix D can be used. It requires measurement of thermodynamic variables: potential temperature through the layer, pressure, and mixing ratio. If on the other hand scattering occurs throughout the depth of the mixed layer, then the reflectivity can be estimated from heat and moisture fluxes (Rabin, 1983). It requires measurements or estimates of fluxes at the earth's surface. Direct measurements of fluxes have limited accuracy and can suffer from horizontal variability. In either case there may be insects or other point targets that may make measurement interpretation more difficult.

## 4.2 Case Studies - Examples of Weak Reflection in January

We have examined Doppler spectra from very cold days in January because then the atmosphere is stable; hence the reflectivity from refractive index fluctuations is lowest. Also, after cold front passage, there are no insects to contaminate the measurements (of course, debris could be present). We present results of measurements on three cold days of January 1985.

### 4.2.1 January 16, 1985

Several spectra were collected on this day in order to test wind mapping in clear air and nonprecipitating clouds. A cool front passed over the radar site before noon. The temperature at the surface was 4°C at 0600 CST; it dropped to 2°C at 0900 CST after frontal passage, then warmed to 7°C at 1500 CST, and fell back to 4°C at 1800 CST. The rawinsonde wind soundings from 0600 and 1800 CST (Fig. 4.1) indicate strong shear between the surface and 600 m and considerable variability in the first kilometer both before and after the front's passage. Hence, extrapolation of wind data from near the ground (<600 m) to higher altitudes would be difficult.

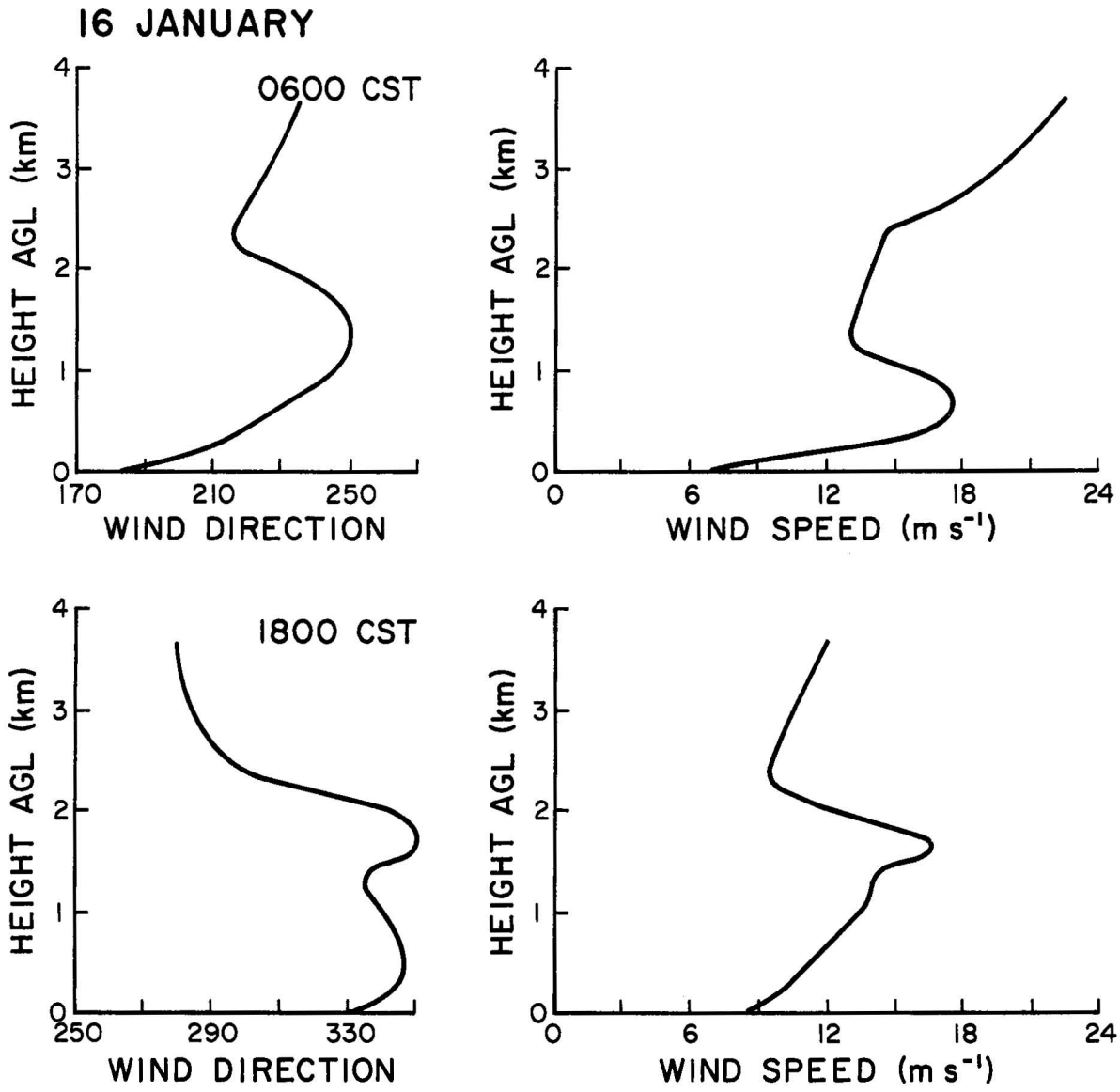


*Figure 4.1.--Wind speed and direction from two soundings on January 16, 1985.*

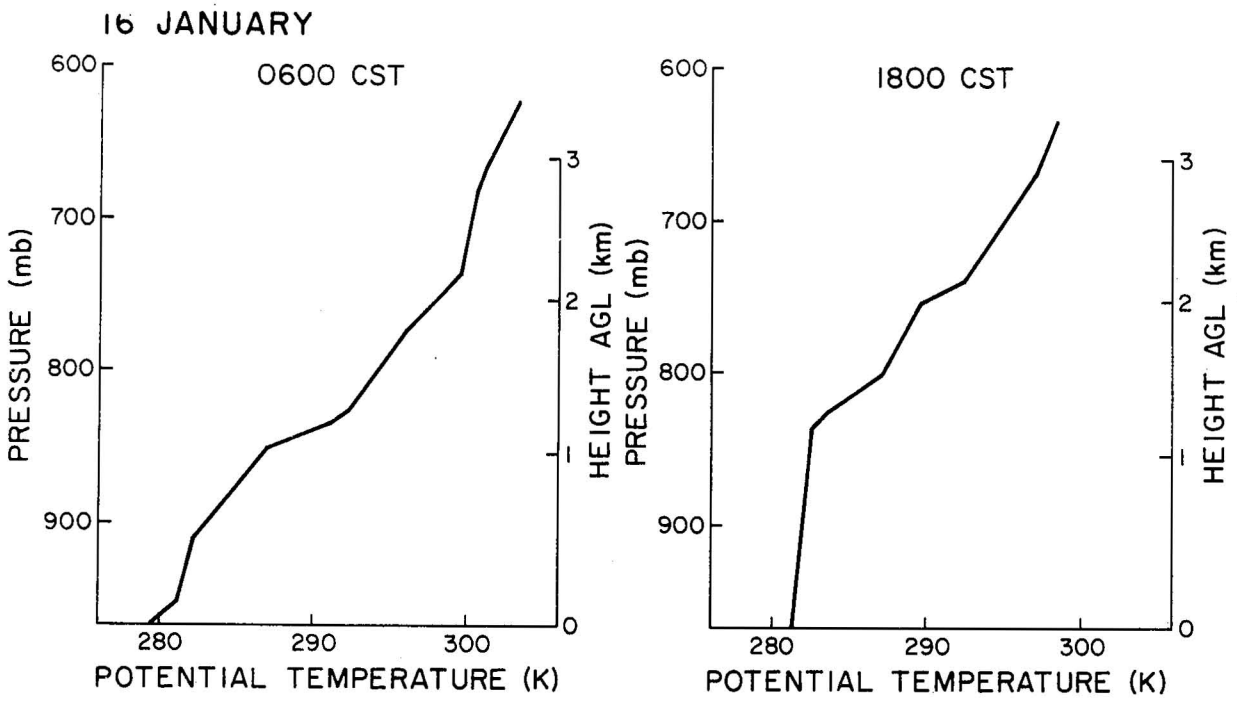


*Figure 4.2.--Potential temperature from two soundings on January 16, 1985.*

The potential temperature profile at 0600 CST (Fig. 4.2) suggests the possibility that the surface layer and a layer at about 1 km could have enhanced mixing and therefore increased reflectivity. A later sounding at 1800 CST shows that the height of the mixed layer has grown to 1.2 km. Sixteen spectra from consecutive range locations are shown on Figs. 4.3 - 4.6. A cold front was moving through the data collection area north of Oklahoma City at the time the spectra in Fig. 4.3 were collected. Thus, spectra from the first three range locations were produced by the southerly winds. The spectral widths, $\sigma_v$, range from 1 to 2 $ms^{-1}$ and the effective reflectivity factor, $Z_e$, from -17 to -14 dBZ (see Appendix E for details of the calculations). The bimodal spectra from the fourth to ninth range locations are produced by the cold front air that is moving toward the radar and by the relatively warm environmental air overriding the front as illustrated in Fig. 4.7. The strong spectra have widths of about 2 $ms^{-1}$ and reflectivities of 0 dBZ. Spectra from the environmental flow (Fig. 4.4) are enhanced in a layer between 300 and 500 m, spectral widths are about 1.5 $ms^{-1}$, and reflec-

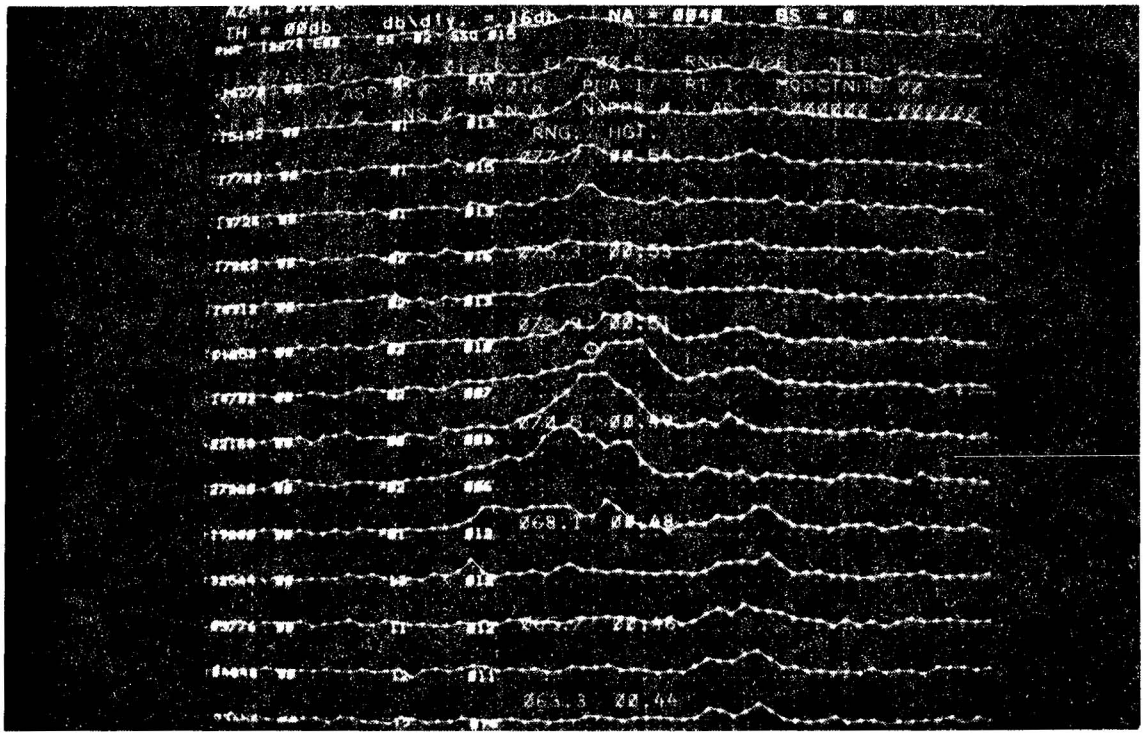

*Figure 4.3.--Sixteen consecutive spectra collected at 0930 CST on January 16, 1985. The distance to the first range gate is 63.3 km as indicated on the display, and the gates are 1.2 km apart. Heights of beam center above ground (km) are also indicated next to the ranges. Spectra are in logarithmic units with 16 dB/div. The velocity scale is from -34 to 34 $ms^{-1}$, and there are 64 spectral coefficients spaced about 1 $ms^{-1}$ apart. Forty spectra were averaged in order to obtain these plots. Azimuth is 12.6° and elevation is 0.4°.*

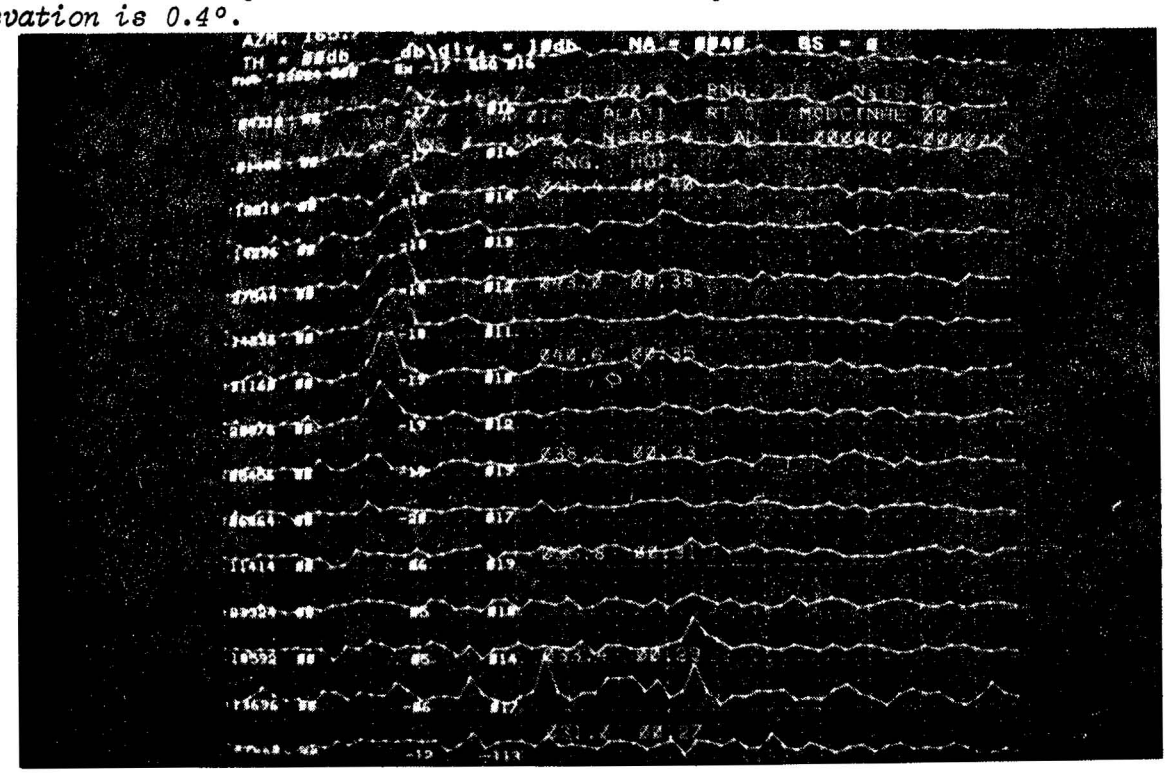

*Figure 4.4.--Consecutive spectra collected at 0935 CST (see Fig. 4.3). The azimuth is 165.7°, the vertical scale is 10 dB/div, and distance to first range gate is 31 km.*

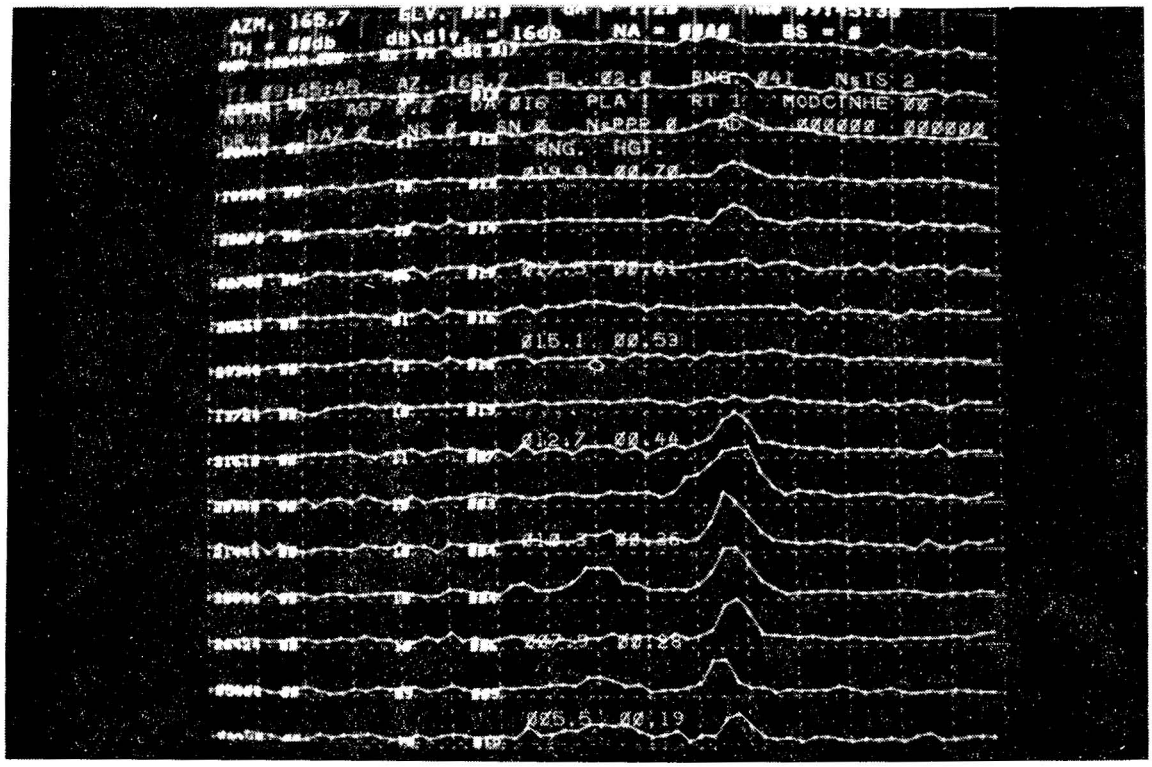


*Figure 4.5.--Consecutive spectra collected at 0945 CST (see Fig. 4.3). The azimuth is 165.7°, elevation is 2°, and distance to first range gate is 5.5 km.*

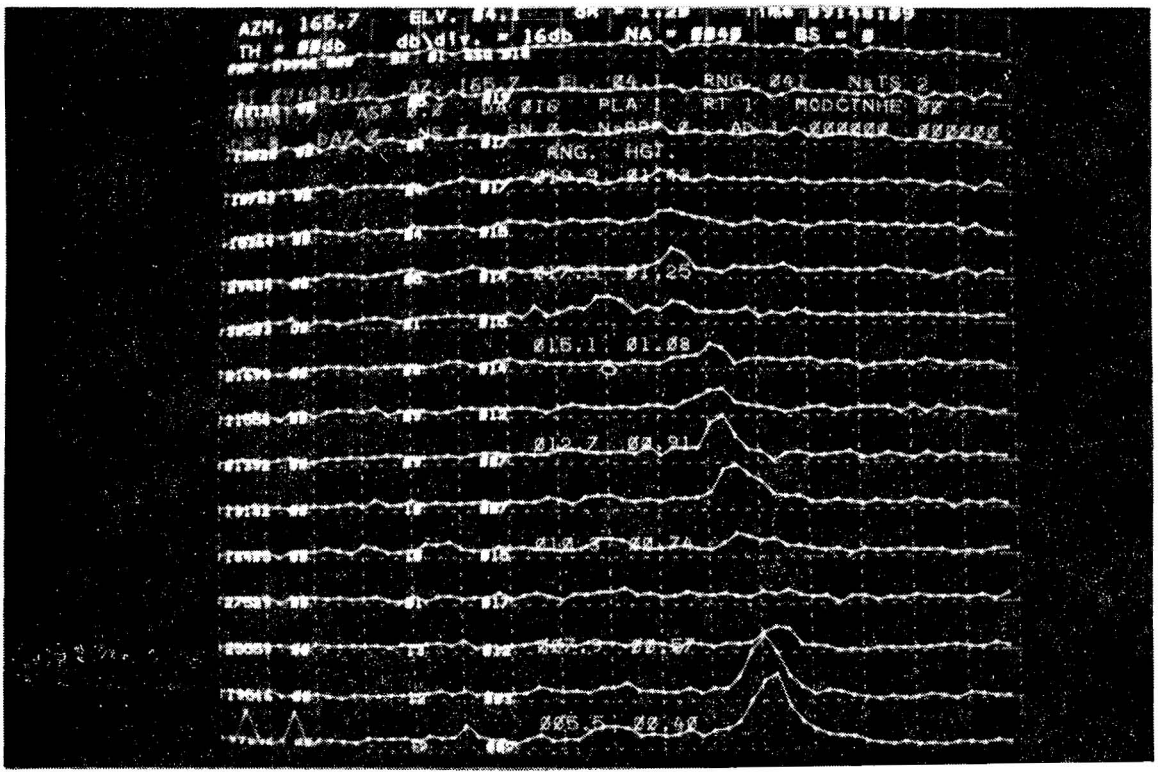


*Figure 4.6.--Consecutive spectra collected at 0948 CST. Azimuth and distance to first range gate are as in Fig. 4.5. Elevation is 4.1°.*

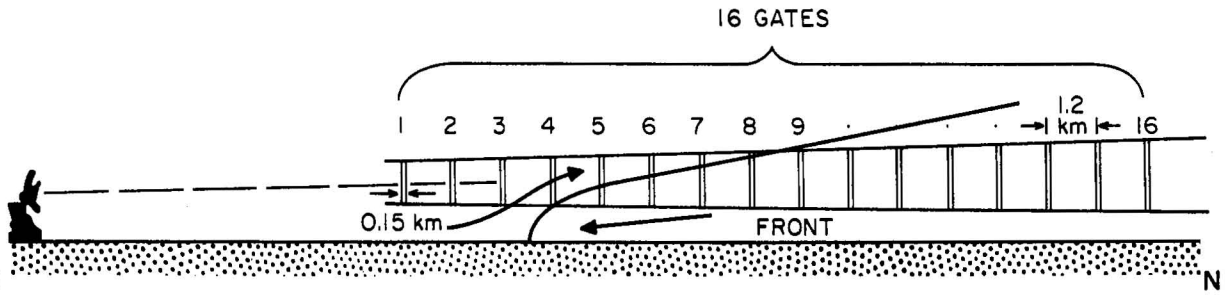


*Figure 4.7.--Measurement geometry. Sixteen range gates are positioned so that several of them sample both the front and the environmental air motion.*

tivity is -14 dBZ. At this range (30-40 km) the signal below the layer is weak and not readily apparent. However, closer to the radar (5-12 km in Fig. 4.5), we see that all the mixed layer contributes to the reflections and furthermore, that there are weak echoes between 700 m and 1.25 km (Fig. 4.6). We do not know if these are from elevated layers or clouds. We estimate the spectral widths to be about 0.7 m $s^{-1}$ (Fig. 4.5, 4.6) and the reflectivities vary from -23 to -28 dBZ. The strongest reflectivity (0 dBZ) occurs at the frontal interface. It could also be influenced by particles made airborne by the wind. We compute the $C_n^2$ for the more typical values of reflectivities (-14 to -28 dBZ). From (E.7) we find $C_n^2$ between $10^{-13.2}$ and $10^{-14.6}$ $m^{-2/3}$. We have more confidence in the lower values that we observed ($-28 < Z_e < -23$) because these were measured nearer the radar (5 to 15 km) where the resolution volumes are much smaller and therefore more likely to be uniformly filled with irregularities. Therefore more representative values for $C_n^2$ range from $10^{-14.1}$ to $10^{-14.6}$ $m^{-2/3}$. This range of values corresponds to the lower end of $C_n^2$ observed by Gossard (1977) in maritime air.

Because the soundings are not representative of the conditions in the boundary layer that existed during radar operations, we cannot obtain theoretical values for the reflectivity nor the structure constant.

4.2.2 January 18, 1985

This was also a cool day after the passage of a cold front. Winds at the surface were northerly (Fig. 4.8) and the potential temperature profile suggests a strong but shallow surface inversion layer at 0600 CST which is completely mixed out at 1800 CST (Fig. 4.9). Clouds were present over most of Oklahoma during our measurements (Fig. 4.10). The spectra (collected between 1200 and 1300 CST) suggest that the surface layer was about 200 m deep (Fig. 4.11a) and that there was another region of enhanced reflectivity extending from 400 m to about 1.2 km (Fig. 4.11b). Measured values of $C_n^2$ and reflectivity factor for these two layers are:

Lower layer $Z_e$ = -8.5 to -11 dBZ, $C_n^2 = 10^{-12.6}$ to $10^{-12.9}$ $m^{-2/3}$
Upper layer $Z_e$ = -12.5 dBZ, $C_n^2 = 10^{-13}$ $m^{-2/3}$.

Because it was cloudy we expect that the strong inversion near ground did not erode very much by 1200 CST when the measurements were made. Therefore the reflectivity of the lower layer is strong and compares poorly with the theoretical value of -17 dBZ ($C_n^2$ of $10^{-13.5}$ $m^{-2/3}$) based on the 0600 CST sounding (Fig. 4.9). The higher measured values can be explained by the uncertainty in the gradients of potential temperature, which must have been weaker at 1200 CST. For example, if we have a gradient that is one-half the value at 0600 CST we get a $Z_e$ = -10 dBZ. We do not have the potential temperature profile of the higher layer and hence cannot compute its reflectivity.

We also used this opportunity to estimate the cloud thickness. For that purpose a signal was transmitted through a shrouded, vertically pointing antenna. Spectra at two different times present definite evidence of a cloud layer (Fig. 4.12a and 4.12b).

At 0905 CST the layer extends between 4 and 5.5 km; surface observation from Oklahoma City put the cloud base height at 4 km. At 1200 CST the surface observation estimates the cloud base to be at 2.6 km, and we see in Fig. 4.12b that the radar estimated base is at 2.2 km. So on days like this, spatially continuous profiles of velocities could be obtained from the surface to about 6 km.

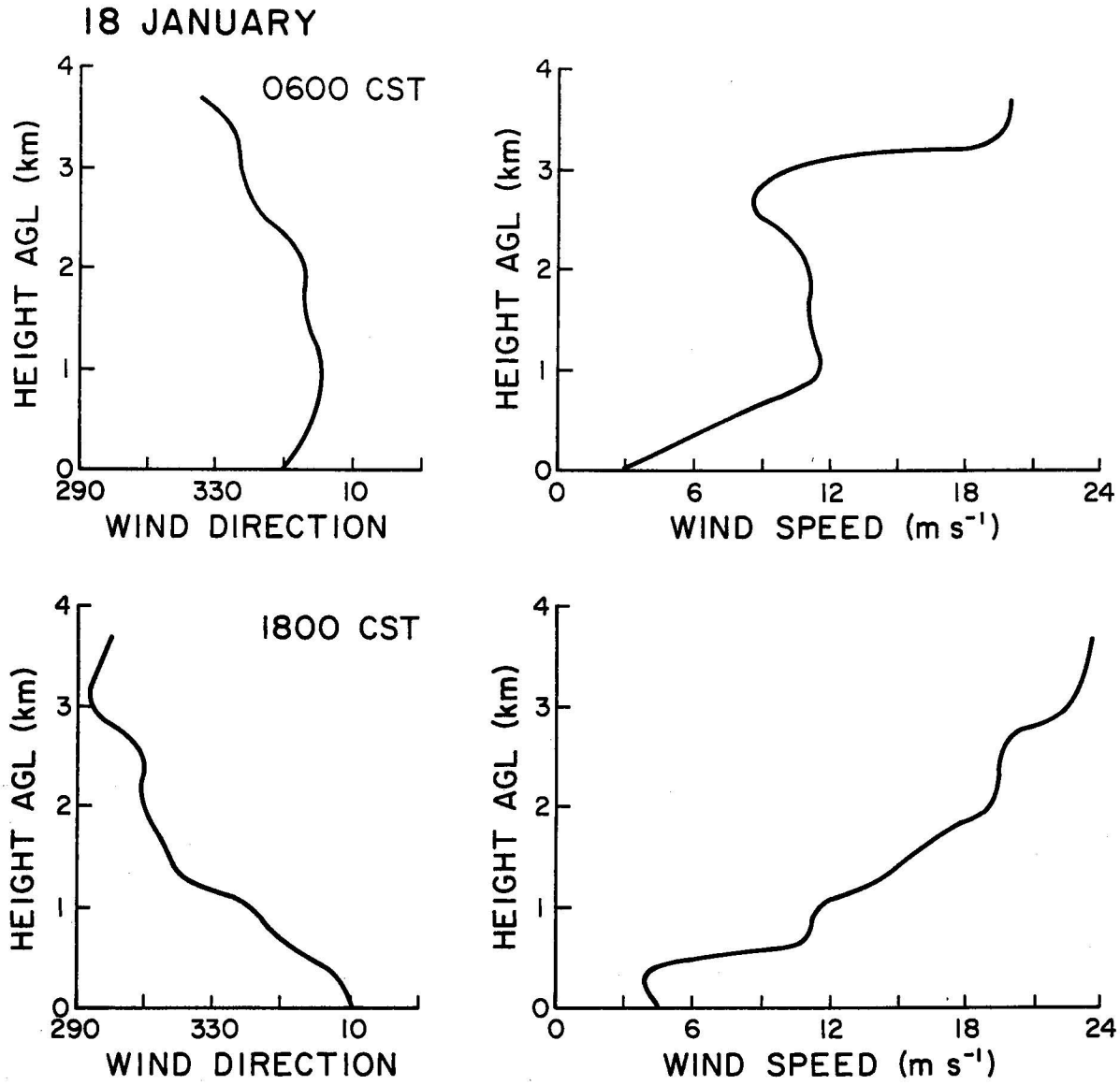


*Figure 4.8.--Wind speed and direction from two soundings on January 18, 1985.*

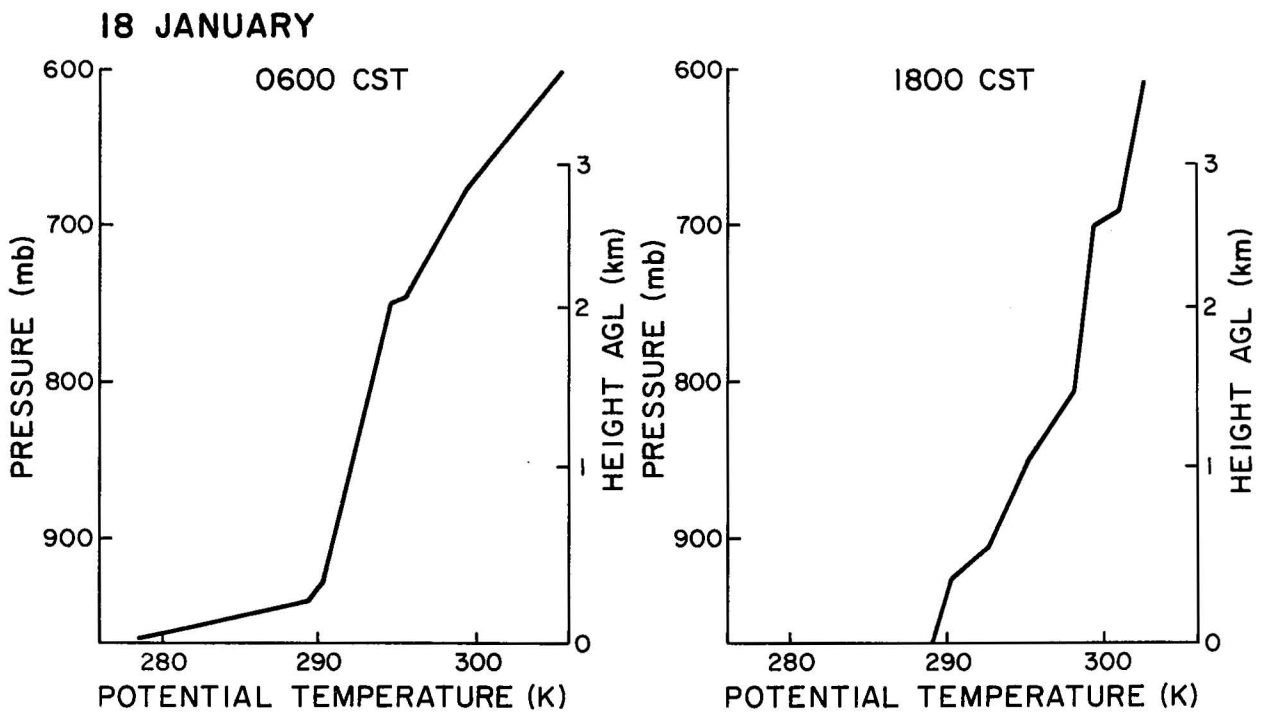


*Figure 4.9.--Potential temperature from two soundings on January 18, 1985.*

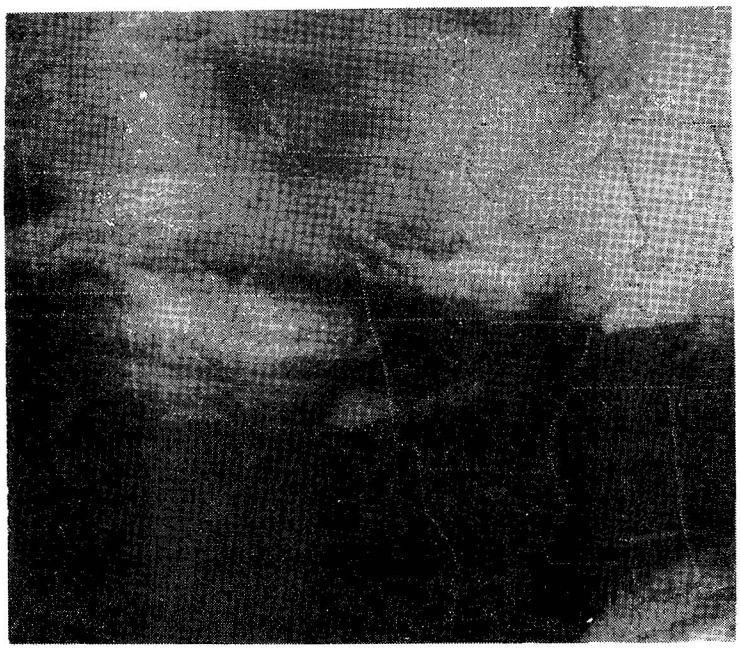

*Figure 4.10.--Satellite picture of Oklahoma, January 18, 1985, at 1030 CST.*

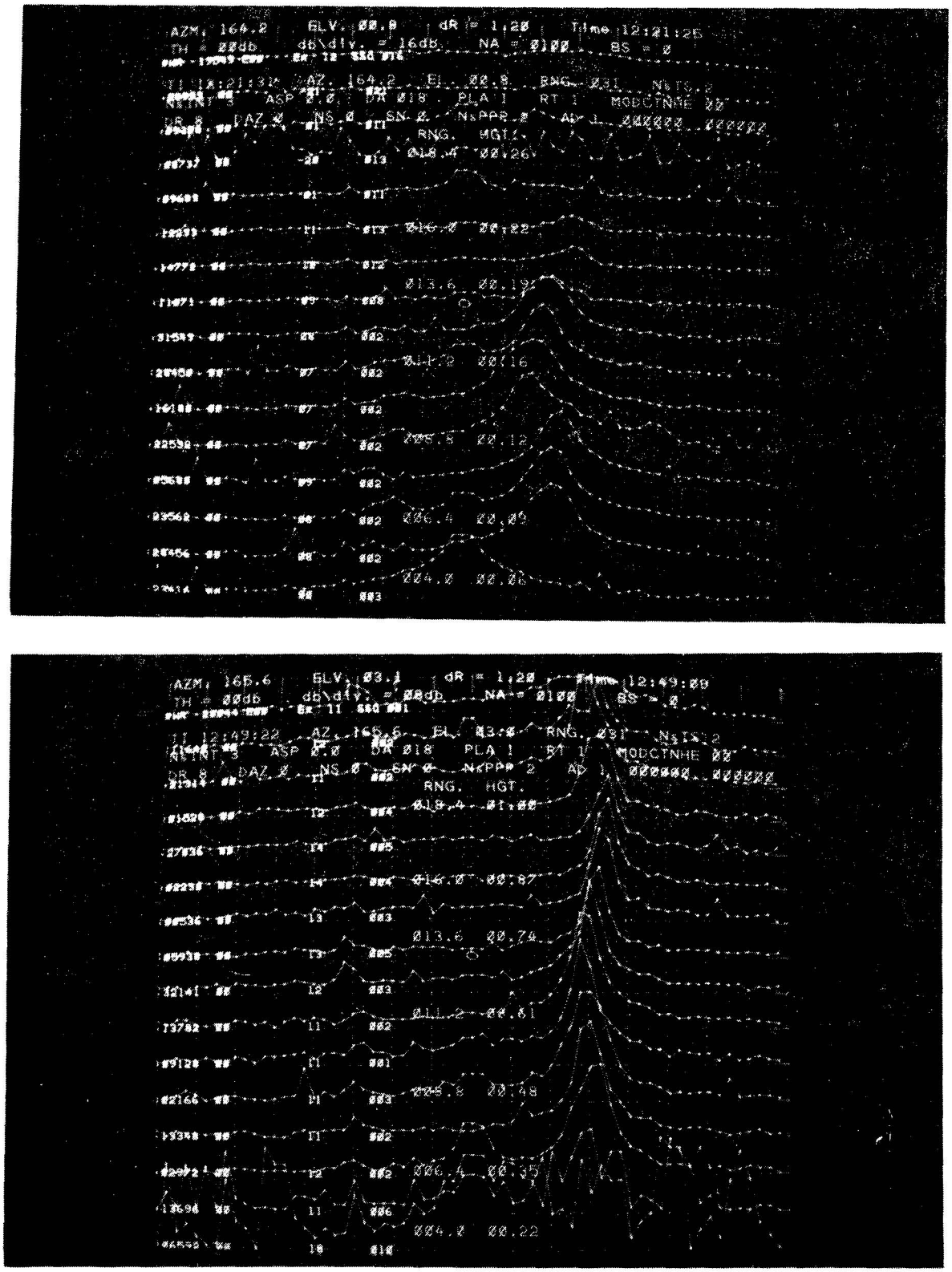

*Figure 4.11.--Sixteen consecutive spectra collected at 1221 CST on January 18, 1985. The range to the first gate is 4 km and the gates are spaced 1.2 km apart. (a) Vertical scale is 16 dB/ div; one hundred spectra were averaged in order to obtain plots on this figure. Azimuth is 164.2° and elevation is 0.8°. (b) Vertical scale is 8 dB/div; azimuth=165.6° and elevation = 3.1°.*

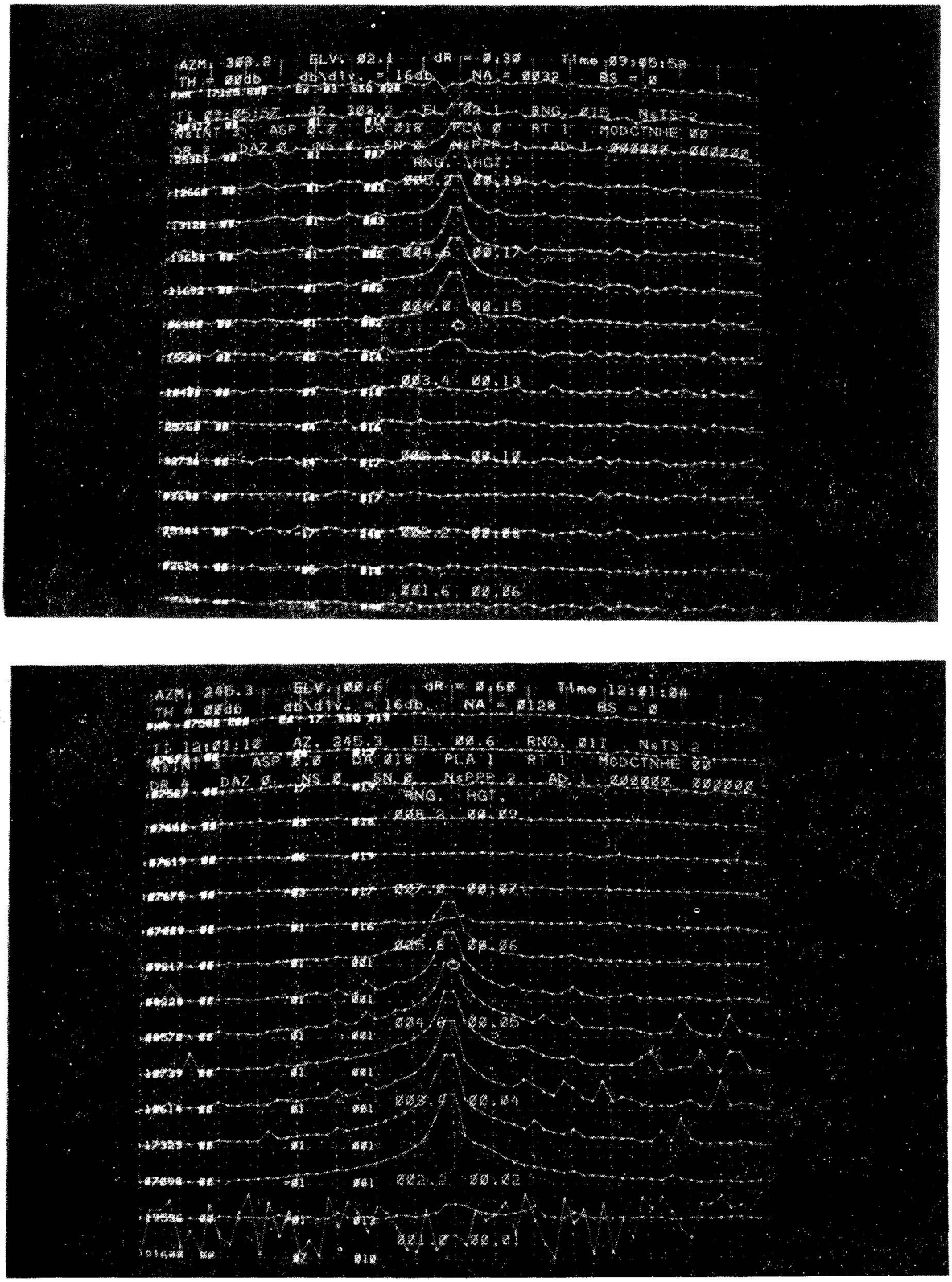


*Figure 4.12.--Doppler spectra at vertical incidence. (a) Time is 0906 CST and range gates are spaced 300 m apart. The spectral coefficient at zero Doppler velocity has been replaced with the adjacent left value. Thirty two spectra were averaged and the vertical scale is 16 dB/div. (b) Time is 1201 CST, 128 spectra were averaged, and gate spacing is 600 m.*

4.2.3 January 21, 1985

On this day temperatures were -10°C at the surface, and winds were from the northwest; there were high cirrus clouds over part of Oklahoma (Fig. 4.13), but these did not produce measurable echoes. Height profiles of windspeed and direction from the morning (0600 CST) sounding show considerable shear in the low levels, indicating again that radar measurements from near the ground would not extrapolate correctly to higher altitudes. Note that an abrupt change in speed occurs 1 km above ground, which is slightly above the height where radar measurements were possible on this day (Fig. 4.14).

Doppler spectra collected at 1200 CST (Fig. 4.15) show an enhanced layer between 500 and 800 m. Because the antenna was pointing in the downwind direction, we can compare the windspeeds with rawinsonde observations. Radar winds varied from about 4 $ms^{-1}$ to 7 $ms^{-1}$. These values are about 4 $ms^{-1}$ lower than the rawinsonde observations at 0600 CST and are equal to or greater than the observations at 1800 CST. But if we average the two rawinsonde observations we obtain a very good comparison with the radar measured winds. The reflectivity factor and $C_n^2$ in the middle of this layer are estimated to be $Z_e$ = -25.6 dBZ and $C_n^2 = 10^{-14.4}\ m^{-2/3}$, which are comparable with the lower

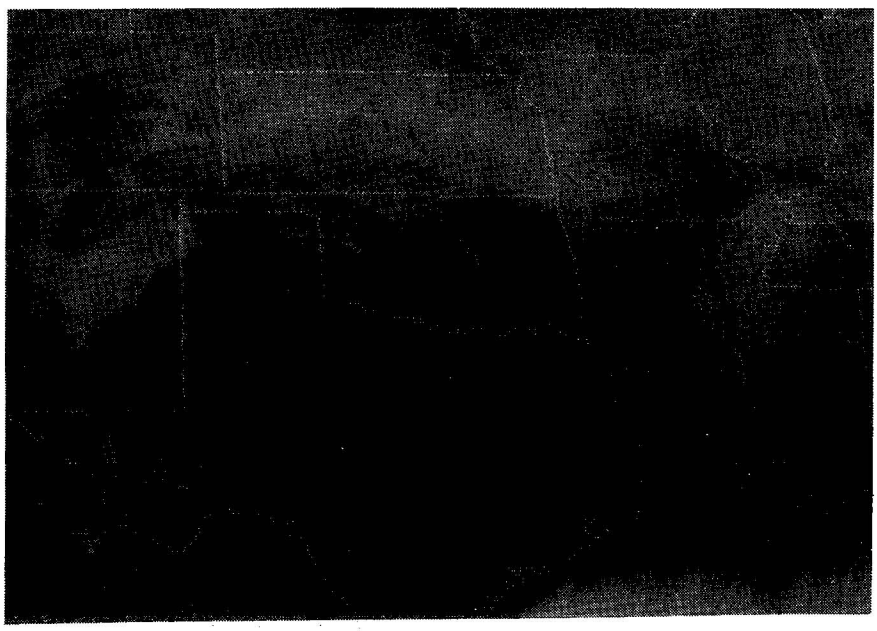

*Figure 4.13.--Visible satellite picture at 0930 CST on January 21, 1985.*

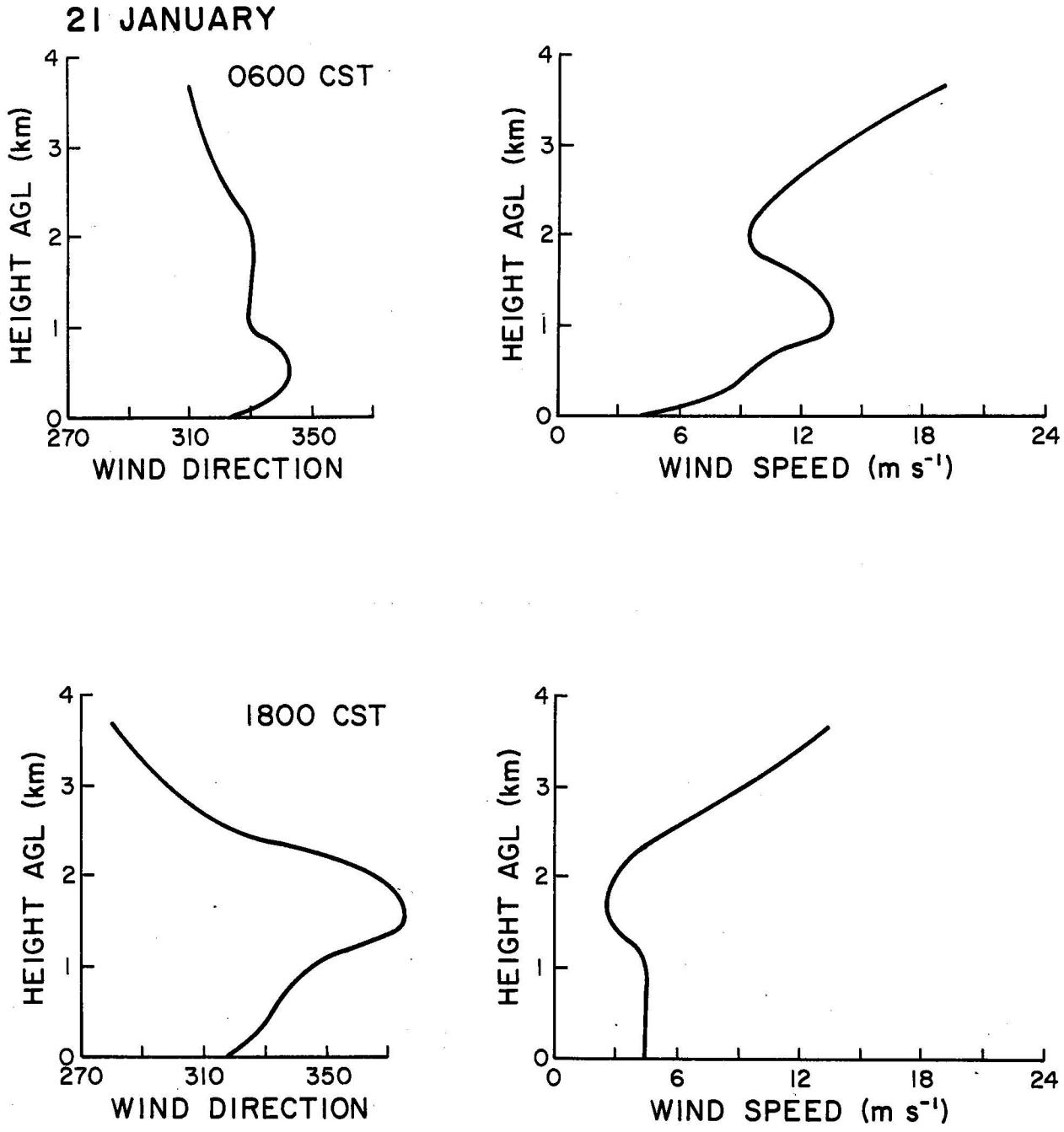


*Figure 4.14.--Wind speed and direction at 0600 CST and 1800 CST on January 21, 1985.*

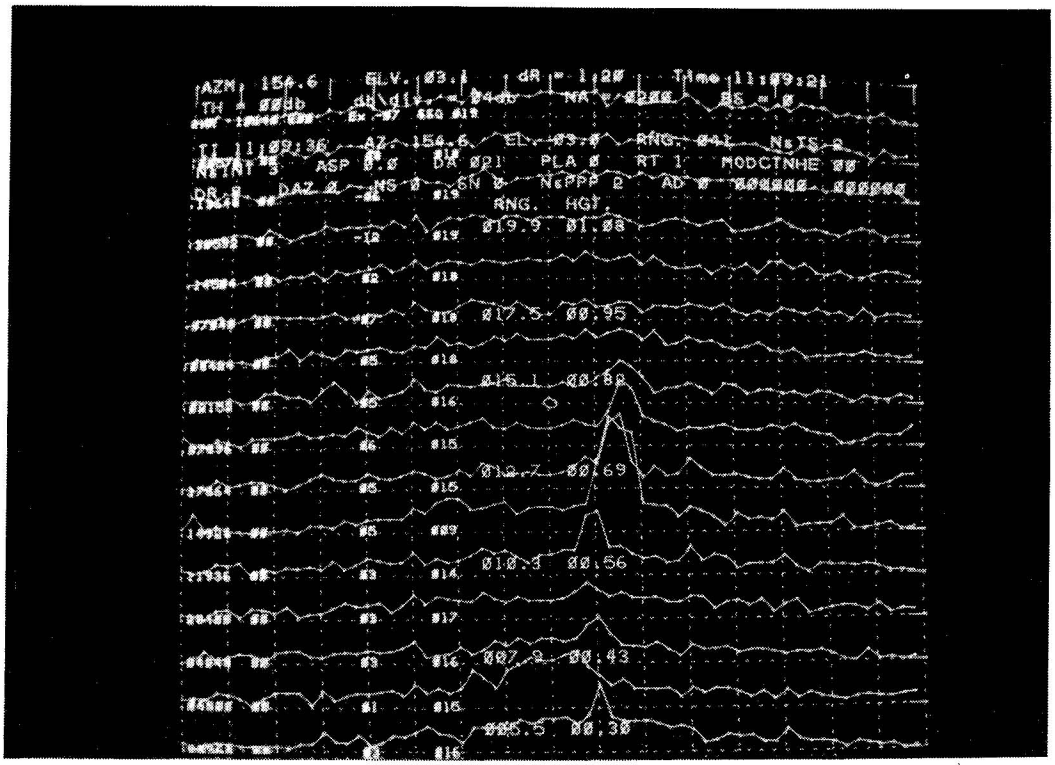


*Figure 4.15.--Doppler spectra on January 21, 1985. Number of averaged spectra is 200, elevation angle is 3.1°, azimuth is 154.6°, and the scale is 4 dB/div. The time is 1109 CST.*

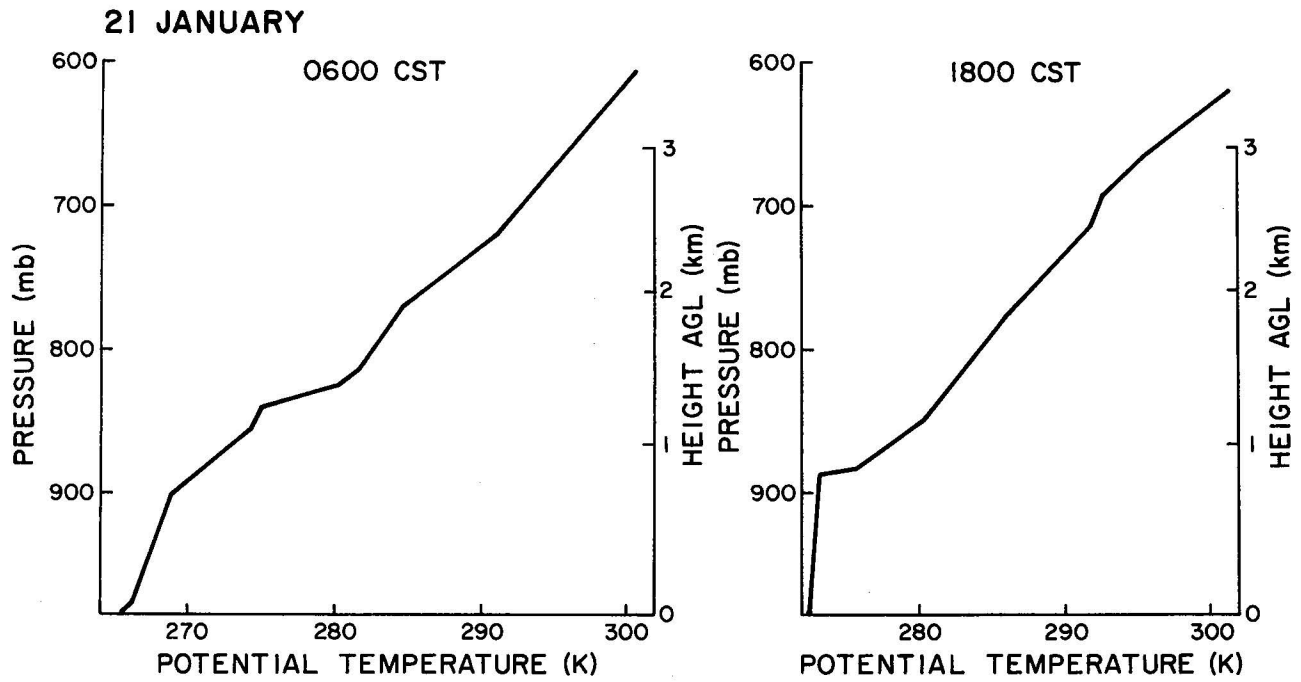


*Figure 4.16.--Potential temperature profiles at 0600 and 1800 CST on January 21, 1985.*

values seen on January 16th. With time, the height of enhanced reflectivity grew to about 1 km but the values of $Z_e$ and $C_n^2$ did not change appreciably. Plots of potential temperature (Fig. 4.16) show that the inversion was very weak at 0600 CST near the ground and that the mixed layer extended to about 0.8 km by 1800 CST.

Results of the measurements for the three winter days are summarized in Table 4.1. Reflectivities in clear air were less than -10 dBZ and were produced by turbulent mixing of refractive index gradients. These were confined to a few relatively thin layers, one of which was from the ground to a few hundred meters. The higher layer had a weaker reflectivity (less than -20 dBZ) and extended from about 0.5 km to an upper height that grew with time to about 1.2 km. Spectral widths in all cases were between 0.6 and 1.3 $ms^{-1}$.

Table 4.1.--Measured Reflectivity Factor of Clear Air

| Date | Time | Range (km) | Height (km) | Reflectivity factor (dBZ) | Structure constant ($m^{-2/3}$) | Comments |
|---|---|---|---|---|---|---|
| Jan. 16 | 0900-1000 CST | 6 | <0.6 | -28 | $10^{-14.6}$ | Two layers |
| | | 10 | 0.7-1.2 | -23 | $10^{-14.1}$ | Ahead of cold front |
| | | 40 | 0.3-0.5 | -14 | $10^{-13.2}$ | Behind the cold front |
| Jan. 18 | 1200-1300 CST | 8 | <0.2 | -10 | $10^{-12.8}$ | Strong inversion |
| | | 10 | 0.4-1.2 | -12.5 | $10^{-13}$ | Cloudy; clouds had measurable Z |
| Jan. 21 | 1100 CST | 11 | 0.5-0.8 | -25.6 | $10^{-14.3}$ | Cloudy but no measureable Z from clouds |

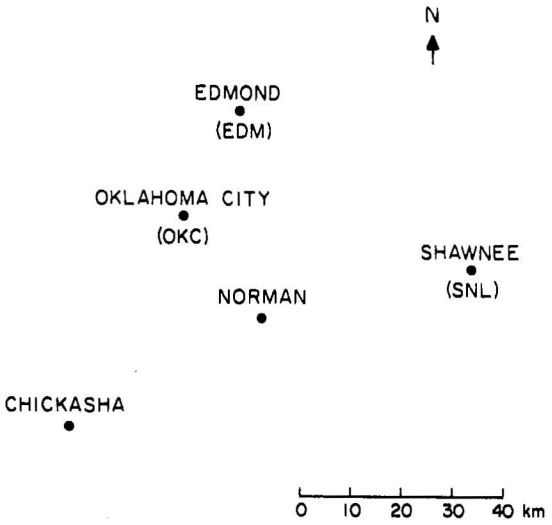


*Figure 4.17.--Relative position of instruments used to observe the quiescent atmosphere on May 27, 1983.*

## 4.3 Example of Strong Reflections on May 27, 1983

We have conducted an experiment for the purpose of relating the radar reflectivity factor Z to the integrated water vapor content as measured by a ground-based radiometer. Results of this experiment that are pertinent to measurement of velocities in clear air are presented in this section. So far we have analyzed only one day of data. Besides the radar and radiometer there was a lidar at Chickasha (40 km SW of Norman) operated by the University of Wisconsin, and a set of rawinsonde measurements. The relative positions of these instruments with respect to the Norman Doppler radar are shown in Fig. 4.17.

Doppler radar data collection began at 0800 in the morning, local standard time (LST), and volume scans (PPI) were collected every 30 minutes thereafter until 1600 LST. Radar parameters during this data collection are listed in Table 4.2

We have calculated the equivalent reflectivity factor from histograms of the reflectivities in an annulus between 40 km and 50 km from the radar. First a modal value of the histogram was found, then three digital categories on either side of the peak were used for a weighted average (first moment) calculation. This allowed us to edit some data automatically and also to obtain a considerably better resolution than the 1 dB width of our digital categories for reflectivity.

Table 4.2.--Radar Parameters on May 27, 1983

| | |
|---|---|
| Peak power | 600 kW |
| Pulse repetition time | 2.3 ms |
| Pulse length | 1 μs |
| Beamwidth (one-way 3 dB) | 0.8° |
| Number of samples for velocity (pulse pair) estimation | 64 |
| Equivalent number of samples for reflectivity estimation | 64 |
| Antenna rotation rate | 6° $s^{-1}$ |

Vertical profiles of reflectivities obtained in this manner are shown in Figs. 4.18a and 4.18b. Note that the lowest observation height is about 400 m because the lowest elevation angle was 0.4° and the average distance to the resolution volumes was 45 km. A 4/3 earth radius model for bending of rays in a stratified atmosphere was used in our calculations. The reflectivity values and the height profiles typify non-stormy spring days in Oklahoma. The gradual increase of reflectivities at all heights until about 1130 LST is most likely caused by the rise of the mixed layer under the influence of solar heating. From 1130 until about 1500 the profile develops a peak in reflectivity that is slightly below the top of the mixed layer. The growth of the mixed layer is witnessed from the rawinsonde data (Fig. 4.19a). At 0600 the layer top deduced from the potential temperature is at about 300 m, and by 0900 it reaches 600 m. The mixing ratio profiles for this day show a definite increase after 1430 LST and there is a steady increase in total precipitable water measured by the microwave radiometer (Fig. 4.20). This may be partly responsible for the increase in reflectivity, which at 10 cm wavelengths is influenced both by temperature and humidity irregularities. The lidar-determined heights of the mixed layer (Fig. 4.21) are consistent with the rawinsondes, and show that the thickness of the entrainment zone was about 200 to 400 m. The location of the peak reflectivity coincides with the bottom of the entrainment zone in Fig. 4.21. We propose that this increase in

reflectivity is caused by the temperature fluxes that tend, later in the day, to build maximum value away from the earth's surface.

However, it is instructive to compare the measured reflectivity with theoretical values. First we use the theory based on temperature and moisture flux values (Rabin 1983) and later a theory based on turbulent mixing of shear layers (Appendix D). Comparison with thermal flux theory is seen in Fig. 4.22 for a ratio of sensible heat flux (H) to surface evaporation (E) (i.e., Bowen ratio) of $\beta = 0.002$. The theoretical curve of reflectivity versus incoming solar radiation (S) in Fig. 4.22 does not change for small Bowen ratios ($\beta < 0.02$). For larger Bowen ratios the curve shifts toward lower reflectivities. The theoretical value of reflectivity shown in the figure is an upper limit because we have assumed that all incoming solar radiation is transformed into fluxes (i.e., $S = H + E$), mostly moisture flux. Thus, reflection and long wave radiative loss from the earth's surface are neglected, as well as heat diffusion into the earth. The general trend of the measured reflectivity at 500 m agrees well with the theoretical model. This reinforces our belief that the mixed layer driven by solar fluxes is mainly responsible for the reflectivity through fluctuations of the refractive index. This finding does not exclude contribution from insects, which may also be distributed throughout the mixed layer. Reflectivity change at two heights in Fig. 4.23 definitely demonstrates the connection with solar radiation. As expected, the maximum at a height of 1 km lags (by about 2 hours) the maximum at 0.5 km.

Calculated values of $C_n^2$ and reflectivity from the theory of turbulent breakdown of shear layers (see Appendix D for calculation details) are listed in Table 4.3 for three different times and four discernible layers.

A quick comparison with measured values in Fig. 4.18a reveals that the computed effective reflectivity factors from strong layers are generally higher. However, the spread of $C_n^2$ values is just too large for a definite conclusion. Because the mixing ratio profile (Figure 4.19b) is very noisy we have also used the average gradient of the mixing ratio (2 g $kg^{-1}$ $km^{-1}$) over the 1 km depth to compute the $C_n^2$. Using this smaller value of the mixing ratio gradient means that most of the contribution to $C_n^2$ comes from the potential temperature gradient. We see that the agreement is better and that the theoretical values of the reflectivity factor are about 2-3 dB lower than

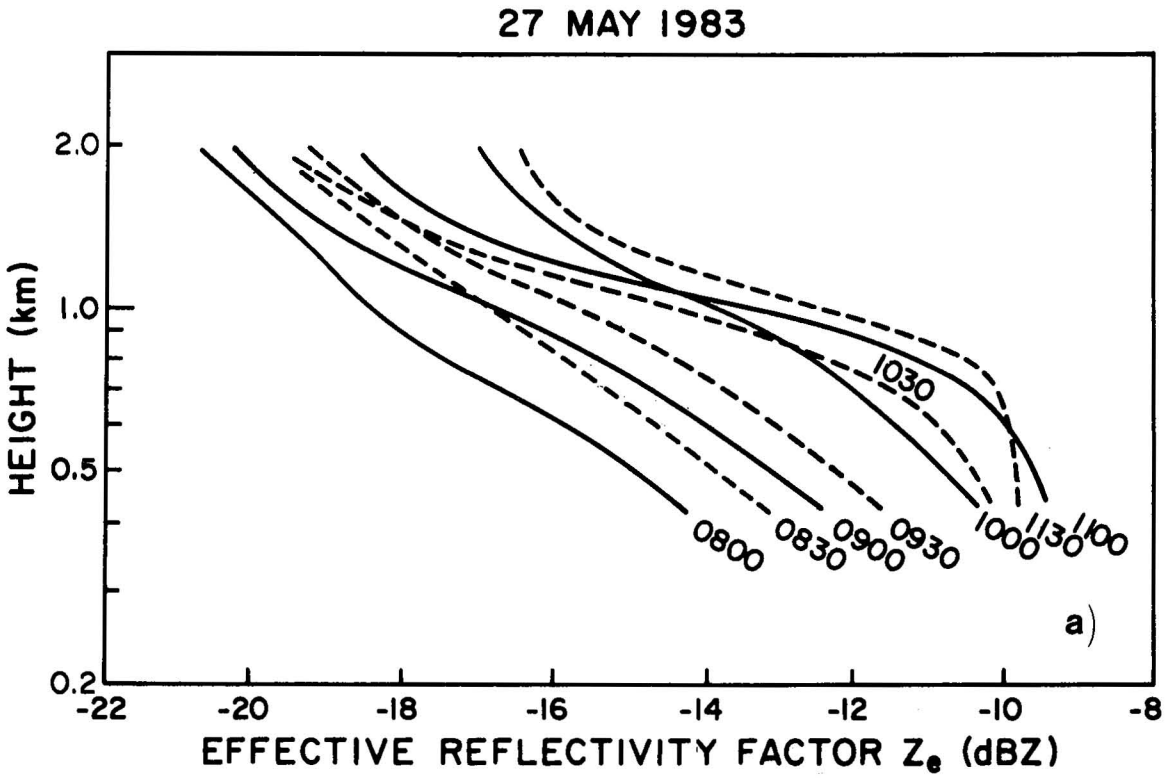


*Figure 4.18.--Height profiles of reflectivity factor (dBZ) on 27 May 1983, taken (a) every 30 min between 0800 and 1130 LST, and (b) from 1130 until 1600 LST.*

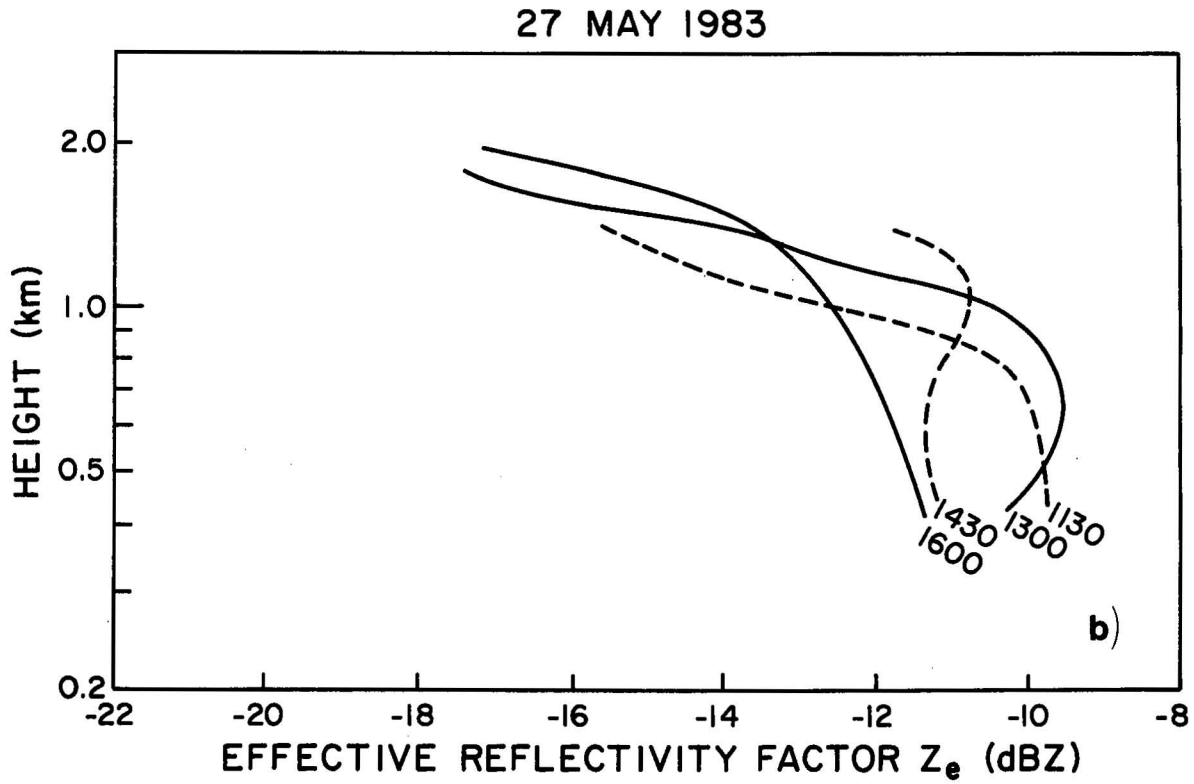

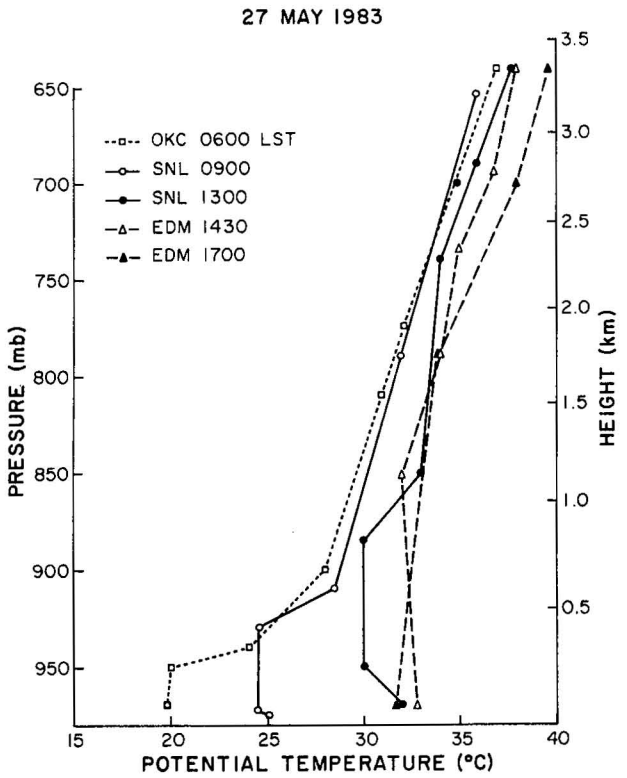


*Figure 4.19a.--Potential temperature versus pressure (height), from three stations at five different times.*

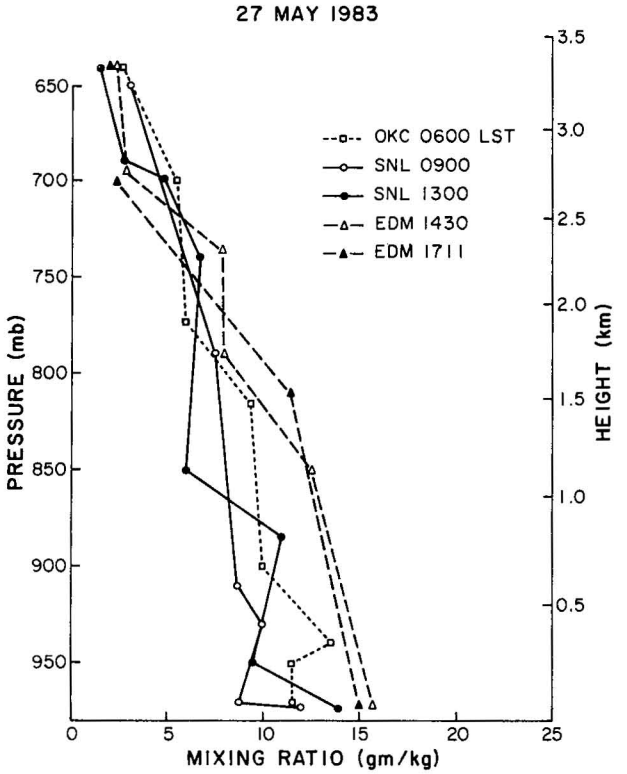


*Figure 4.19b.--Mixing ratio versus pressure (height).*

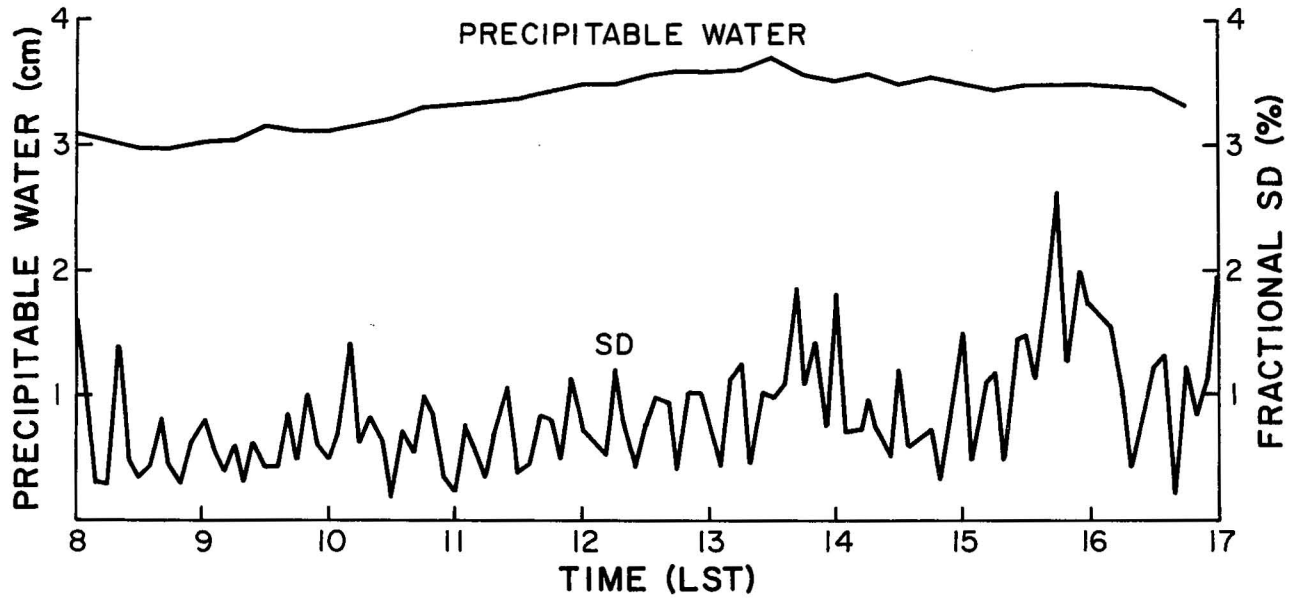


*Figure 4.20.--Precipitable water and its standard deviation on May 27, 1983. Data were obtained from 5-min. averages of a radiometer output.*

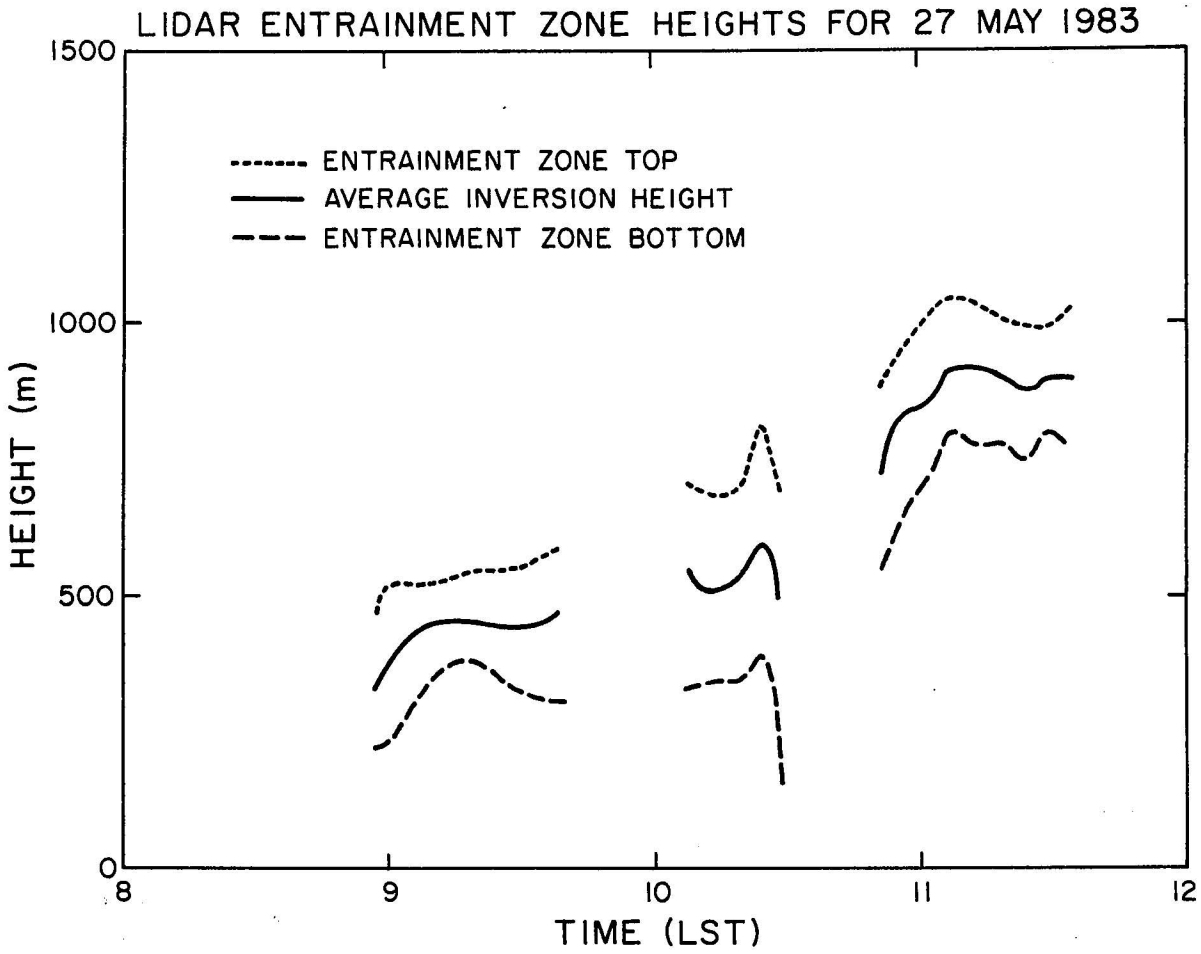


*Figure 4.21.--Entrainment zone heights obtained with lidar. (Courtesy of R. Stull, University of Wisconsin, Department of Meteorology)*

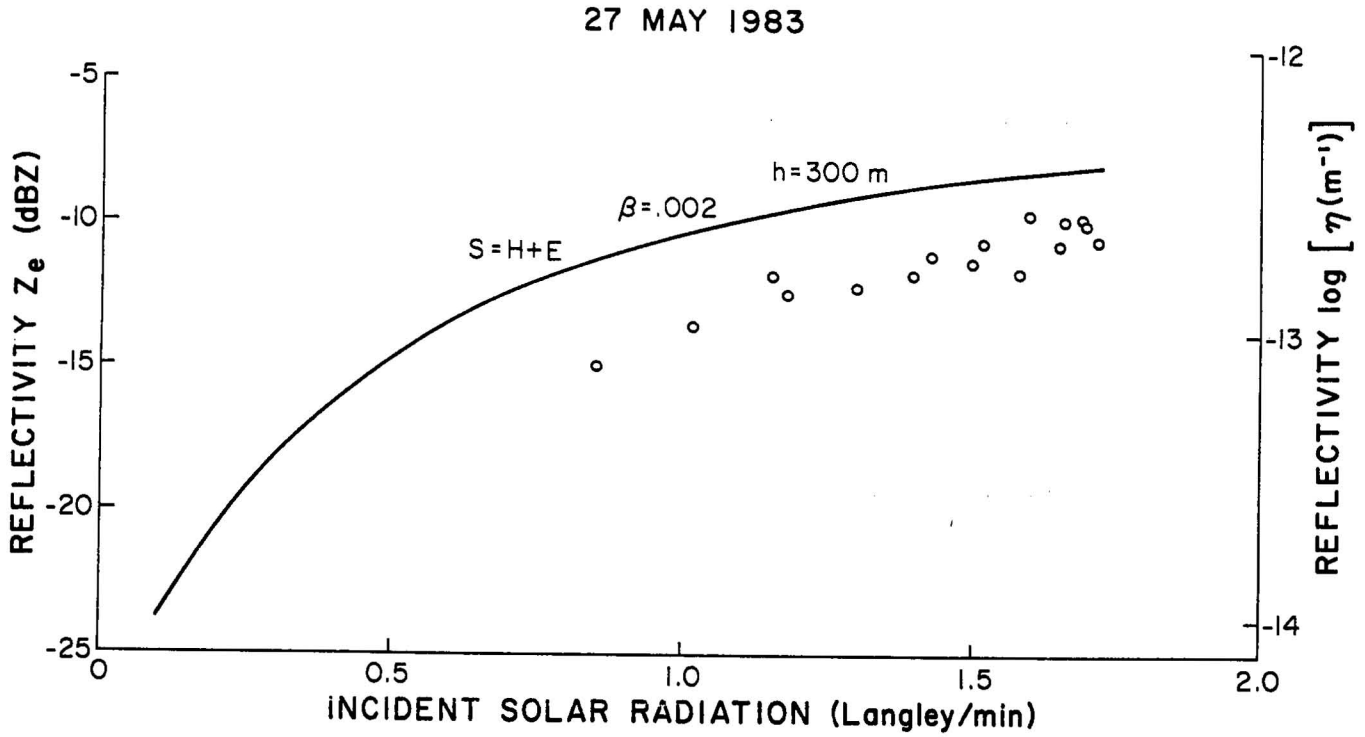


*Figure 4.22.--Predicted reflectivity at 300 m above wet ground (Bowen ratio of .002) from the solar fluxes and measured reflectivity between 0800-1600 LST on May 27, 1983.*

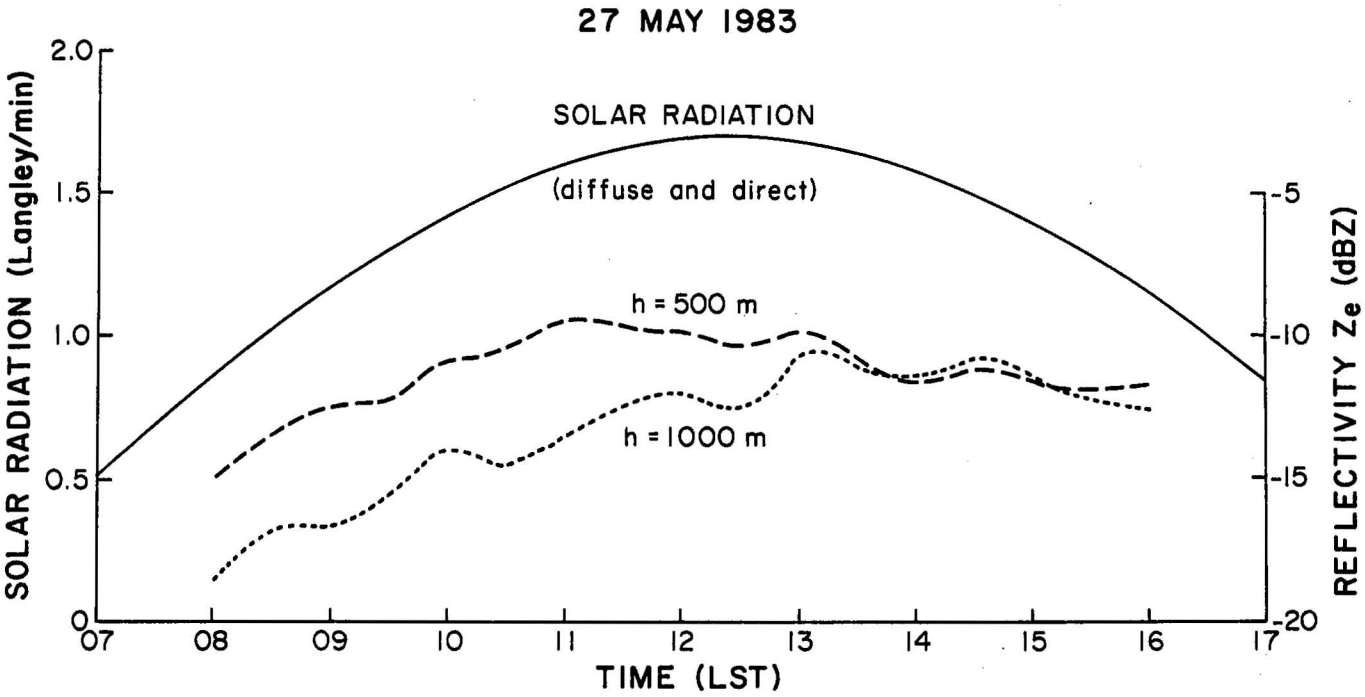


*Figure 4.23.--Variation of the effective reflectivity factor with time at two different heights.*

Table 4.3.--Computed Reflectivity Factor and $C_n^2$ on May 27, 1983 From Rawinsonde Data

| Station | OKC | OKC | SNL | SNL |
|---|---|---|---|---|
| Time (LST) | 6 | 6 | 9 | 13 |
| Mean height (m) | 250 | 500 | 500 | 900 |
| $C_n^2$ ($m^{-2/3}$)* | $9.8 \times 10^{-14}$ | $3.7 \times 10^{-13}$ | $1.7 \times 10^{-13}$ | $1.1 \times .10^{-12}$ |
| Reflectivity factor (dBZ)* | -12.1 | -6.3 | -9.6 | -1.7 |
| $C_n^2$ ($m^{-2/3}$)† | $9.3 \times 10^{-14}$ | $5.1\ 10^{-14}$ | $5.9 \times 10^{-14}$ | $4.6 \times 10^{-14}$ |
| Reflectivity factor (dBZ)† | -12.3 | -14.9 | -14.3 | -15.4 |

*) From maximum gradients of mixing ratio
†) From an average gradient of mixing ratio of 2 g $kg^{-1}$ $km^{-1}$

measurements because the moisture contribution has been neglected. Nevertheless, if there were no other mechanisms controlling the reflectivity (for example, clouds), the layers would be detectable since they have larger $C_n^2$ than the ones measured during the three winter days.

Our measured reflectivities (Fig. 4.18a and b) at 500 m above ground imply a $C_n^2$ between $10^{-12.8}$ and $10^{-13.4}$, and we have no evidence of distributed layers either from rawinsonde or radar measurements. Furthermore, later soundings do not show isolated layers. So if refractive index irregularities dominate the scattering process they must be associated with temperature and moisture fluxes originating at the ground. Note on Fig. 4.22 that our measured reflectivities are below the upper limit imposed by a realistic Bowen ratio. Even though convective mixing can account for the reflectivity as witnessed by the similarity of the data to the theoretical curve in Fig. 4.21, we must bear in mind that enhanced convection will also bring more insects to higher altitudes. Thus the trend of reflectivity increase with time would be the same for both mechanisms (insects or refractive index fluctuations).

There are two factors that point toward significant contribution from insects. First, the reflectivity profiles with height (Rabin, 1983) based on

increased insect distributions should fall exponentially (linearly on the log scale) just as is the case for most of our profiles. Second, (a) our values of $C_n^2$ inferred from measured reflectivity are at least two orders of magnitude higher than values measured with an FM-CW radar by Chadwick and Moran (1980); (b) they are two orders of magnitude higher than the aircraft measurements of Ochs and Lawrence (1972); (c) they are about two orders of magnitude larger than Gossard's (1977) estimates based on radiosonde measurements; and (d) about one order of magnitude larger than values in the center of an inversion measured with a spaced refractometer by Bean et al. (1971).

An example of a velocity azimuth display (VAD) for this day is shown in Fig. 4.24. The data used were in the range interval from 40 to 50 km. Altogether 45 consecutive (in range) velocities were averaged along each radial. To eliminate outliers, only those velocities within 12 m $s^{-1}$ of the modal value were averaged. The least-squares fit was made to the zeroth, first, and second harmonic over the 360° circle. The wind profile from such a VAD is shown in Figs. 4.25a and 4.25b. Winds from three nearby rawinsondes (see Fig. 4.17 for locations) are also included, and we note a very good agreement between all these instruments.

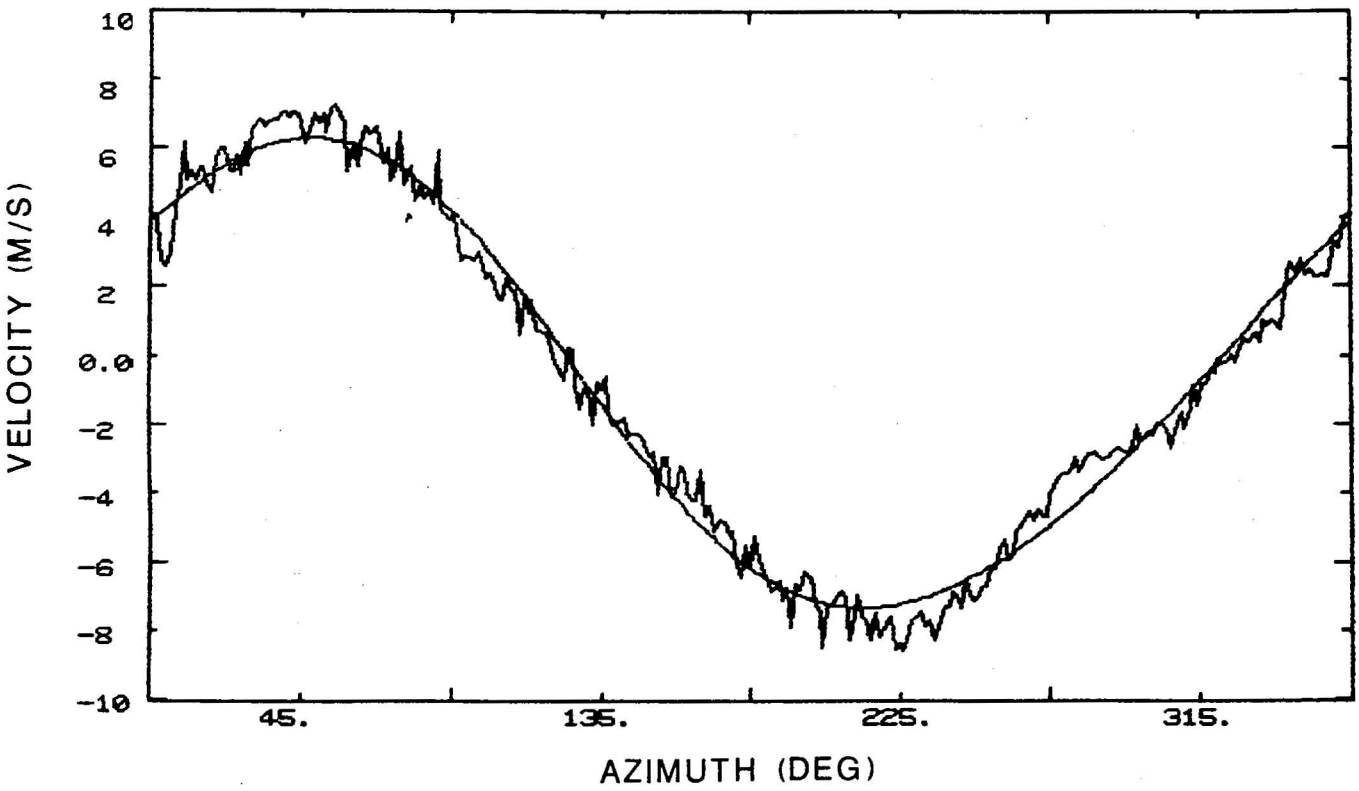


*Figure 4.24.--A velocity azimuth display (VAD) on May 27, 1983. Data for this display were collected between 1510 and 1535 LST. The smooth curve is a least-squares fitted sum of three harmonics.*

## 4.4 Summary of 1983 Experiments

The Interim Operational Test Facility (IOTF) of the National Weather Service conducted a test in the spring of 1983 in Norman, Oklahoma. One of the objectives was to obtain from the VAD the vertical profiles of wind. Altogether there were 24 operational days in April and May and 18 days in June. These observations were conducted between 1200 and 2100 CST. On 3 out of the 24 days in April and May (after cold frontal passages) the reflectivities were below -15 dBZ so that reliable winds at 1 to 2 km above ground could not be obtained. In June, winds through the boundary layer were always obtainable. During these tests pulse pair derived velocities were analyzed, which, at low signal to noise ratios, are more prone to contamination by ground clutter and point targets. If spectral processing were used, we believe that we would have obtained profiles of winds in the boundary layer on these days as well.

Another noteworthy observation was that the days of little echo were also fair weather days. Strong low-level winds brought stronger signal. All the low-level jets that occurred were detectable. The average difference between the VAD and the rawinsonde winds was less than 1%. On most days, wind velocities were measured reliably to about 4 km above ground level with little or no cloud cover present.

## 4.5 Measurements at Wallops Island

Measurements made in the early seventies at Wallops Island are in accord with our findings. The Wallops Island radar has a 60 ft diameter antenna and peak power of 3 MW, which translates to a power-aperture product that is about 17 times larger than the one for the Norman radar. The wavelength is also 10 cm, yet observation of reflectivities on an RHI display (Fig. 4.26) show layers extending to 4 km and no more. Actually at the earlier time there seems to be only one layer at 8 km and the rest are below 1 km. Later in the day the layers appear at most heights below 4 km and are especially strong at 4 km and below 1 km. Recently, NSSL scientists repeated measurements at Wallops Island and used coherent processing (pulse pair) to display velocity fields in an RHI format. Again there was no echo above 6 km but the radar did not operate at peak sensitivity. We must conclude then that measurements between 1 and 4 to 6 km are

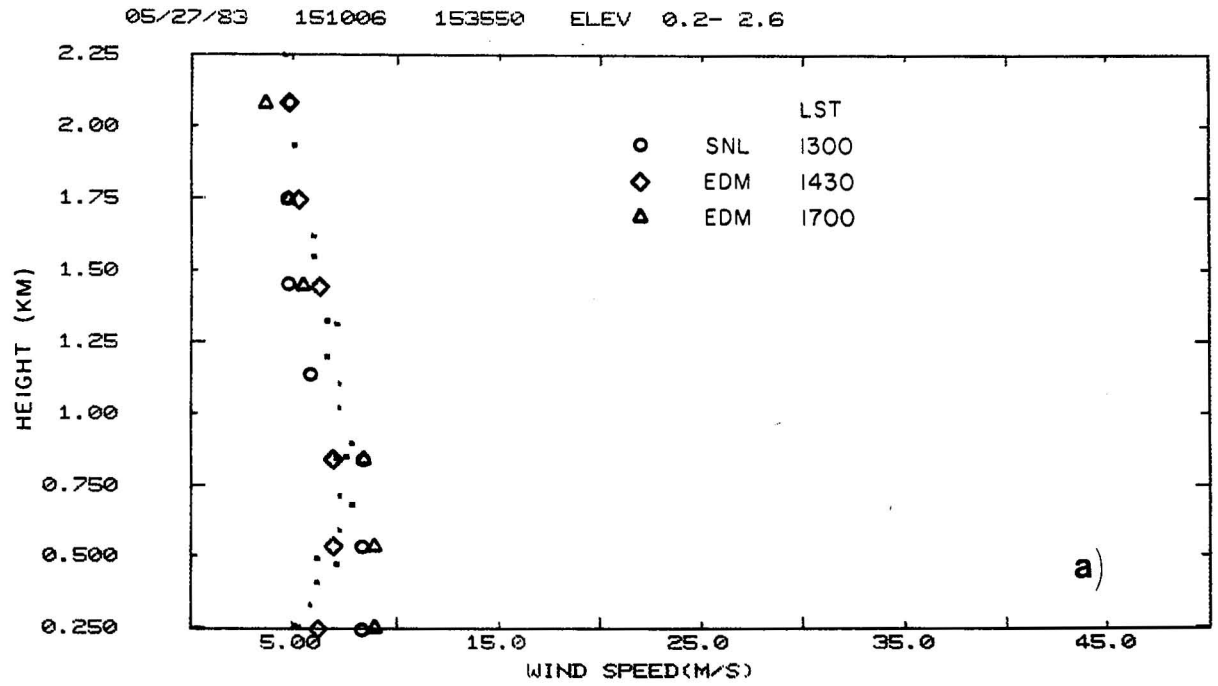


*Figure 4.25.--Wind profile obtained from VADs on May 27, 1983 between 1510 and 1535 LST together with winds from three rawinsondes: a) wind speed; b) wind direction.*

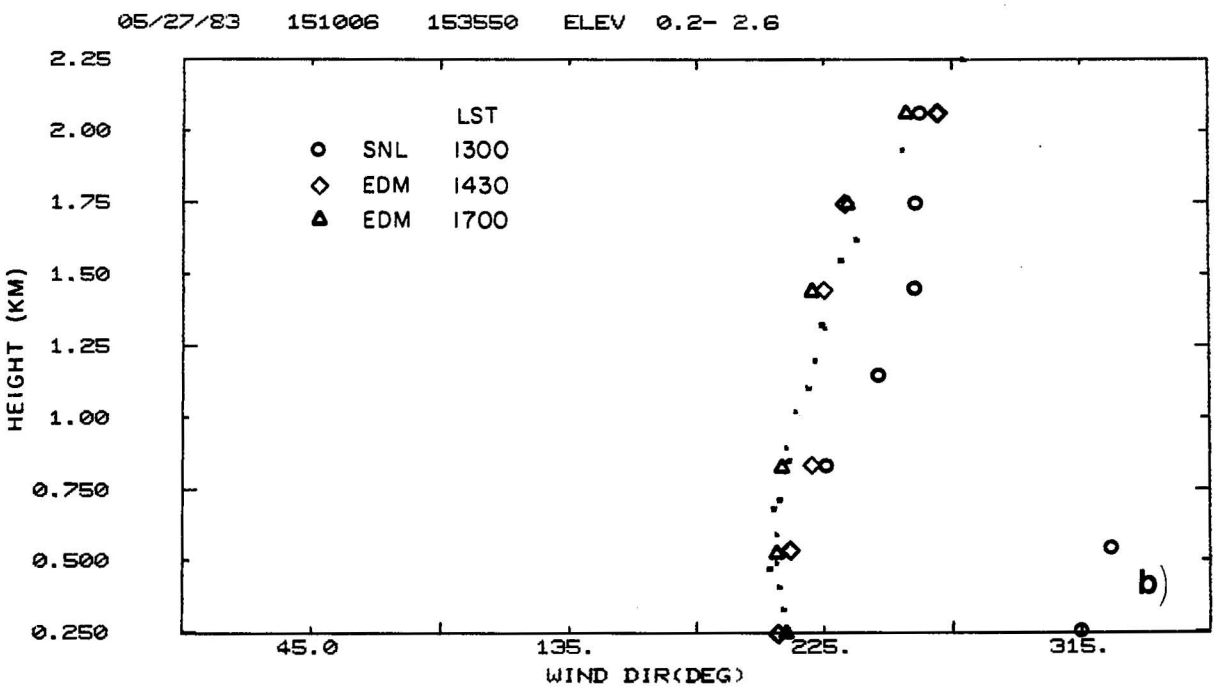

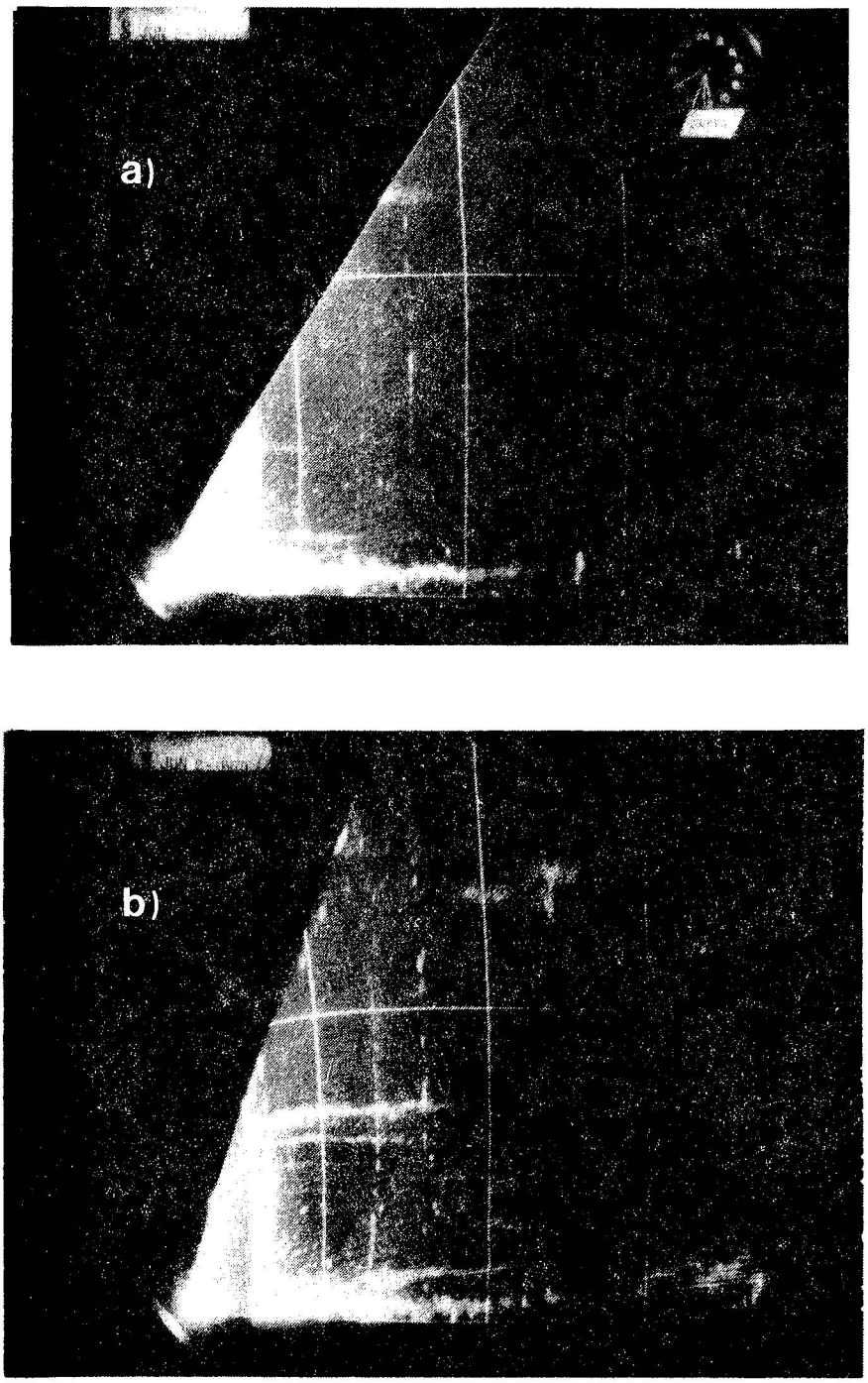


*Figure 4.26.--RHI display of reflectivity on 2 June 1970 from Wallops Island radar. The height mark is at 6.1 km and range marks are 9.3 km apart. (a) at 0735 CST; (b) at 1335 LST.*

not always possible. At higher altitudes they may be rare if the radar wavelength is 10 cm.

## 5. CONCLUSIONS

It has been our experience from the limited measurements in Oklahoma and Colorado that radars with a 10 cm wavelength will always measure some echo to about a few hundred meters above ground. These weak echoes are from refractive index irregularities and are weakest in winter months and when the atmosphere is very stable. In order to measure winds under these conditions it is necessary to employ Doppler spectral analysis. We have shown examples of Doppler spectra from which values of the structure constant $C_n^2$ and effective reflectivity factor $Z_e$ were calculated. The $Z_e$ ranged from -10 to -28 dBZ in January and could be explained with the theory of turbulent mixing of layers. Reflectivity factors in the spring are typically larger than -15 dBZ and for the one case analyzed could be explained by convective mixing of humidity and potential temperature gradients. The presence of insects is also significant during the warmer months in Oklahoma. Until recently we had no independent means to discriminate between insects and refractive index fluctuations. However, a radar having dual polarization capability may help us to discriminate between the two mechanisms.

It is important to note that during warmer months measurements are possible through the boundary layer and very often above it. The presence of a low-level jet (2 to 4 km above ground) was always detectable.

Our results for 10 cm wavelength radars cannot always be extrapolated to shorter wavelengths. If turbulence is in the inertial subrange and all other radar parameters are equal, then signal to noise ratios are proportional to $\lambda^{5/3}$ for clear air. If particles are scatterers, the proportionality is $\lambda^{-2}$ .

To extrapolate our clear air data to a wavelength of 3 cm would require turbulent eddies of size $\lambda/2 = 1.5$ cm to be in the inertial subrange. It is not known how often this is the case in the planetary boundary layer. As a matter of fact not enough data are available for us to ascertain how often turbulent eddies of size 5 cm are in the inertial subrange above the boundary layer. Our own experience and that of others is that there may be intermittent layers below 6 km within which there are energetic eddies that produce echoes for 10 cm radars. Most often, turbulence on scales of 5 cm at these heights is in the dissipative regime so there are no detectable echoes or there are big gaps between layers.

Thus, routine measurements above the boundary layer at centimeter wavelengths are not possible and other means must be sought to make such measurements.

One possibility is to take advantage of other natural scatterers. This prompted us to examine the occurrence of precipitation and clouds in the continental U.S.A. Overall, 38% of the time there are enough clouds to allow measurements to at least 3 km. There is scattered light precipitation 12% of the time, and the remaining 26% of the time rain is reaching the ground somewhere near the radar.

## REFERENCES


Bean, B.R., R.E. McGavin, R.B. Chadwick, and B.D. Warner, 1971: Preliminary results of utilizing the high resolution FM radar as a boundary-layer probe. Bound. Layer Meteor., 1, 466-473.

Brewster, K.A., 1985: Kinetic energy evolution in a developing severe thunderstorm. CIMMS report No. 59, Norman, OK.

Chadwick, R.B., and K.P. Moran, 1980: Long-term measurements of $C_n^2$ in the boundary layer. Radio Sci., 15 (2), 355-361.

Doviak, R.J., and D.S. Zrnic', 1984: Doppler Radar and Weather Observations. Academic Press, Orlando, Florida, 458 pp.

Draper, N.R., and H. Smith, 1981: Applied Regression Analysis. Wiley, New York, NY, 709 pp.

Ference, M., Jr., 1951: Instruments and techniques for meteorological measurements. Compendium of Meteorology (Thomas F. Malone, ed.), American Meteorological Society, Boston, Mass., 1207-1222.

Gossard, E.E., 1977: Refractive index variance and its height variation distribution in different air masses, Radio Sci., 12 (1), 89-105.

Grantham, D.D., and A.J. Kantor, 1967: Distributions of radar echoes over the United States. Air Force Cambridge Research Laboratory report AFCRL-67-0232.

Hoehne, W.E., 1980: Precision of National Weather Service upper air measurements. NOAA Tech. Memo. NWS T&DE-16, August, 23 pp.

Koscielny, A.J., R.J. Doviak, and R. Rabin, 1982: Statistical considerations in the estimation of divergence from single Doppler radar and application to prestorm boundary layer observation. J. Appl. Meteorology, 21, 197-210.

Ochs, G.R., and R.S. Lawrence, 1972: Temperature and $C_n^2$ profiles measured over land and ocean to 3 km above the surface. Tech. Rep. ERL 251-WPL22, NOAA/ERRL Wave Propagation Laboratory, Boulder, CO.

Rabin, R.M., 1983: Radar reflectivity in clear boundary layer and its relation to surface fluxes. Preprints, 21st Conf. Radar Meteor., Amer. Meteor. Soc., Boston, Mass., 646-649.

Ruffner, J.A., and F.E. Bair, ed., 1977: The Weather Almanac. 2nd ed. Avon Books, New York, NY, 728 pp.

Vasiloff, S.V., and E.A. Brandes 1984: An investigation of the transition from multicell to supercell storms. Preprints, 22nd Conf. Radar Meteor., Amer. Meteor. Soc., Boston, Mass., 77-82.

## ACKNOWLEDGMENTS

Several members of the Laboratory contributed to the material in this report. Glen Anderson operated the radar, and Albert Koscielny provided the displays for the winter experiment. Yosefa Gal-Chen, Albert Koscielny, and Randy Rausch developed and ran the software for wind profiles and reflectivity measurements. Edward Brandes, Steven Vasiloff, and Keith Brewster supplied dual Doppler analysis wind fields and profiles, and R.J. Doviak supplied the photos from his 1970 experiment at Wallops Island. Roland Stull (University of Wisconsin) had given lidar data. Stimulating inquiries by Don Snider (U.S. Army Atmospheric Science Lab) contributed considerably to this work. Artwork was performed by Joan Kimpel and photography by Robert Goldsmith. This research was supported by the U.S. Army Atmopsheric Science Laboratory Project AM2A8305 under Project Order No. ASL-84-8024.

# APPENDIX A

## TABLES OF RADAR ECHO

### A.1 Climates[1] for the Six Stations

Sacramento - Mild climate with an abundance of sunshine year-round. Cloudless skies prevail during the summer and also largely during the spring and autumn. The summers are dry with warm days. During the winter "rainy season" (December through February) over half of the annual precipitation falls, yet rain in measurable amounts occurs only on about 10 days each month.

Amarillo - Wide-ranging climate with large departures from normal precipitation and large and rapid temperature changes, especially in winter. Amarillo generally has cool winters and warm summers. Three-fourths of the annual precipitation falls between April and September during thunderstorm activity.

Minneapolis - Continental climate with wide variations in temperature, ample summer rainfall, and scanty winter precipitation. Minneapolis generally has very cold winters and mild summers.

Kansas City - Climate similar to that of Minneapolis. However, it is not as cold in winter and warmer in summer.

New York - A mild climate with continental influence predominating although oceanic influence is by no means absent. Since weather systems approach from the west, New York City experiences higher temperatures in summer and lower ones in winter than would otherwise be expected in a coastal area. Precipitation is moderate and distributed fairly evenly throughout the year. Most of the rainfall from May to October is from thunderstorms.

Key West - Tropical marine climate with long, warm summers and mild winters. The marine influence is evidenced by the low daily range in temperature. During summer and autumn, rainfall is abundant with fairly dry conditions occurring during winter and early spring.

---

[1]From Ruffner and Bair (1977)

Table A.1. Percentage frequency of radar echoes within 100 nautical miles of the radar site for January. An * refers to probabilities less than 0.1%.

| | Height (kft above sea level) | | | | | | |
|---|---|---|---|---|---|---|---|
| STATION | 0-4.9 | 5-9.9 | 10-14.9 | 15-19.9 | 20-24.9 | 25-29.9 | 30+ |
| Sacramento | 23.4 | 23.4 | 22.9 | 15.6 | 6.8 | 1.7 | 0.5 |
| Santa Catalina | 16.4 | 15.7 | 7.1 | 2.8 | 0.4 | * | * |
| Missoula | 40.0 | 40.0 | 32.8 | 9.8 | 0.6 | 0.1 | * |
| Minneapolis | 24.7 | 24.4 | 20.2 | 9.6 | 1.9 | 0.2 | * |
| Des Moines | 22.6 | 22.6 | 18.7 | 9.6 | 2.4 | 0.3 | 0.1 |
| Chicago | 33.7 | 25.4 | 15.2 | 6.1 | 1.4 | 0.5 | 0.2 |
| Detroit | 36.2 | 34.6 | 25.5 | 12.7 | 3.5 | 0.5 | 0.1 |
| Kansas City | 25.2 | 25.2 | 23.3 | 13.4 | 5.0 | 0.7 | 0.4 |
| St. Louis | 24.8 | 24.8 | 22.8 | 12.4 | 3.7 | 1.8 | 1.2 |
| Wichita | 16.9 | 16.9 | 15.8 | 12.0 | 5.7 | 0.7 | 0.1 |
| Amarillo | 12.5 | 12.5 | 12.3 | 8.8 | 3.1 | 0.3 | * |
| Oklahoma City | 11.7 | 11.6 | 11.4 | 7.0 | 3.1 | 0.7 | 0.1 |
| Little Rock | 28.0 | 28.0 | 24.5 | 18.3 | 8.9 | 3.2 | 1.6 |
| Fort Worth | 20.6 | 20.6 | 19.4 | 16.5 | 9.0 | 3.0 | 0.5 |
| Lake Charles | 40.2 | 40.1 | 38.8 | 32.3 | 25.5 | 13.1 | 7.2 |
| New Orleans | 40.3 | 40.3 | 38.6 | 33.3 | 24.3 | 10.5 | 6.4 |
| Galveston | 36.8 | 36.7 | 34.6 | 28.5 | 20.2 | 10.9 | 4.9 |
| Brownsville | 18.6 | 18.6 | 15.4 | 8.1 | 2.5 | 0.4 | 0.2 |
| Evansville | 33.5 | 32.1 | 25.3 | 15.1 | 4.5 | 1.9 | 0.9 |
| Cincinnati | 35.4 | 34.5 | 28.9 | 18.0 | 7.8 | 2.2 | 0.7 |
| Buffalo | 65.6 | 53.9 | 21.2 | 10.0 | 3.1 | 0.3 | * |
| New York | 41.7 | 41.6 | 38.8 | 29.1 | 13.4 | 3.3 | 0.8 |
| Atlantic City | 36.3 | 36.2 | 33.1 | 25.5 | 10.5 | 3.2 | 0.4 |
| Washington | 37.2 | 37.1 | 34.8 | 25.8 | 17.0 | 4.8 | 0.4 |
| Wilmington | 37.8 | 37.8 | 31.6 | 22.6 | 11.2 | 3.1 | 1.2 |
| Charleston | 39.1 | 39.0 | 37.7 | 31.6 | 19.1 | 6.9 | 3.3 |
| Daytona | 44.9 | 44.9 | 42.1 | 35.0 | 22.3 | 10.3 | 2.6 |
| Apalachicola | 34.9 | 34.7 | 34.2 | 29.0 | 19.6 | 9.6 | 3.7 |
| Tampa | 43.4 | 43.3 | 40.1 | 31.4 | 19.9 | 9.2 | 3.0 |
| Miami | 56.6 | 56.5 | 52.3 | 37.5 | 18.5 | 6.6 | 1.7 |
| Key West | 58.5 | 58.5 | 55.8 | 42.8 | 23.5 | 11.0 | 4.3 |

Table A.2. Percentage frequency of radar echoes for April.

| STATION | Height (kft above sea level) 0-4.9 | 5-9.9 | 10-14.9 | 15-19.9 | 20-24.9 | 25-29.9 | 30+ |
|---|---|---|---|---|---|---|---|
| Sacramento | 31.8 | 31.8 | 31.7 | 27.3 | 17.5 | 5.6 | 1.2 |
| Santa Catalina | 17.4 | 17.1 | 14.1 | 7.4 | 4.8 | 1.7 | 0.4 |
| Missoula | 43.7 | 43.7 | 42.7 | 24.8 | 7.3 | 1.6 | 0.5 |
| Minneapolis | 44.1 | 44.1 | 41.8 | 32.9 | 19.2 | 9.6 | 5.3 |
| Des Moines | 49.7 | 49.7 | 47.7 | 41.1 | 27.8 | 17.6 | 12.3 |
| Chicago | 35.1 | 35.0 | 31.9 | 23.7 | 15.8 | 9.4 | 5.6 |
| Detroit | 42.4 | 42.4 | 38.2 | 28.3 | 14.2 | 7.7 | 4.5 |
| Kansas City | 44.7 | 44.7 | 44.3 | 41.4 | 30.5 | 21.4 | 14.9 |
| St. Louis | 44.4 | 44.4 | 43.7 | 39.9 | 28.2 | 18.2 | 11.3 |
| Wichita | 35.4 | 35.4 | 35.4 | 34.6 | 28.5 | 19.8 | 13.6 |
| Amarillo | 20.1 | 20.1 | 20.0 | 18.5 | 12.3 | 7.4 | 3.5 |
| Oklahoma City | 29.6 | 29.6 | 29.6 | 28.5 | 22.7 | 17.1 | 13.6 |
| Little Rock | 42.8 | 42.7 | 42.2 | 39.2 | 32.4 | 21.9 | 14.7 |
| Fort Worth | 34.9 | 34.9 | 34.8 | 33.5 | 30.2 | 23.8 | 18.4 |
| Lake Charles | 39.0 | 38.9 | 37.8 | 34.5 | 29.4 | 20.5 | 14.1 |
| New Orleans | 44.9 | 44.9 | 44.6 | 42.1 | 35.9 | 27.3 | 20.1 |
| Galveston | 26.3 | 26.3 | 26.3 | 23.6 | 20.3 | 15.2 | 10.0 |
| Brownsville | 15.6 | 15.6 | 14.7 | 12.5 | 8.7 | 5.6 | 3.5 |
| Evansville | 53.8 | 53.5 | 49.2 | 38.0 | 19.5 | 11.3 | 6.8 |
| Cincinnati | 49.2 | 49.2 | 45.6 | 32.6 | 20.3 | 13.7 | 8.9 |
| Buffalo | 50.0 | 49.9 | 34.5 | 20.7 | 8.4 | 2.5 | 1.2 |
| New York | 48.3 | 48.2 | 46.0 | 38.3 | 24.6 | 9.7 | 3.3 |
| Atlantic City | 38.1 | 38.0 | 36.0 | 31.5 | 20.4 | 5.8 | 2.3 |
| Washington | 42.7 | 42.7 | 40.9 | 32.4 | 21.2 | 9.2 | 3.3 |
| Wilmington | 40.2 | 39.9 | 36.2 | 25.7 | 15.9 | 8.3 | 4.0 |
| Charleston | 42.5 | 42.5 | 41.8 | 38.7 | 27.6 | 16.1 | 9.1 |
| Daytona | 32.7 | 32.7 | 30.8 | 25.3 | 18.2 | 12.1 | 8.2 |
| Apalachicola | 23.8 | 23.8 | 23.7 | 20.5 | 15.3 | 10.0 | 7.6 |
| Tampa | 25.2 | 25.2 | 24.9 | 21.2 | 17.3 | 11.3 | 8.2 |
| Miami | 56.5 | 56.4 | 52.8 | 41.9 | 27.3 | 18.5 | 13.3 |
| Key West | 50.8 | 50.8 | 49.2 | 40.4 | 25.7 | 15.8 | 9.4 |

Table A.3. Percentage frequency of radar echoes for July.

| STATION | Height (kft above sea level) 0-4.9 | 5-9.9 | 10-14.9 | 15-19.9 | 20-24.9 | 25-29.9 | 30+ |
|---|---|---|---|---|---|---|---|
| Sacramento | 13.2 | 13.2 | 13.2 | 13.2 | 13.1 | 10.8 | 7.6 |
| Santa Catalina | 3.0 | 3.0 | 2.9 | 2.2 | 1.2 | 0.3 | 0.1 |
| Missoula | 43.7 | 43.7 | 43.5 | 41.3 | 35.8 | 25.2 | 17.1 |
| Minneapolis | 49.6 | 49.6 | 49.6 | 48.8 | 43.8 | 31.4 | 22.9 |
| Des Moines | 50.1 | 50.1 | 49.8 | 49.4 | 45.7 | 36.8 | 27.3 |
| Chicago | 34.9 | 34.8 | 34.1 | 31.6 | 25.8 | 18.5 | 14.6 |
| Detroit | 46.7 | 46.7 | 46.2 | 44.9 | 37.6 | 26.1 | 16.8 |
| Kansas City | 52.2 | 52.2 | 52.2 | 52.0 | 49.3 | 41.7 | 32.5 |
| St. Louis | 47.1 | 47.1 | 47.1 | 47.1 | 44.0 | 35.8 | 25.1 |
| Wichita | 52.8 | 52.8 | 52.7 | 52.5 | 50.9 | 42.6 | 29.7 |
| Amarillo | 54.5 | 54.5 | 54.5 | 54.2 | 52.3 | 43.3 | 34.0 |
| Oklahoma City | 43.0 | 43.0 | 43.0 | 42.9 | 40.0 | 31.5 | 23.0 |
| Little Rock | 54.2 | 54.2 | 54.1 | 53.8 | 51.3 | 44.5 | 35.4 |
| Fort Worth | 32.1 | 32.1 | 32.1 | 32.1 | 31.2 | 27.0 | 20.7 |
| Lake Charles | 59.8 | 59.8 | 59.8 | 59.4 | 57.5 | 53.1 | 44.5 |
| New Orleans | 79.8 | 79.8 | 79.7 | 79.2 | 76.8 | 68.7 | 58.3 |
| Galveston | 51.5 | 51.5 | 51.5 | 51.3 | 48.8 | 41.3 | 33.1 |
| Brownsville | 38.7 | 38.7 | 38.6 | 35.8 | 27.4 | 17.0 | 9.5 |
| Evansville | 52.2 | 52.2 | 51.7 | 49.2 | 40.3 | 28.5 | 20.7 |
| Cincinnati | 51.8 | 51.8 | 51.3 | 49.1 | 41.8 | 33.6 | 24.0 |
| Buffalo | 45.9 | 45.9 | 44.8 | 39.1 | 29.8 | 19.3 | 13.5 |
| New York | 51.3 | 51.3 | 51.0 | 87.5 | 44.9 | 35.9 | 24.0 |
| Atlantic City | 43.1 | 43.1 | 42.3 | 41.0 | 35.8 | 26.9 | 17.5 |
| Washington | 52.9 | 52.9 | 52.4 | 48.2 | 39.3 | 26.8 | 17.0 |
| Wilmington | 70.0 | 70.0 | 68.7 | 60.5 | 50.3 | 37.3 | 25.3 |
| Charleston | 75.7 | 75.7 | 75.5 | 73.9 | 68.6 | 59.7 | 47.2 |
| Daytona | 83.7 | 83.7 | 83.7 | 82.0 | 76.5 | 65.6 | 52.5 |
| Apalachicola | 81.1 | 81.1 | 81.0 | 79.6 | 75.2 | 64.7 | 53.6 |
| Tampa | 90.1 | 90.1 | 90.1 | 88.8 | 84.1 | 75.9 | 65.2 |
| Miami | 91.6 | 91.6 | 91.5 | 90.7 | 87.0 | 76.3 | 62.5 |
| Key West | 87.8 | 87.8 | 87.7 | 86.6 | 82.2 | 72.1 | 58.6 |

Table A.4. Percentage frequency of radar echoes for October.

| STATION | Height (kft above sea level) | | | | | | |
|---|---|---|---|---|---|---|---|
| | 0-4.9 | 5-9.9 | 10-14.9 | 15-19.9 | 20-24.9 | 25-29.9 | 30+ |
| Sacramento | 25.0 | 25.0 | 24.4 | 22.5 | 16.4 | 6.2 | 1.2 |
| Santa Catalina | 11.8 | 11.4 | 9.8 | 7.0 | 3.1 | 0.6 | * |
| Missoula | 36.2 | 36.2 | 35.8 | 29.8 | 9.5 | 3.2 | 1.0 |
| Minneapolis | 23.9 | 23.9 | 23.1 | 18.9 | 10.0 | 4.3 | 1.8 |
| Des Moines | 25.7 | 25.7 | 25.6 | 23.2 | 17.7 | 11.1 | 7.0 |
| Chicago | 25.1 | 24.8 | 19.9 | 13.4 | 7.8 | 3.4 | 1.3 |
| Detroit | 36.2 | 36.1 | 31.7 | 23.2 | 13.2 | 6.0 | 2.4 |
| Kansas City | 26.9 | 26.9 | 26.8 | 24.7 | 17.3 | 8.5 | 5.2 |
| St. Louis | 26.9 | 26.9 | 26.8 | 24.9 | 17.0 | 9.7 | 3.4 |
| Wichita | 20.5 | 20.5 | 20.5 | 19.3 | 15.4 | 10.2 | 5.0 |
| Amarillo | 13.6 | 13.6 | 13.6 | 13.6 | 12.6 | 8.2 | 4.1 |
| Oklahoma City | 17.2 | 17.2 | 17.2 | 16.4 | 13.4 | 9.7 | 5.5 |
| Little Rock | 25.1 | 25.1 | 24.9 | 22.6 | 15.2 | 10.1 | 7.1 |
| Fort Worth | 22.3 | 22.3 | 22.2 | 21.9 | 19.6 | 15.3 | 10.6 |
| Lake Charles | 33.1 | 33.1 | 33.1 | 32.5 | 28.6 | 22.5 | 15.1 |
| New Orleans | 37.2 | 37.2 | 37.1 | 36.0 | 31.2 | 23.5 | 15.5 |
| Galveston | 33.6 | 33.6 | 33.6 | 33.0 | 30.0 | 23.0 | 15.7 |
| Brownsville | 54.1 | 54.1 | 53.9 | 46.5 | 31.4 | 16.4 | 8.9 |
| Evansville | 27.5 | 27.5 | 26.7 | 22.8 | 12.8 | 6.6 | 3.1 |
| Cincinnati | 26.9 | 26.9 | 26.1 | 23.0 | 14.9 | 7.7 | 4.2 |
| Buffalo | 29.8 | 29.7 | 22.7 | 10.8 | 4.3 | 1.0 | 0.3 |
| New York | 35.2 | 35.2 | 35.2 | 32.0 | 21.9 | 10.4 | 5.0 |
| Atlantic City | 26.7 | 26.7 | 24.8 | 20.7 | 13.4 | 6.1 | 1.9 |
| Washington | 29.0 | 29.0 | 28.6 | 24.7 | 16.4 | 6.9 | 2.7 |
| Wilmington | 38.3 | 38.3 | 37.3 | 27.7 | 16.8 | 8.8 | 4.2 |
| Charleston | 39.7 | 39.7 | 38.8 | 34.3 | 26.0 | 18.8 | 13.6 |
| Daytona | 58.9 | 58.9 | 57.8 | 53.5 | 42.2 | 30.5 | 19.6 |
| Apalachicola | 23.7 | 23.5 | 22.4 | 20.0 | 16.4 | 11.0 | 7.1 |
| Tampa | 45.1 | 45.0 | 43.6 | 36.9 | 28.0 | 17.8 | 10.3 |
| Miami | 78.9 | 78.9 | 77.9 | 72.7 | 65.9 | 51.8 | 34.5 |
| Key West | 81.1 | 81.1 | 80.7 | 77.2 | 67.3 | 51.7 | 36.3 |

Table A.5. Diurnal Variations in Radar Echo Frequencies.

| Station | 1-3 | 4-6 | 7-9 | 10-12 | 13-15 | 16-18 | 19-21 | 22-24 | LST |
|---|---|---|---|---|---|---|---|---|---|
| **January** | | | | | | | | | |
| Sacramento | 20.8 | 20.5 | 21.2 | 20.8 | 25.6 | 26.3 | 27.6 | 27.6 | |
| Amarillo | 12.9 | 12.2 | 12.2 | 11.6 | 10.2 | 10.8 | 14.4 | 15.8 | |
| Minneapolis | 18.3 | 16.5 | 24.3 | 29.9 | 28.5 | 30.7 | 27.4 | 21.9 | |
| Kansas City | 20 | 21 | 20 | 23 | 25 | 22 | 21 | 22 | |
| New York | 45.9 | 40.6 | 44.1 | 43.3 | 42.4 | 39.2 | 38.0 | 40.1 | |
| Key West | 57.3 | 57.7 | 62.2 | 67.3 | 65.7 | 55.4 | 50.7 | 52.0 | |
| **April** | | | | | | | | | |
| Sacramento | 27.4 | 26.7 | 25.9 | 27.5 | 36.4 | 41.8 | 39.2 | 30.0 | |
| Amarillo | 20.4 | 15.6 | 17.1 | 14.9 | 16.4 | 27.0 | 25.7 | 23.3 | |
| Minneapolis | 43.2 | 37.5 | 43.6 | 50.2 | 45.0 | 48.9 | 44.9 | 40.1 | |
| Kansas City | 39.8 | 41.5 | 46.3 | 45.5 | 50.0 | 49.0 | 46.9 | 39.8 | |
| New York | 41.1 | 42.7 | 43.5 | 45.8 | 50.4 | 53.2 | 57.3 | 52.2 | |
| Key West | 43.1 | 52.1 | 53.0 | 56.8 | 58.2 | 51.5 | 48.3 | 44.0 | |
| **July** | | | | | | | | | |
| Sacramento | 6.8 | 6.9 | 6.6 | 10.1 | 22.7 | 28.9 | 12.2 | 6.3 | |
| Amarillo | 50.9 | 42.3 | 40.3 | 38.3 | 53.5 | 74.0 | 73.8 | 62.4 | |
| Minneapolis | 45.9 | 49.4 | 52.1 | 47.7 | 57.0 | 55.5 | 47.6 | 41.5 | |
| Kansas City | 48.7 | 57.3 | 58.7 | 56.3 | 53.7 | 60.4 | 43.4 | 40.1 | |
| New York | 45.5 | 41.6 | 43.0 | 46.3 | 59.7 | 64.1 | 57.6 | 51.8 | |
| Key West | 80.8 | 85.5 | 85.1 | 88.8 | 94.1 | 96.7 | 92.7 | 78.5 | |
| **October** | | | | | | | | | |
| Sacramento | 23.1 | 24.1 | 24.7 | 19.9 | 24.9 | 33.3 | 26.0 | 23.7 | |
| Amarillo | 11.5 | 11.5 | 12.2 | 12.0 | 13.7 | 17.6 | 16.8 | 13.6 | |
| Minneapolis | 23.3 | 18.5 | 22.9 | 20.5 | 24.9 | 27.4 | 27.3 | 25.8 | |
| Kansas City | 25.1 | 24.8 | 28.6 | 25.7 | 22.7 | 28.0 | 30.5 | 29.3 | |
| New York | 34.2 | 33.3 | 32.9 | 32.1 | 37.8 | 42.7 | 35.8 | 32.4 | |
| Key West | 78.8 | 82.0 | 81.8 | 83.1 | 83.0 | 80.9 | 82.4 | 76.8 | |

Table A.6. Radar echo coverage probabilities for a six station sample. An * refers to probabilities less than 1%.

SACRAMENTO

**January**

| Echo Coverage % | 1-3 | 4-6 | 7-9 | 10-12 | 13-15 | 16-18 | 19-21 | 22-24 | 1-24 | LST |
|---|---|---|---|---|---|---|---|---|---|---|
| 0 | 79 | 80 | 79 | 79 | 74 | 74 | 72 | 76 | 77 | |
| 1-30 | 6 | 8 | 6 | 6 | 6 | 6 | 9 | 7 | 6 | |
| 31-70 | 4 | 6 | 4 | 8 | 6 | 8 | 8 | 8 | 7 | |
| 71-100 | 10 | 8 | 11 | 8 | 13 | 12 | 10 | 9 | 11 | |

**April**

| | | | | | | | | | | |
|---|---|---|---|---|---|---|---|---|---|---|
| 0 | 73 | 73 | 74 | 72 | 64 | 58 | 61 | 70 | 68 | |
| 1-30 | 8 | 8 | 7 | 8 | 13 | 14 | 13 | 9 | 10 | |
| 31-70 | 8 | 5 | 7 | 4 | 7 | 10 | 15 | 13 | 9 | |
| 71-100 | 12 | 14 | 12 | 15 | 18 | 19 | 10 | 7 | 13 | |

**July**

| | | | | | | | | | | |
|---|---|---|---|---|---|---|---|---|---|---|
| 0 | 93 | 93 | 93 | 90 | 77 | 71 | 88 | 94 | 87 | |
| 1-30 | 4 | 7 | 5 | 11 | 21 | 24 | 9 | 4 | 11 | |
| 31-70 | 1 | 1 | 2 | * | 4 | 3 | * | 1 | 2 | |
| 71-100 | 2 | 1 | 0 | 0 | 0 | 0 | 2 | 2 | 1 | |

**October**

| | | | | | | | | | | |
|---|---|---|---|---|---|---|---|---|---|---|
| 0 | 77 | 76 | 75 | 80 | 75 | 67 | 74 | 76 | 75 | |
| 1-30 | 10 | 8 | 6 | 5 | 12 | 14 | 7 | 7 | 9 | |
| 31-70 | 8 | 11 | 10 | 4 | 6 | 9 | 7 | 5 | 7 | |
| 71-100 | 6 | 6 | 7 | 11 | 8 | 12 | 11 | 10 | 9 | |

Table A.6 (continued)

AMARILLO

January

| Echo Coverage % | 1-3 | 4-6 | 7-9 | 10-12 | 13-15 | 16-18 | 19-21 | 22-24 | 1-24 | LST |
|---|---|---|---|---|---|---|---|---|---|---|
| 0 | 87 | 88 | 88 | 88 | 90 | 89 | 86 | 84 | 88 | |
| 1-30 | 6 | 6 | 8 | 5 | 4 | 5 | 4 | 6 | 5 | |
| 31-70 | 3 | 5 | 3 | 3 | 4 | 5 | 7 | 5 | 4 | |
| 71-100 | 4 | 2 | 2 | 4 | 3 | 3 | 4 | 5 | 3 | |

April

| | | | | | | | | | | |
|---|---|---|---|---|---|---|---|---|---|---|
| 0 | 80 | 84 | 83 | 85 | 84 | 73 | 74 | 77 | 80 | |
| 1-30 | 13 | 11 | 15 | 10 | 9 | 18 | 15 | 16 | 14 | |
| 31-70 | 6 | 5 | 4 | 4 | 5 | 6 | 7 | 7 | 6 | |
| 71-100 | 1 | 1 | * | 2 | 4 | 5 | 3 | 2 | 2 | |

July

| | | | | | | | | | | |
|---|---|---|---|---|---|---|---|---|---|---|
| 0 | 49 | 58 | 60 | 62 | 46 | 26 | 26 | 38 | 46 | |
| 1-30 | 23 | 24 | 25 | 28 | 34 | 40 | 42 | 38 | 32 | |
| 31-70 | 15 | 12 | 10 | 8 | 17 | 21 | 22 | 15 | 15 | |
| 71-100 | 12 | 8 | 7 | 3 | 5 | 13 | 9 | 11 | 8 | |

October

| | | | | | | | | | | |
|---|---|---|---|---|---|---|---|---|---|---|
| 0 | 88 | 88 | 88 | 88 | 86 | 82 | 83 | 86 | 86 | |
| 1-30 | 6 | 6 | 5 | 7 | 6 | 11 | 10 | 7 | 7 | |
| 31-70 | 5 | 3 | 6 | 1 | 4 | 5 | 4 | 5 | 4 | |
| 71-100 | 2 | 4 | 3 | 5 | 3 | 4 | 4 | 2 | 3 | |

Table A.6 (continued)

## MINNEAPOLIS

### January

| Echo Coverage % | 1-3 | 4-6 | 7-9 | 10-12 | 13-15 | 16-18 | 19-21 | 22-24 | 1-24 | LST |
|---|---|---|---|---|---|---|---|---|---|---|
| 0 | 82 | 84 | 76 | 70 | 72 | 69 | 73 | 78 | 75 | |
| 1-30 | 8 | 6 | 7 | 6 | 6 | 4 | 6 | 4 | 6 | |
| 31-70 | 4 | 4 | 6 | 10 | 8 | 7 | 7 | 4 | 6 | |
| 71-100 | 8 | 8 | 12 | 15 | 16 | 21 | 15 | 14 | 13 | |

### April

| | | | | | | | | | | |
|---|---|---|---|---|---|---|---|---|---|---|
| 0 | 57 | 62 | 56 | 50 | 55 | 51 | 55 | 60 | 56 | |
| 1-30 | 11 | 9 | 13 | 15 | 12 | 14 | 10 | 14 | 13 | |
| 31-70 | 12 | 13 | 10 | 9 | 11 | 13 | 12 | 11 | 11 | |
| 71-100 | 21 | 18 | 21 | 25 | 22 | 22 | 23 | 17 | 21 | |

### July

| | | | | | | | | | | |
|---|---|---|---|---|---|---|---|---|---|---|
| 0 | 54 | 51 | 48 | 52 | 43 | 44 | 52 | 58 | 50 | |
| 1-30 | 25 | 24 | 22 | 22 | 32 | 25 | 25 | 25 | 25 | |
| 31-70 | 12 | 17 | 16 | 16 | 9 | 16 | 10 | 9 | 14 | |
| 71-100 | 10 | 9 | 16 | 12 | 16 | 17 | 13 | 9 | 12 | |

### October

| | | | | | | | | | | |
|---|---|---|---|---|---|---|---|---|---|---|
| 0 | 77 | 82 | 77 | 80 | 75 | 73 | 73 | 74 | 76 | |
| 1-30 | 11 | 6 | 11 | 12 | 9 | 10 | 13 | 13 | 11 | |
| 31-70 | 5 | 8 | 5 | 5 | 5 | 7 | 6 | 5 | 5 | |
| 71-100 | 8 | 6 | 8 | 5 | 11 | 12 | 10 | 10 | 8 | |

Table A.6 (continued)

**KANSAS CITY**

**January**

| Echo Coverage % | 1-3 | 4-6 | 7-9 | 10-12 | 13-15 | 16-18 | 19-21 | 22-24 | 1-24 | LST |
|---|---|---|---|---|---|---|---|---|---|---|
| 0 | 80 | 79 | 80 | 77 | 75 | 78 | 79 | 78 | 78 | |
| 1-30 | 4 | 5 | 4 | 4 | 11 | 3 | 5 | 3 | 5 | |
| 31-70 | 4 | 5 | 6 | 7 | 5 | 6 | 5 | 6 | 5 | |
| 71-100 | 13 | 12 | 11 | 11 | 9 | 13 | 13 | 13 | 12 | |

**April**

| | | | | | | | | | | |
|---|---|---|---|---|---|---|---|---|---|---|
| 0 | 60 | 58 | 54 | 54 | 50 | 51 | 53 | 60 | 55 | |
| 1-30 | 16 | 16 | 14 | 17 | 18 | 19 | 17 | 16 | 17 | |
| 31-70 | 14 | 18 | 16 | 14 | 18 | 16 | 19 | 14 | 16 | |
| 71-100 | 11 | 10 | 18 | 17 | 16 | 15 | 13 | 12 | 14 | |

**July**

| | | | | | | | | | | |
|---|---|---|---|---|---|---|---|---|---|---|
| 0 | 51 | 43 | 41 | 44 | 46 | 40 | 57 | 60 | 48 | |
| 1-30 | 21 | 25 | 27 | 29 | 31 | 43 | 33 | 26 | 29 | |
| 31-70 | 17 | 20 | 18 | 16 | 12 | 9 | 8 | 11 | 14 | |
| 71-100 | 11 | 14 | 16 | 13 | 11 | 10 | 4 | 5 | 11 | |

**October**

| | | | | | | | | | | |
|---|---|---|---|---|---|---|---|---|---|---|
| 0 | 75 | 75 | 71 | 74 | 77 | 72 | 70 | 71 | 73 | |
| 1-30 | 10 | 13 | 15 | 11 | 7 | 10 | 17 | 9 | 12 | |
| 31-70 | 6 | 5 | 7 | 10 | 7 | 11 | 10 | 10 | 8 | |
| 71-100 | 9 | 9 | 6 | 4 | 9 | 8 | 5 | 8 | 7 | |

Table A.6 (continued)

**NEW YORK**

**January**

| Echo Coverage % | 1-3 | 4-6 | 7-9 | 10-12 | 13-15 | 16-18 | 19-21 | 22-24 | 1-24 | LST |
|---|---|---|---|---|---|---|---|---|---|---|
| 0 | 54 | 59 | 56 | 57 | 58 | 61 | 62 | 60 | 58 | |
| 1-30 | 12 | 10 | 16 | 17 | 18 | 12 | 14 | 18 | 15 | |
| 31-70 | 12 | 12 | 11 | 9 | 7 | 13 | 9 | 8 | 10 | |
| 71-100 | 22 | 20 | 18 | 18 | 19 | 14 | 17 | 16 | 18 | |

**April**

| | | | | | | | | | | |
|---|---|---|---|---|---|---|---|---|---|---|
| 0 | 59 | 57 | 56 | 54 | 50 | 47 | 43 | 48 | 52 | |
| 1-30 | 15 | 14 | 13 | 17 | 13 | 11 | 17 | 18 | 14 | |
| 31-70 | 11 | 11 | 13 | 10 | 14 | 15 | 23 | 13 | 14 | |
| 71-100 | 15 | 17 | 16 | 18 | 24 | 28 | 18 | 19 | 19 | |

**July**

| | | | | | | | | | | |
|---|---|---|---|---|---|---|---|---|---|---|
| 0 | 54 | 58 | 57 | 54 | 40 | 36 | 42 | 48 | 49 | |
| 1-30 | 25 | 25 | 22 | 25 | 25 | 25 | 30 | 32 | 26 | |
| 31-70 | 13 | 12 | 12 | 10 | 17 | 23 | 13 | 10 | 14 | |
| 71-100 | 10 | 7 | 10 | 13 | 20 | 18 | 15 | 11 | 13 | |

**October**

| | | | | | | | | | | |
|---|---|---|---|---|---|---|---|---|---|---|
| 0 | 66 | 67 | 67 | 68 | 62 | 57 | 64 | 68 | 65 | |
| 1-30 | 12 | 17 | 18 | 14 | 14 | 18 | 16 | 13 | 15 | |
| 31-70 | 8 | 8 | 8 | 9 | 11 | 10 | 9 | 9 | 9 | |
| 71-100 | 12 | 6 | 8 | 10 | 12 | 15 | 11 | 9 | 10 | |

Table A.6 (continued)

KEY WEST

**January**

| Echo Coverage % | 1-3 | 4-6 | 7-9 | 10-12 | 13-15 | 16-18 | 19-21 | 22-24 | 1-24 | LST |
|---|---|---|---|---|---|---|---|---|---|---|
| 0 | 43 | 42 | 38 | 33 | 34 | 45 | 49 | 48 | 42 | |
| 1-30 | 23 | 20 | 26 | 28 | 39 | 30 | 28 | 23 | 27 | |
| 31-70 | 22 | 22 | 24 | 23 | 15 | 15 | 16 | 19 | 19 | |
| 71-100 | 14 | 16 | 14 | 15 | 13 | 12 | 9 | 11 | 13 | |

**April**

| | | | | | | | | | | |
|---|---|---|---|---|---|---|---|---|---|---|
| 0 | 57 | 48 | 47 | 43 | 42 | 48 | 52 | 56 | 49 | |
| 1-30 | 20 | 28 | 31 | 39 | 42 | 38 | 31 | 26 | 32 | |
| 31-70 | 12 | 12 | 13 | 10 | 8 | 12 | 11 | 7 | 10 | |
| 71-100 | 11 | 12 | 8 | 6 | 6 | 2 | 7 | 11 | 8 | |

**July**

| | | | | | | | | | | |
|---|---|---|---|---|---|---|---|---|---|---|
| 0 | 19 | 14 | 15 | 11 | 6 | 3 | 7 | 22 | 12 | |
| 1-30 | 22 | 21 | 15 | 21 | 24 | 35 | 35 | 27 | 24 | |
| 31-70 | 16 | 23 | 25 | 25 | 30 | 35 | 27 | 19 | 25 | |
| 71-100 | 44 | 42 | 47 | 44 | 41 | 29 | 31 | 34 | 40 | |

**October**

| | | | | | | | | | | |
|---|---|---|---|---|---|---|---|---|---|---|
| 0 | 21 | 18 | 18 | 17 | 17 | 19 | 18 | 23 | 19 | |
| 1-30 | 13 | 13 | 18 | 23 | 21 | 22 | 23 | 15 | 19 | |
| 31-70 | 26 | 27 | 31 | 33 | 28 | 26 | 26 | 31 | 29 | |
| 71-100 | 38 | 43 | 35 | 29 | 35 | 34 | 31 | 32 | 34 | |

Table A.7. Average number of clear, cloudy and precipitation days per year.

| City | Clear[1] | Cloudy[2] | No. Yrs.[3] | Precip. (at a pt.)[4] |
|---|---|---|---|---|
| Birmingham, AL | 99 | 154 | (32) | 118 |
| Mobile, AL | 100 | 146 | (27) | 124 |
| Flagstaff, AZ | 168 | 100 | (26) | 75 |
| Phoenix, AZ | 213 | 70 | (38) | 34 |
| Little Rock, AR | 121 | 147 | (33) | 104 |
| Eureka, CA | 78 | 188 | (65) | 118 |
| Fresno, CA | 202 | 93 | (26) | 44 |
| Los Angeles, CA | 185 | 74 | (33) | 34 |
| Sacramento, CA | 190 | 102 | (27) | 58 |
| San Diego, CA | 151 | 98 | (35) | 41 |
| Colorado Springs, CO | 129 | 114 | (27) | 86 |
| Denver, CO | 115 | 116 | (41) | 88 |
| Hartford, CT | 76 | 178 | (21) | 128 |
| Wilmington, DE | 94 | 164 | (28) | 116 |
| Washington, DC | 102 | 158 | (27) | 112 |
| Miami, FL | 76 | 117 | (26) | 129 |
| Daytona Beach, FL | 93 | 135 | (32) | 115 |
| Atlanta, GA | 108 | 146 | (41) | 116 |
| Chicago, IL | 91 | 168 | (33) | 123 |
| Indianapolis, IN | 90 | 174 | (44) | 123 |
| Des Moines, IA | 102 | 168 | (26) | 106 |
| Topeka, KS | 112 | 156 | (29) | 95 |
| New Orleans, LA | 109 | 134 | (27) | 114 |
| Caribou, ME | 57 | 207 | (34) | 160 |
| Boston, MA | 99 | 161 | (40) | 128 |
| Detroit, MI | 80 | 177 | (32) | 131 |
| Duluth, MN | 75 | 186 | (27) | 135 |
| Jackson, MS | 108 | 151 | (12) | 113 |
| St. Louis, MO | 101 | 160 | (27) | 110 |
| Helena, MT | 82 | 180 | (35) | 96 |
| Omaha, NE | 113 | 147 | (40) | 100 |
| Las Vegas, NV | 216 | 66 | (27) | 24 |
| Albany, NY | 71 | 184 | (37) | 135 |
| Buffalo, NY | 56 | 204 | (32) | 168 |
| New York, NY | 107 | 133 | (42) | 121 |
| Asheville, NC | 99 | 157 | (11) | 129 |

| | | | | |
|---|---|---|---|---|
| Oklahoma City, OK | 140 | 128 | (27) | 82 |
| Portland, OR | 69 | 229 | (27) | 153 |
| Philadelphia, PA | 91 | 160 | (30) | 116 |
| Providence, RI | 102 | 161 | (30) | 125 |
| Charleston, SC | 102 | 151 | (30) | 115 |
| Rapid City, SD | 110 | 142 | (30) | 95 |
| Sioux Falls, SD | 105 | 156 | (30) | 107 |
| Memphis, TN | 118 | 150 | (30) | 107 |
| Amarillo, TX | 161 | 100 | (30) | 68 |
| Dallas, TX | 140 | 132 | (30) | 79 |
| El Paso, TX | 196 | 71 | (30) | 45 |
| Houston, TX | 93 | 166 | (30) | 108 |
| San Antonio, TX | 110 | 136 | (30) | 80 |
| Salt Lake City, UT | 128 | 132 | (30) | 88 |
| Burlington, VT | 58 | 203 | (30) | 152 |
| Richmond, VA | 103 | 55 | (30) | 114 |
| Seattle, WA | 56 | 228 | (30) | 161 |
| Spokane, WA | 90 | 189 | (30) | 115 |
| Charleston, WV | 58 | 190 | (30) | 149 |
| Milwaukee, WI | 96 | 169 | (30) | 123 |
| Cheyenne, WY | 107 | 131 | (30) | 97 |
| Average = | 110.5 | 149 | | 105.6 |
| Standard Error = | 39.4 | 37.4 | | 32.8 |

[1] number of days when cloud cover is 0.3 or less

[2] number of days when cloud cover is 0.8 or more

[3] number of years used to compute data

[4] number of days when measured precipitation is 0.01 inches or greater

## APPENDIX B

## MAXIMUM DETECTION RANGE OF WEATHER RADAR

The backscattered signal power received from a resolution volume at range $r_o$ is expressed as [Doviak and Zrnic', 1984]

$$\overline{P}_r(\text{mW}) = \frac{\pi^5 10^{-17} g^2 P_t(\text{W}) \ell^2 \ell_r \tau_s(\mu\text{s}) \theta_1^2(\text{deg}) |K_w|^2 Z_e(\text{mm}^6\text{m}^{-3})}{6.75 \times 2^{14} \ell n 2 \, r_o^2(\text{km}) \lambda^2(\text{cm})} \qquad \text{(B.1)}$$

where $\overline{P}_r$ is the average received power, $P_t$ is the transmitted peak power, $\ell$ is path attenuation including waveguide losses, $\ell_r$ is receiver loss due to finite bandwidth, $\tau_s$ is pulse width, $\theta_1$ is the one-way 3 dB beamwidth of the antenna, g is antenna gain, $\lambda$ is wavelength, and $Z_e$ is the effective reflectivity factor. The symbols in parentheses indicate the units of measure. $|K_w|^2 = 0.93$ is a constant.

For a circular aperture antenna we can approximate the 3 dB one-way pattern beamwidth $\theta_1$ with

$$\theta_1 = \frac{1.27\lambda}{D} \qquad \text{(radians)} \qquad \text{(B.2)}$$

where D is the diameter of the aperture. To obtain a relation between maximum detection range $r_m$ and power aperture product ($P_tA$), we define a quantity $P_z$ as the ratio of minimum detectable signal $P_{min}$ and reflectivity factor $Z_e$;

$$P_z\ (\text{dB}) = 10 \log \left[\frac{P_{min}(\text{mW})}{Z_e(\text{mm}^6\text{m}^{-3})}\right] \qquad \text{(B.3)}$$

$$= N\ (\text{dBm}) + \text{SNR}_{min}(\text{dB}) - Z_e(\text{dBZ})$$

where N is the noise power and $\text{SNR}_{min}$ is the minimum signal-to-noise ratio for measurement.

An empirical R-$Z_e$ relation of the type

$$Z_e = 200\ R^{1.6} \qquad \text{(B.4)}$$

can be used to relate rainfall rate R(mm $\text{hr}^{-1}$) to the reflectivity factor. The antenna gain is expressed as

$$g = \frac{4\pi A \eta_a}{\lambda^2} \qquad (B.5)$$

where A is the aperture area and $\eta_a$ is the aperture efficiency. A typical value for the aperture efficiency of an antenna with -25 dB sidelobe levels is 0.58.

For a properly designed radar system, the loss in waveguides, radome, etc. is of the order 6 dB. Assuming a matched receiver, a loss of 2.3 dB can be expected in the receiver. The loss due to atmospheric path attenuation is small ($\lesssim$ 0.5 dB) when the propagation medium between the resolution volume and the radar antenna has little precipitation. At shorter wavelengths ($\lambda$<3 cm) path attenuation increases, thus affecting the maximum detectable range. In our calculation we neglect this path loss. Using a total system loss of 8.3 dB, aperture efficiency of 0.58 and pulse width of 1 $\mu$s we arrive at a relation between $r_m$ and $P_tA$. Substituting (B.2), (B.3) and (B.5) in (B.1) we have the maximum detection range as

$$r_m = \left[\frac{1.21 \times 10^{-16} P_t A \ (kW \cdot m^2)}{\lambda^4(m)\ 10^{(0.1 \times P_z)}}\right]^{1/2} \ (km) \qquad (B.6)$$

Figures B.1, B.2, and B.3 show the dependence of $r_m$ on the power aperture product $P_tA$ at 10, 5, and 3 cm. $P_z$ is shown as a parameter. The relations (B.3) and (B.4) are combined in Fig. B.4 to facilitate easy calculation of $P_z$ as a function of rainfall rate R and minimum detectable signal by the receiver. As an example, consider a radar that operates at a wavelength of 10 cm and has a 10 m diameter parabolic dish with peak power $P_t$ = 100 kW. We find $P_tA \cdot 10^{-4} \approx 0.78$, and if the noise level is at -110 dBm and $SNR_{min}$ = -0 dB we find from Fig. B.1 that a cloud with a reflectivity of 10 dBZ would be detected up to about 100 km in range. A cirrus cloud with a reflectivity of 2 dBZ would be detectable only to about 45 km.

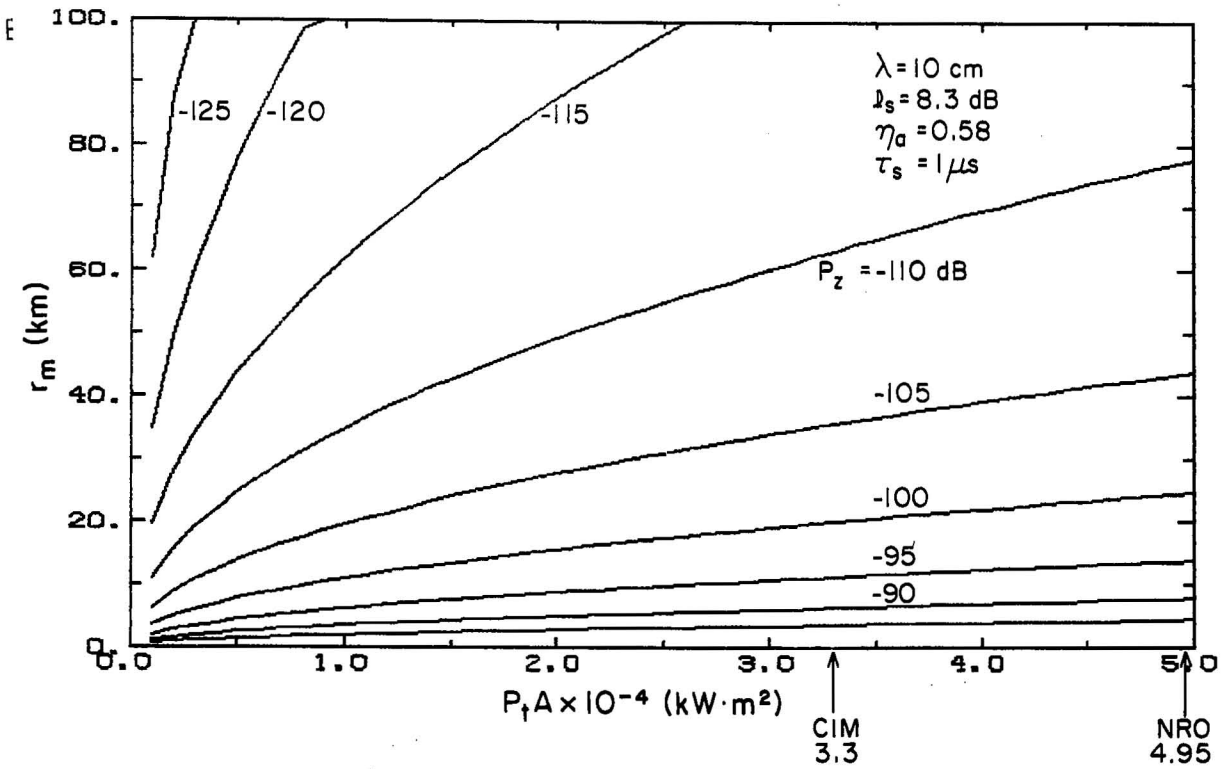


*Figure B.1.--Maximum detection range versus power-aperture product at λ = 10 cm.*

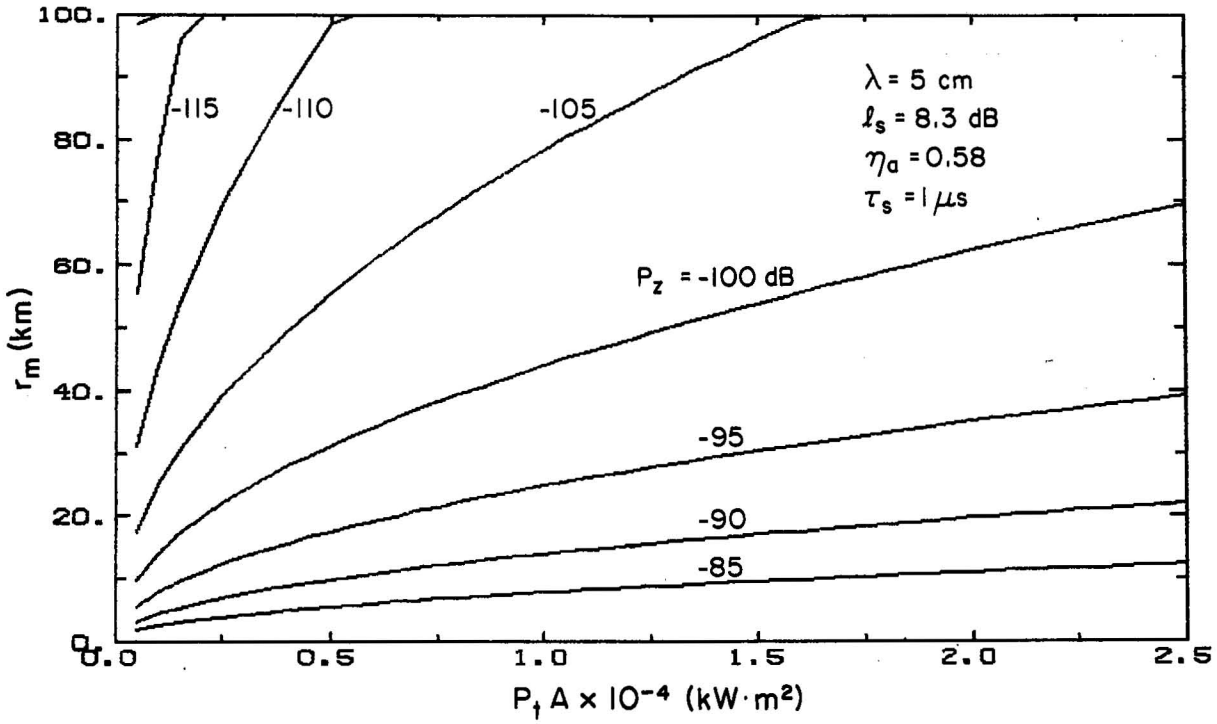


*Figure B.2.--Maximum detection range versus power-aperture product at λ = 5 cm.*

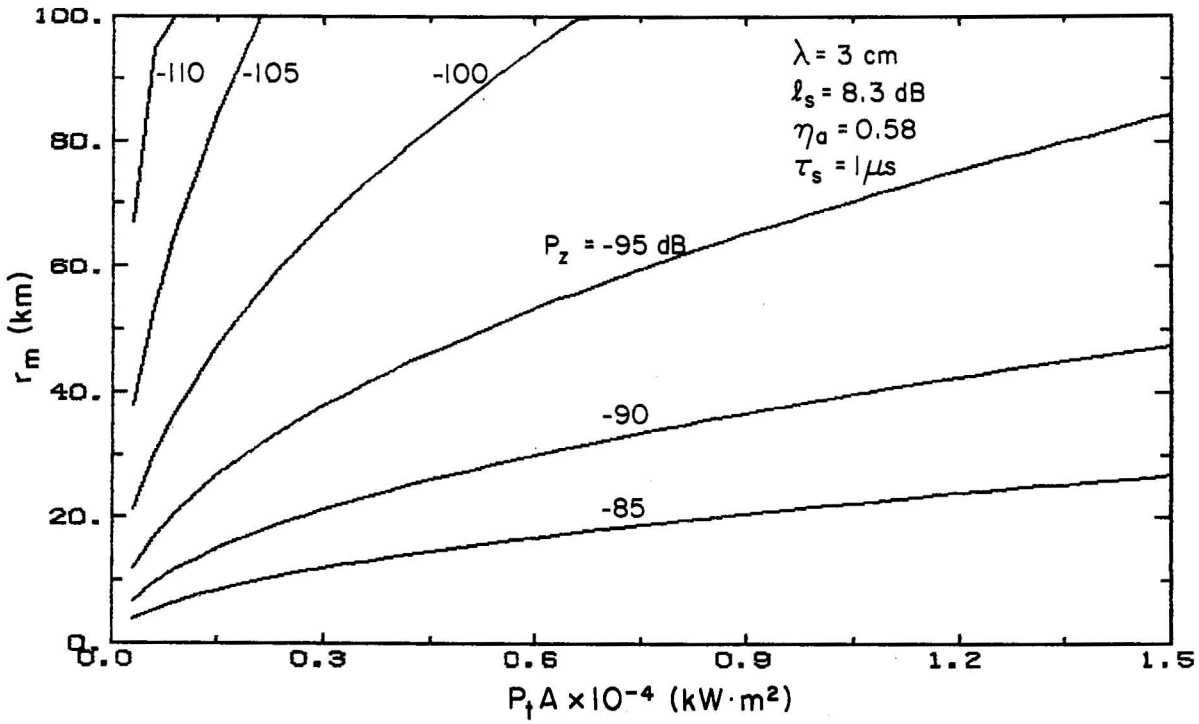


*Figure B.3.--Maximum detection range versus power-aperture product at $\lambda$ = 3 cm.*

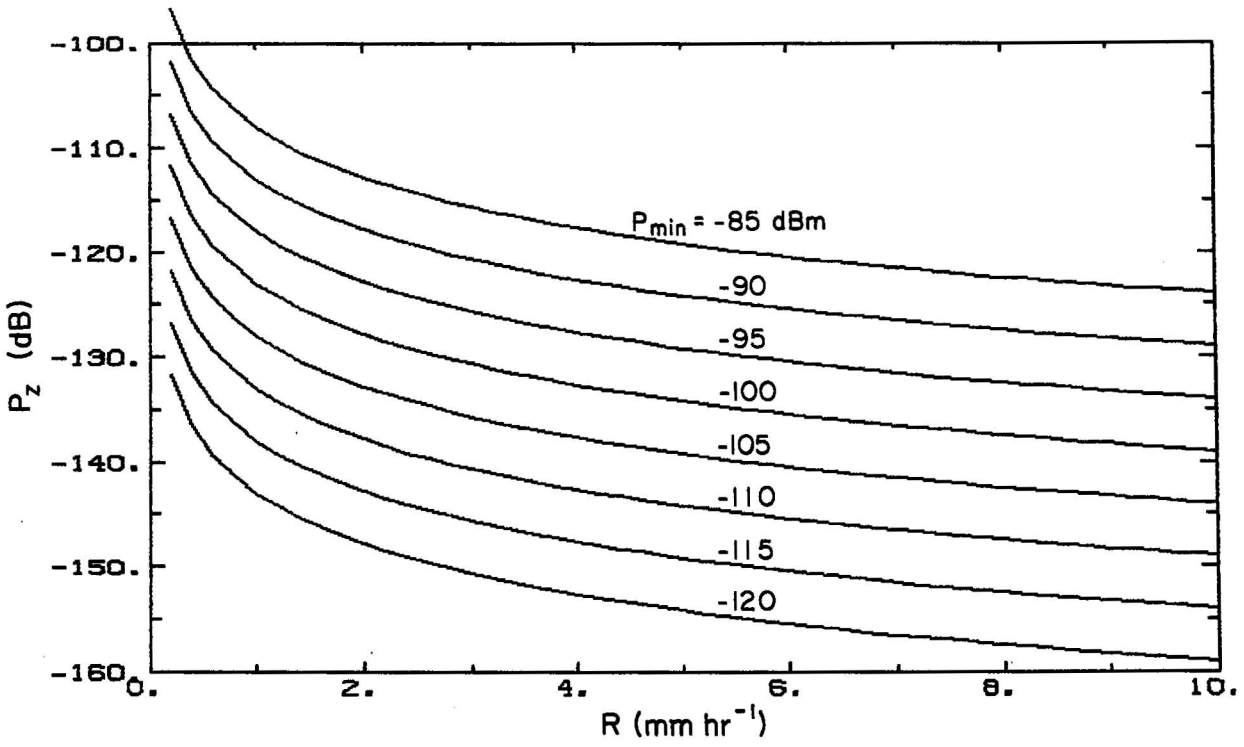


*Figure B.4.--$P_z$ versus rainfall rate.*

## APPENDIX C
## LEAST-SQUARES FIT OF RANGE-AVERAGED VELOCITIES

For radial velocity data processed within a sector, the least-squares estimates of the uniform wind components are

$$\begin{bmatrix} \hat{u}_o \\ \hat{v}_o \end{bmatrix} = \begin{bmatrix} \sum_i^{\Delta\phi} \sum_j^{\Delta r} \sin^2\phi_i \cos^2\theta'_{ej} & \sum_i^{\Delta\phi} \sum_j^{\Delta r} \sin\phi_i \cos\phi_i \cos^2\theta'_{ej} \\ \sum_i^{\Delta\phi} \sum_j^{\Delta r} \sin\phi_i \cos\phi_i \cos^2\theta'_{ej} & \sum_i^{\Delta\phi} \sum_j^{\Delta r} \cos^2\phi_i \cos^2\theta'_{ej} \end{bmatrix}^{-1} \times \begin{bmatrix} \sum_i^{\Delta\phi} \sum_j^{\Delta r} \hat{v}_{ij} \sin\phi_i \cos\theta'_{ej} \\ \sum_i^{\Delta\phi} \sum_j^{\Delta r} \hat{v}_{ij} \cos\phi_i \cos\theta'_{ej} \end{bmatrix} . \quad (C.1)$$

Assuming a flat earth and no beam bending, $\theta'_e$ is independent of range (i.e., of j) and constant (and equal to $\theta_e$) so that (C.1) can be rewritten as

$$\begin{bmatrix} \hat{u}_o \\ \hat{v}_o \end{bmatrix} = \frac{1}{\cos\theta_e} \begin{bmatrix} \sum_i^{\Delta\phi} \sin^2\phi_i & \sum_i^{\Delta\phi} \sin\phi_i \cos\phi_i \\ \sum_i^{\Delta\phi} \sin\phi_i \cos\phi_i & \sum_i^{\Delta\phi} \cos^2\phi_i \end{bmatrix}^{-1} \times \begin{bmatrix} \sum_i^{\Delta\phi} \bar{v}_i \sin\phi_i \\ \sum_i^{\Delta\phi} \bar{v}_i \cos\phi_i \end{bmatrix} \quad (C.2)$$

where $\bar{v}_i \equiv n_r^{-1} \sum_j^{\Delta r} v_{ij}$. Therefore, estimates obtained from processing range averaged velocity data along an arc (C.2) are equivalent to those obtained from processing data within a sector (C.1) if the earth's curvature and beam bending can be ignored and $\Delta r$ is sufficiently small so that effects of vertical wind shear can be ignored.

Because the earth is spherical and radar beams are refracted, a sufficient and necessary condition for (C.1) and (C.2) to be approximately equal is that $\theta_c$ be nearly constant over the averaging interval. Evaluating (3.1) for typical values of r, $\theta_e$, and assuming a 4/3 effective earth's radius model, $\theta_c$ is on the order of $5 \times 10^{-3}$ radians. (Typical values are r = 50 km and $\theta_e < 10°$.) For a symmetric averaging interval of length $\Delta r$, the maximum variation of $\theta_c$ from its value at the midpoint of the averaging interval is

$$\Delta\theta_{c_{max}} \approx \frac{\partial\theta_c}{\partial r} \Delta r/2$$

which, for an averaging interval of length 10 km is on the order of $10^{-4}$ radians. Because relative changes in $\theta_c$ are small ($\leq 2\%$), to a good approximation $\theta_c$ can be considered constant and equal to its value at the center of the averaging interval.

## APPENDIX D

## STRUCTURE CONSTANT FROM TURBULENT MIXING IN SHEAR LAYERS

We briefly explain calculations of the $C_n^2$ for turbulent layers. The pertinent formula can be found in Doviak and Zrnic (1984, Eq. 11.149) and it reads

$$C_n^2 = \frac{a^2 \varepsilon^{2/3} T_1 R_f}{(1-R_f) g \, d\langle\theta\rangle/dz} \cdot \left(\frac{K_\phi}{K_H}\right) \cdot 10^{-12} \left(\frac{d\langle\phi\rangle}{dz}\right)^2 \qquad (D.1)$$

where $K_\phi/K_H \approx 1$ when shear is the main turbulence generator, $T_1$ is the mean temperature of the turbulent layer, and $\varepsilon$ is the eddy dissipation rate. For light turbulence $\varepsilon$ is about $3 \times 10^{-3}$ $m^2 s^{-3}$. $R_f$ is the flux Richardson number taken to be 0.25, and $a^2$ is a dimensionless constant between 3.2 and 4. The acceleration due to gravity is g, and the quantities $d\langle\theta\rangle/dz$ and $d\langle\phi\rangle/dz$ are the gradients of potential temperature and potential refractive index at the height of observation. This last quantity can be written as

$$\phi = (77.6/\theta)\,(P_o + 4810\, P_{wo}/\theta) \qquad (D.2)$$

where $P_{wo} = P_w(P_o/P)$ is the potential water vapor pressure, P is atmospheric pressure, $P_o$ = 1000 mb, and $P_w$ is the water vapor pressure. $P_w$ is related to the mixing ratio m by

$$P_w = \frac{mP}{m+0.622} \quad \text{(mbar)} \qquad (D.3)$$

Height profiles of $\theta$ and m provide all the information needed to evaluate (D.1). We identified layers from obviously large changes in $\theta$ with height and have used the center of a layer to evaluate the gradients.

## APPENDIX E

## ESTIMATION OF THE REFLECTIVITY FACTOR AND THE STRUCTURE CONSTANT FROM DOPPLER SPECTRA

If the weather signal has Gaussian spectrum shape and the receiver noise is white, the reflectivity factor can be estimated as follows:

First one must determine the signal to noise ratio (SNR):

$$SNR(dB) = 10 \log (10^{\alpha/10}-1) - 10 \log (2v_a/\sqrt{2\pi}\ \sigma_v) \qquad (E.1)$$

where $\alpha$ is the distance between spectral peak and the noise level, $v_a$ is the unambiguous velocity and $\sigma_v$ is the spectrum width (Fig. E.1). From the width, $\Delta$, of the spectrum 4.3 dB below the peak we find

$$\sigma_v = \Delta/2\sqrt{2} \qquad (E.2)$$

Now the radar equation (Appendix B) with the parameters from Table E.1 yields

$$Z_e(dBZ) = 10 \log P_r(mW) + 20 \log r(km) + 70.4 \qquad (E.3)$$

From E.1 and the known noise power (-114 dBm) the received power becomes

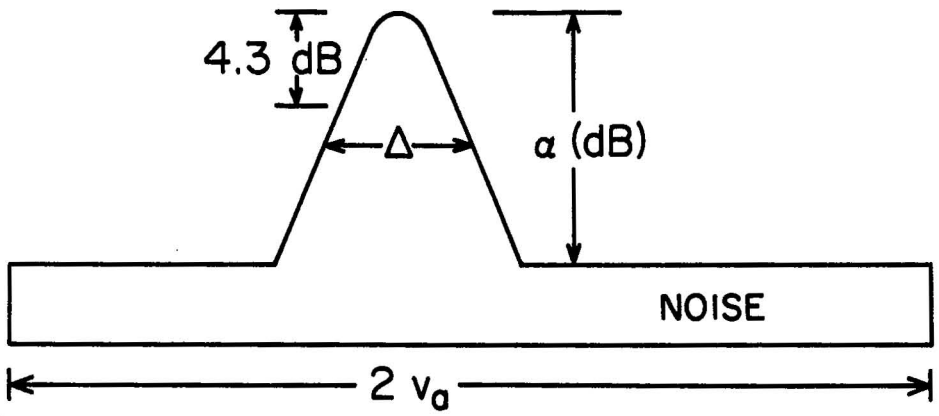


*Figure E.1.--A Gaussian signal spectrum in white noise. Measurable quantities $\alpha$ and $\Delta$ are indicated; $v_a$ is the unambiguous velocity.*

$$10 \log P_r(mW) = SNR - 114 \qquad (E.4)$$

so that

$$Z_e(dBZ) = SNR + 20 \log r(km) - 43.6 \qquad (E.5)$$

The effective reflectivity factor $Z_e$ can be related to the structure constant $C_n^2$ by means of the equation for unit volume reflectivity (i.e., cross section per unit volume):

$$\eta = 0.38 \lambda^{-1/3} C_n^2 = \pi^5 \lambda^{-4} |K_w|^2 Z_e \qquad (E.6)$$

where all units are in the MKS system. So for $Z_e$ in dBZ, $|K_w|^2 = 0.93$, and $\lambda = 0.1$ m we get

$$\log C_n^2 = -11.8 + 0.1 Z_e \qquad (E.7)$$

TABLE E.1--Norman radar parameters

| | |
|---|---|
| Transmitted power $P_t$ | 750 kW |
| Antenna gain g | 46.8 dB |
| One-way (3 dB) beamwidth $\theta_1$ | 0.8° |
| Pulse length $\tau$ | 1 μs |
| Wavelength $\lambda$ | 10.52 cm |
| Waveguide and radome losses $\ell^2$ | 4 dB |
| Receiver filter loss $\ell_r$ | 2.5 dB |
| Pulse repetition frequency $T_s$ | 768 μs |

## NATIONAL SEVERE STORMS LABORATORY

The NSSL Technical Memoranda, beginning at No. 28, continue the sequence established by the U.S. Weather Bureau National Severe Storms Project, Kansas City, Missouri. Numbers 1-22 were designated NSSP Reports. Numbers 23-27 were NSSL Reports, and 24-27 appeared as subseries of Weather Bureau Technical Notes. These reports are available from the National Technical Information Service, Operations Division, Springfield, Virginia 22151, a microfiche version for $4.00 or a hard copy, cost dependending upon the number of pages. NTIS numbers are given below in parenthesis.

No. 1 National Severe Storms Project Objectives and Basic Design. Staff, NSSP. March 1961. 16 p. (PB-168207)

No. 2 The Development of Aircraft Investigations of Squall Lines from 1956-1960. Brent B. Goddard. 34 p. (PB-168208)

No. 3 Instability Lines and Their Environments as Shown by Aircraft Soundings and Quasi-Horizontal Traverses. Dansey T. Williams. February 1962. 15 p. (PD-168209)

No. 4 On the Mechanics of the Tornado. J. R. Fulks. February 1962. 33 p. (PD-168210)

No. 5 A Summary of Field Operations and Data Collection by the National Severe Storms Project in Spring 1961. Jean T. Lee. March 1962. 47 p. (PB 165095)

No. 6 Index to the NSSP Surface Network. Tetsuya Fujita. April 1962. 32 p. (PB-168212)

No. 7 The Vertical Structure of Three Dry Lines as Revealed by Aircraft Traverses. E. L. McGuire. April 1962. 10 p. (PB-168213)

No. 8 Radar Observations of a Tornado Thunderstorm in Vertical Section. Ralph J. Donaldson, Jr. April 1962. 21 p. (PB-174859)

No. 9 Dynamics of Severe Convective Storms. Chester W. Newton. July 1962. 44 p. (PB-163319)

No. 10 Some Measured Characteristics of Severe Storms Turbulence. Roy Steiner and Richard H. Rhyne. July 1962. 17 p. (N62-16401)

No. 11 A Report of the Kinematic Properties of Certain Small-Scale Systems. Dansey T. Williams. October 1962. 22 p. (PB-168216)

No. 12 Analysis of the Severe Weather Factor in Automatic Control of Air Route Traffic. W. Boynton Beckwith. December 1962. 67 p. (PB-168217)

No. 13 500-Kc./Sec. Sferics Studies in Severe Storms. Douglas A. Kohl and John E. Miller. April 1963. 36 p. (PB-168218)

No. 14 Field Operations of the National Severe Storms Project in Spring 1962. L. D. Sanders. May 1963. 71 p. (PB-168219)

No. 15 Penetrations of Thunderstorms by an Aircraft Flying at Supersonic Speeds. G. P. Roys. Radar Photographs and Gust Loads in Three Storms of 1961 Rough Rider. Paul W. J. Schumacher. May 1963. 19 p. (PB-168220)

No. 16 Analysis of Selected Aircraft Data from NSSP Operations, 1962. Tetsuya Fujita. May 1963. 29 p. (PB-168221)

No. 17 Analysis Methods for Small-Scale Surface Network Data. Dansey T. Williams. August 1963. 20 p. (PB-168222)

No. 18 The Thunderstorm Wake of May 4, 1961. Dansey T. Williams. August 1963. 233 p. (PB-168223)

No. 19 Measurements by Aircraft of Condensed Water in Great Plains Thunderstorms. George P. Roys and Edwin Kessler. July 1966. 17 p. (PB-173048)

No. 20 Field Operations of the National Severe Storms Project in Spring 1963. J. T. Lee, L. D. Sanders, and D. T. Williams. January 1964. 68 p. (PB-168224)

No. 21 On the Motion and Predictability of Convective Systems as Related to the Upper Winds in a Case of Small Turning of Wind with Height. James C. Fankhauser. January 1964. 36 p. (PB 168225)

No. 22 Movement and Development Patterns of Convective Storms and Forecasting the Probability of Storm Passage at a Given Location. Chester W. Newton and James C. Fankhauser. January 1964. 53 p. (PB-168226)

No. 23 Purposes and Programs of the National Severe Storms Laboratory, Norman, Oklahoma. Edwin Kessler. December 1964. 17 p. (PB-166675)

No. 24 Papers on Weather Radar, Atmospheric Turbulence, Sferics and Data Processing. NSSL Staff. August 1965. 139 p. (AD-621586)

No. 25 A Comparison of Kinematically Computed Precipitation with Observed Convective Rainfall. James C. Fankhauser. September 1965. 28 p. (PB-168445)

No. 26 Probing Air Motion by Doppler Analysis of Radar Clear Air Returns. Roger M. Lhermitte. May 1966. 37 p. (PB-170636)

No. 27 Statistical Properties of Radar Echo Patterns and the Radar Echo Process. Larry Armijo. May 1966. The Role of the Kutta-Joukowski Force in Cloud Systems with Circulation. J. L. Goldman. May 1966. 34 p. (PB-170756)

No. 28 Movement and Predictability of Radar Echoes. James Warren Wilson. November 1966. 30 p. (PB-173972)

No. 29 Notes on Thunderstorm Motions, Heights, and Circulations. T. W. Harrold, W. T. Roach, and Kenneth E. Wilk. November 1966. 51 p. (AD-644899)

No. 30 Turbulence in Clear Air Near Thunderstorms. Anne Burns, Terence W. Harrold, Jack Burnham, and Clifford S. Spavins. December 1966. 20 p. (PB-173992)

No. 31 Study of a Left-Moving Thunderstorm of 23 April 1964. George R. Hammond. April 1967. 75 p. (PB-174681)

No. 32 Thunderstorm Circulations and Turbulence Studies from Aircraft and Radar Data. James C. Fankhauser and J. T. Lee. April 1967. 32 p. (PB-174860)

No. 33 On the Continuity of Water Substance. Edwin Kessler. April 1967. 125 p. (PB-175840)

No. 34 Note on Probing Balloon Motion by Doppler Radar. Robert M. Lhermitte. July 1967. 14 p. (PB-175930)

No. 35 A Theory for the Determination of Wind and Precipitation Velocities with Doppler Radars. Larry Armijo. August 1967. 20 p. (PB-176376)

No. 36 A Preliminary Evaluation of the F-100 Rough Rider Turbulence Measurement System. U. O. Lappe. October 1967. 25 p. (PB-177037)

No. 37 Preliminary Quantitative Analysis of Airborne Weather Radar. Lester P. Merritt. December 1967. 32 p. (PB-177188)

No. 38 On the Source of Thunderstorm Rotation. Stanley L. Barnes. March 1968. 28 p. (PB-178990)

No. 39 Thunderstorm-Environment Interactions Revealed by Chaff Trajectories in the Mid-Troposphere. James C. Fankhauser. June 1968. 14 p. (PB-179659)

No. 40 Objective Detection and Correction of Errors in Radiosonde Data. Rex L. Inman. June 1968. 50 p. (PB-180284)

No. 41 Structure and Movement of the Severe Thunderstorms of 3 April 1964 as Revealed from Radar and Surface Mesonetwork Data Analysis. Jess Charba and Yoshikazu Sasaki. October 1968. 47 p. (PB-183310)

No. 42 A Rainfall Rate Sensor. Brian E. Morgan. November 1968. 10 p. (PB-183979)

No. 43 Detection and Presentation of Severe Thunderstorms by Airborne and Ground-based Radars: A Comparative Study. K. E. Wilk, J. K. Carter, and J. T. Dooley. February 1969. 56 p. (PB-183572)

No. 44 A Study of a Severe Local Storm of 16 April 1967. George Thomas Haglund. May 1969. 54 p. (PB-184970)

No. 45 On the Relationship Between Horizontal Moisture Convergence and Convective Cloud Formation. Horace R. Hudson. March 1970. 29 p. (PB-191720)

No. 46 Severe Thunderstorm Radar Echo Motion and Related Weather Events Hazardous to Aviation Operations. Peter A. Barclay and Kenneth E. Wilk. June 1970. 63 p. (PB-192498)

No. 47 Evaluation of Roughness Lengths at the NSSL-WKY Meteorological Tower. Leslie D. Sanders and Allen H. Weber. August 1970. 24 p. (PB-194587)

No. 48 Behavior of Winds in the Lowest 1500 ft. in Central Oklahoma: June 1966 - May 1967. Kenneth C. Crawford and Horace R. Hudson. August 1970. 57 p. (N71-10615)

No. 49 Tornado Incidence Maps. Arnold Court. August 1970. 76 p. (COM-71-00019)

No. 50 The Meteorologically Instrumented WKY-TV Tower Facility. John K. Carter. September 1970. 18 p. (COM-71-00108)

No. 51 Papers on Operational Objective Analysis Schemes at the National Severe Storms Forecast Center. Rex L. Inman. November 1970. 91 p. (COM-71-00136)

No. 52 The Exploration of Certain Features of Tornado Dynamics Using a Laboratory Model. Neil B. Ward. November 1970. 22 p. (COM-71-00139)

No. 53 Rawinsonde Observation and Processing Techniques at the National Severe Storms Laboratory. Stanley L. Barnes, James H. Henderson and Robert J. Ketchum. April 1971. 245 p. (COM-71-00707)

NO. 54 Model of Precipitation and Vertical Air Currents. Edwin Kessler and William C. Bumgarner. June 1971. 93 p. (COM-71-00911)

No. 55 The NSSL Surface Network and Observations of Hazardous Wind Gusts. Operations Staff. June 1971. 20 p. (COM-71-00910)

No. 56 Pilot Chaff Project at NSSL. Edward A. Jessup. November 1971. 36 p. (COM-72-10106)

No. 57 Numerical Simulation of Convective Vortices. Robert P. Davies-Jones and Glenn T. Vickers. November 1971. 27 p. (COM-72-10269)

No. 58 The Thermal Structure of the Lowest Half Kilometer in Central Oklahoma: December 9, 1966 - May 31, 1967. R. Craig Goff and Horace R. Hudson. July 1972. 53 p. (COM-72-11281)

No. 59 Cloud-to-Ground Lightning Versus Radar Reflectivity in Oklahoma Thunderstorms. Gilbert D. Kinzer. September 1972. 24 p. (COM-73-10050)

No. 60 Simulated Real Time Displays of Doppler Radar Velocity Fields. G. B. Walker and L. D. Hennington. November 1972. 10 p. (COM-73-10515)

No. 61 Gravity Current Model Applied to Analysis of Squall-Line Gust Front. Jess Charba. November 1972. 58 p. (COM-73-10410)

No. 62 Mesoscale Objective Map Analysis Using Weighted Time-Series Observations. Stanley L. Barnes. March 1973. 60 p. (COM-73-10781)

No. 63 Observations of Severe Storms on 26 and 28 April 1971. Charles L. Vlcek. April 1973. 19 p. (COM-73-11200)

No. 64 Meteorological Radar Signal Intensity Estimation. Dale Sirmans and R. J. Doviak. September 1973. 80 p. (COM-73-11923/2AS)

No. 65 Radiosonde Altitude Measurement Using Double Radiotheodolite Techniques. Stephan P. Nelson. September 1973. 20 p. (COM-73-11932/9AS)

No. 66 The Motion and Morphology of the Dryline. Joseph T. Schaefer. September 1973. 81 p. (COM-74-10043)

No. 67 Radar Rainfall Pattern Optimizing Technique. Edward A. Brandes. March 1974. 16 p. (COM-74-10906/AS)

No. 68 The NSSL/WKY-TV Tower Data Collection Program: April-July 1972. R. Craig Goff and W. David Zittel. May 1974. 45 p. (COM-74-11334/AS)

No. 69 Papers on Oklahoma Thunderstorms, April 29-30, 1970. Stanley L. Barnes, Editor. May 1974. 147 p. (COM-74-11474/AS)

No. 70 Life Cycle of Florida Keys' Waterspouts. Joseph H. Golden. June 1974. 147 p. (COM-74-11477/AS)

No. 71 Interaction of Two Convective Scales Within a Severe Thunderstorm: A Case Study. and Thunderstorm Wake Vortex Structure and Aerodynamic Origin. Leslie R. Lemon. June 1974. 43 p. (COM-74-11642/AS)

NO. 72 Updraft Properties Deduced from Rawinsoundings. Robert P. Davies-Jones and James H. Henderson. October 1974. 117 p. (COM-75-10583/AS)

No. 73 Severe Rainstorm at Enid, Oklahoma - October 10, 1973. L. P. Merritt, K. E. Wilk, and M. L. Weible. November 1974. 50 p. (COM-75-10583/AS)

No. 74 Mesonetwork Array: Its Effect on Thunderstorm Flow Resolution. Stanley L. Barnes. October 1974. 16 p. (COM-75-10248/AS)

No. 75 Thunderstorm-Outflow Kinematics and Dynamics. R. Craig Goff. December 1975. 63 p. (PB-250808/AS)

No. 76 An Analysis of Weather Spectra Variance in a Tornadic Storm. Philippe Waldteufel. May 1976. 80 p. (PB-258456/AS)

No. 77 Normalized Indices of Destruction and Deaths by Tornadoes. Edwin Kessler and J. T. Lee. June 1976. 47 p. (PB-260923/AS)

No. 78 Objectives and Accomplishments of the NSSL 1975 Spring Program. K. Wilk, K. Gray, C. Clark, D. Sirmans, J. Dooley, J. Carter, and W. Bumgarner. July 1976. 47 p. (PB-263813/AS)

No. 79 Subsynoptic Scale Dynamics As Revealed By The Use of Filtered Surface Data. Charles A. Doswell III. December 1976. 40 p. (PB-265433/AS)

No. 80 The Union City, Oklahoma Tornado of 24 May 1973. Rodger A. Brown, Editor. December 1976. 235 p. (PB-269443/AS)

No. 81 Mesocyclone Evolution and Tornado Generation Within the Harrah, Oklahoma Storm. Edward A. Brandes. May 1977. 28 p. (PB-271675/AS)

No. 82 The Tornado: An Engineering-Oriented Perspective. Joseph E. Minor, James R. McDonald, and Kishor C. Mehta. December 1977. 196 p. (PB-281860/AS)

No. 83 Spring Program '76. R. Alberty, J. Weaver, D. Sirmans, J. Dooley, and B. Bumgarner. December 1977. 130 p. (PB-280745/AS)

No. 84 Spring Program '77. Peter S. Ray, John Weaver, and NSSL Staff. December 1977. 173 p. (PB-284953/AS)

No. 85 A Dual-Doppler Variational Objective Analysis as Applied to Studies of Convective Storms. Conrad L. Ziegler. November 1978. 116 p. (PB-293581/AS)

No. 86 Final Report on the Joint Doppler Operational Project (JDOP) 1976-78. Prepared by Staff of the National Severe Storms Laboratory, Environmental Research Laboratories; Weather Radar Branch, Air Force Geophysics Laboratory; Equipment Development Laboratory, National Weather Service; and Air Weather Service, United States Air Force. March 1979. 84 p. (PB80-107188/AS)

No. 87 An Analysis of the Clear Air Planetary Boundary Layer Wind Synthesized from NSSL's Dual Doppler-Radar Data. Myron I. Berger and R. J. Doviak. June 1979. 55 p. (PB-300865/AS)

No. 88 The Relationship of the 300-mb Jet Stream to Tornado Occurrence. Carolyn M. Kloth and Robert P. Davies-Jones. July 1980. 62 p. (PB81-118960)

No. 89 A Study of Hail Production in a Supercell Storm Using a Doppler Derived Wind Field and a Numerical Hail Growth Model. Stephan P. Nelson. December 1980. 90 p. (PB81-17822Q)

No. 90 Summary of AEC-ERDA-NRC Supported Research at NSSL 1973-1979. J. T. Lee, Editor. March 1981. 93 p. (PB81-220162)

No. 91 1980 Spring Program Summary. R. J. Doviak, Editor. April 1981. 128 p. (PB81-234940)

No. 92 Multiple Doppler Radar Analysis of Severe Thunderstorms: Designing a General Analysis System. R. A. Brown, C. R. Safford, S. P. Nelson, D. W. Burgess, W. C. Bumgarner, M. L. Weible, and L. C. Fortner. June 1981. 18 p. (PB82-114117)

No. 93 1981 Spring Program Summary. William L. Taylor, Editor. March 1982. 97 p. (PB82-244757)

No. 94 Multiple Doppler Radar Derived Vertical Velocities in Thunderstorms: Part I - Error Analysis and Solution Techniques, Part II - Maximizing Areal Extent of Vertical Velocities. Stephan P. Nelson and Rodger A. Brown. October 1982. 21 p. (PB83-152-553)

No. 95 Single Doppler Velocity Signatures: An Atlas of Patterns in Clear Air/Widespread Precipitation and Convective Storms. Vincent T. Wood and Rodger A. Brown. November 1983. 71 p. (PB84155779)

No. 96 1983 Spring Program Summary. J. T. Dooley, Editor. April 1984. 54 p. (PB84222223)

No. 97 J. P. Finley: The First Severe Storms Forecaster. Joseph G. Galway. November 1984. 32 p. (PB-85175453)